

การสังเคราะห์และพิสูจน์เอกลักษณ์ของสารคอมโพลีตแมงกานีส-เหล็กออกไซด์
เพื่อใช้ในการดูดซับไอออนของโลหะแทรนซิชัน



นางสาววิญญา ก้องเสนาะ

สถาบันวิทยบริการ
จุฬาลงกรณ์มหาวิทยาลัย
วิทยานิพนธ์นี้เป็นส่วนหนึ่งของการศึกษาตามหลักสูตรปริญญาวิทยาศาสตรมหาบัณฑิต

สาขาวิชาเคมี ภาควิชาเคมี

คณะวิทยาศาสตร์ จุฬาลงกรณ์มหาวิทยาลัย

ปีการศึกษา 2548

ISBN 974-17-5853-7

ลิขสิทธิ์ของจุฬาลงกรณ์มหาวิทยาลัย

**SYNTHESIS AND CHARACTERIZATION OF MANGANESE-IRON OXIDE
COMPOSITES FOR ADSORPTION OF TRANSITION METAL IONS**

Miss Khwannapa Kongsanoa

สถาบันวิทยบริการ

A Thesis Submitted in Partial Fulfillment of the Requirements
for the Degree of Master of Science Program in Chemistry

Department of Chemistry

Faculty of Science


Chulalongkorn University

Academic Year 2005

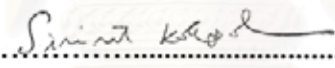
ISBN 974-17-5853-7

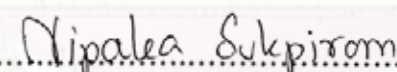
Thesis Title SYNTHESIS AND CHARACTERIZATION OF MANGANESE-
IRON OXIDE COMPOSITES FOR ADSORPTION OF
TRANSITION METAL IONS
By Miss Khwannapa Kongsanoa
Field of Study Chemistry
Thesis Advisor Nipaka Sukpirom, Ph.D.

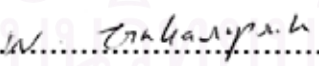
Accepted by the Faculty of Science, Chulalongkorn University in Partial
Fulfillment of the Requirements for the Master's Degree

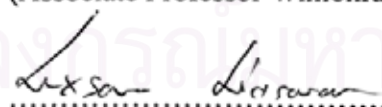

.....Dean of the Faculty of Science
(Professor Piamsak Menasveta, Ph.D.)

THESIS COMMITTEE


.....Chairman
(Associate Professor Sirirat Kokpol, Ph.D.)


.....Thesis Advisor
(Nipaka Sukpirom, Ph.D.)


.....Member
(Associate Professor Wimonrat Trakarnpruk, Ph.D.)


.....Member
(Luxsana Limsavarn, Ph.D.)

ขวัญภา ก้องเสนาะ : การสังเคราะห์และพิสูจน์เอกลักษณ์ของสารคอมโพสิตแมงกานีส-เหล็กออกไซด์เพื่อใช้ในการดูดซับไอออนของโลหะทรานซิชัน (SYNTHESIS AND CHARACTERIZATION OF MANGANESE-IRON OXIDE COMPOSITES FOR ADSORPTION OF TRANSITION METAL IONS) อ. ที่ปรึกษา: ดร. นิปกา สุขภิรมย์
90 หน้า. ISBN 947-17-5853-7

คอมโพสิตของเหล็กออกไซด์และแมงกานีสออกไซด์เตรียมได้ด้วยวิธีต่างๆ ทั้งนี้เพื่อปรับปรุงความสามารถในการดูดซับโลหะหนักและการกรองแยกของตัวดูดซับของเหล็กออกไซด์ วิธีหนึ่งที่สามารถประสบความสำเร็จในการเตรียมคอมโพสิตที่มีการกระจายตัวของอะตอมเหล็กและแมงกานีสทั่วคอมโพสิตโดยสังเกตจากภาพถ่าย SEM-EDX รวมทั้งยังมีพื้นที่ผิว BET สูง คือวิธีการกระจายโครงสร้างและตกตะกอน วิธีนี้ประกอบไปด้วย 2 ขั้นตอน คือ (1) การกระจายโครงสร้างของเบอร์เนสไซต์ (แมงกานีสออกไซด์ที่มีโครงสร้างเป็นชั้น) ด้วยสารละลายเทตระบิวทิลแอมโมเนียมไฮดรอกไซด์ และตามด้วย (2) การตกตะกอนร่วมกับพอลิแคทาไอออนของเหล็กในสารละลายเบส ตรวจสอบคอมโพสิตที่ได้ด้วยเทคนิค XRD และ FT-IR พบว่าประกอบด้วยอนุภาคที่มีความเป็นผลึกขนาดนาโนเมตรของเบอร์เนสไซต์และเกอไทต์ ความสามารถในการดูดซับไอออนของทองแดงและไอออนของตะกั่วของคอมโพสิตที่ได้นี้ดีกว่าความสามารถในการดูดซับไอออนดังกล่าวของของผสมของเบอร์เนสไซต์และเกอไทต์มากถึง 10 - 35% ความสามารถในการกรองแยกคอมโพสิตเหล่านี้ออกจากสารละลายโลหะหนักง่ายกว่าการกรองแยกเกอไทต์ การกรองแยกจะให้สารละลายใสเมื่อตัวดูดซับคือคอมโพสิตที่มีปริมาณเหล็ก 80 % โดยน้ำหนักของโลหะรวม

สถาบันวิทยบริการ
จุฬาลงกรณ์มหาวิทยาลัย

ภาควิชาเคมี..... ลายมือชื่อนิสิตขวัญภา ก้องเสนาะ.....
สาขาวิชา.....เคมี..... ลายมือชื่ออาจารย์ที่ปรึกษานิปกา สุขภิรมย์.....
ปีการศึกษา.....2548.....

4672214523: MAJOR CHEMISTRY

KEY WORD: IRON/MANGANESE/COMPOSITE/EXFOLIATION/PRECIPITATION

KHWANNAPA KONGSANO: SYNTHESIS AND CHARACTERIZATION OF MANGANESE-IRON OXIDE COMPOSITES FOR ADSORPTION OF TRANSITION METAL IONS. THESIS ADVISOR: NIPAKA SUKPIROM, Ph.D., 90 pp., ISBN 974-17-5853-7

The composites of iron oxide and manganese oxide are synthesized using various approaches, in order to improve the heavy metal capacities and filtration quality of iron oxide. The exfoliation-precipitation approach is successful to produce the composites with highly distribution of Fe and Mn over the composites as observed by SEM-EDX, and high BET specific surface area. This approach utilizes two steps (1) the exfoliation of preformed birnessite (layered manganese oxide) using tetrabutylammonium hydroxide solution, and consequently (2) the precipitation with Fe-polycation in basic solution. The composites are comprised of the nanocrystallites of birnessite and goethite, indicating by XRD and FT-IR. The adsorption capacities towards copper and lead ions are much (10-35%) higher than the physical mixtures of pure goethite and birnessite. The filtration qualities of all composites are also improved, comparing to that of pure goethite. The clear filtrate is found using the composite with 80 wt % Fe to total metal as an adsorbent.

สถาบันวิทยบริการ
จุฬาลงกรณ์มหาวิทยาลัย

Department..... Chemistry..... Student's Signature Khwannapa Kongsano.
Field of Study..... Chemistry..... Advisor's Signature Nipaka Sukpirom
Academic..... 2005.....

ACKNOWLEDGEMENTS

Through my years as a graduate student, I have received extensive support from my thesis advisor Dr. Nipaka Sukpirom. She has transformed me into a creative and self-supportive individual, for which I am very grateful. Also, I would like to thank and pay my respect to Associate Professor Dr. Sirirat Kokpol, Associate Professor Dr. Wimonrat Trakarnpruk and Dr. Luxsana Limsavarn as committee members and thesis examiners.

Moreover, I would like to thank Department of Chemistry, Faculty of Science, Chulalongkorn University for providing me resources and facilities. I would like to extend thanks to Dr. Puttaruksa Varanusupakul for giving her time as proposal examiner, Dr. Apichat Imyim for the suggestion on determination of iron content and Dr. Puangfa Unop for the suggestion on adsorption studies.

I also would like to thank the followings: the members of Materials Chemistry and Catalysis Research Unit, Organometallic Group and Supramolecular Research Unit, especially Mr. Tanawat Kanjanaboonmalert, Ms. Parichat Damrongpong, Ms. Auemphon rathanasing, Mr. Nitiphong Jirathiwathanakul, Mr. Nattawut Kaveevivitchai, Ms. Tuanjai Yubolpas, Ms. Pornmanee Khamloet, Mr. Chinawat Sasananan and Mr. Saksit Wongkulab, for their time and assistance. Finally, own thus accomplishment to my family and my friends outside the Chemistry sphere as they always support me and also have faith on me.

CONTENTS

		Page
ABSTRACT IN THAI		iv
ABSTRACT IN ENGLISH		v
ACKNOWLEDGEMENTS		vi
CONTENTS		vii
LIST OF FIGURES		xi
LIST OF TABLES		xiv
LIST OF ABBREVIATIONS		xv
CHAPTER I	INTRODUCTION	1
	1.1 Background.....	1
	1.2 Objectives.....	3
	1.3 Approach and thesis outline.....	4
CHAPTER II	LITERATURE REVIEWS	5
	2.1 Adsorption of cations on manganese oxide and iron oxide.....	5
	2.2 Adsorption of cations on modified surface oxide.....	6
	2.3 Synthesis route for modification surface oxide.....	9
CHAPTER III	THEORY	12
	3.1 Adsorption of metal onto mineral surfaces.....	12
	3.2 Mineral properties.....	13
	3.3 Structural features of iron oxyhydroxides.....	14
	3.4 Structural features of manganese oxide.....	15
	3.4.1 Structural features of birnessite.....	16
	3.4.2 Properties of birnessite.....	17
	3.4.2.1 Intercalation.....	17

	Page
3.4.2.2 Swelling exfoliation/delamination and, reflocculation	17
3.5 Characterization of materials.....	19
3.5.1 Powder X-ray diffraction (XRD).....	19
3.5.2 Scanning electron microscopy and energy dispersive X-ray analysis (SEM-EDX).....	21
3.5.3 Nitrogen adsorption-desorption isotherm.....	22
3.5.4 Determination of iron content in sample.....	23
CHAPTER IV EXPERIMENTS.....	26
4.1 Instruments and apparatus.....	26
4.1.1 Powder X-ray diffraction (XRD).....	26
4.1.2 Scanning electron microscopy and energy dispersive X-ray analysis (SEM-EDX).....	26
4.1.3 Fourier transform infrared (FTIR).....	26
4.1.4 Centrifuge.....	27
4.1.5 Oven and furnace.....	27
4.1.6 Atomic absorption spectroscopy (AAS).....	27
4.1.7 Nitrogen absorptometer.....	27
4.2 Chemicals.....	28
4.3 Synthesis of goethite.....	29
4.4 Synthesis of birnessite.....	29
4.4.1 Solid state method.....	29
4.4.2 Hydrothermal method.....	29
4.5 Synthesis of manganese-iron oxide composites.....	30
4.5.1 Physical mixture.....	30
4.5.2 Co-precipitation	30
4.5.3 Coating.....	31
4.5.4 Exfoliation-precipitation	31

	Page
4.6	Determination of iron content by redox titration..... 32
4.7	Adsorption experiment..... 33
CHAPTER V	RESULTS AND DISCUSSIONS..... 34
5.1	Synthesis and characterization of goethite (α -FeOOH)..... 34
5.1.1	X-ray diffraction (XRD)..... 34
5.1.2	Fourier transform infra-red spectrometer (FT-IR).... 35
5.2	Synthesis and characterization of birnessite..... 36
5.2.1	X-ray diffraction (XRD)..... 37
5.2.2	Fourier transform infra-red spectrometer (FT-IR).... 39
5.3	Synthesis of manganese-iron oxide composites..... 40
5.3.1	Physical mixtures..... 40
5.3.1.1	X-ray diffraction (XRD)..... 40
5.3.1.2	Fourier transform infra-red spectrometer (FT-IR)..... 42
5.3.2	Exfoliation-precipitation 43
5.3.2.1	X-ray diffraction (XRD)..... 43
5.3.2.2	Fourier transform infra-red spectrometer (FT-IR)..... 47
5.3.3	Coating 49
5.3.3.1	X-ray diffraction (XRD)..... 49
5.3.3.2	Fourier transform infra-red spectrometer (FT-IR)..... 51
5.3.4	Coprecipitation 52
5.3.4.1	X-ray diffraction (XRD)..... 52
5.3.4.2	Fourier transform infra-red spectrometer (FT-IR)..... 53

	Page
5.3.5 Structural and chemical properties comparison.....	54
5.3.5.1 X-ray diffraction (XRD).....	54
5.3.5.2 Fourier transform infra-red spectrometer (FT-IR).....	55
5.3.5.3 SEM-EDX.....	57
5.3.5.4 Determination of iron content in composite.....	59
5.3.5.5 N ₂ adsorption-desorption isotherms.....	61
5.4 Adsorption.....	62
5.4.1 Birnessite.....	62
5.4.2 Composites.....	63
5.5 Properties of NtEP composite.....	65
5.5.1 X-ray diffraction (XRD).....	65
5.5.2 Fourier transform infra-red spectrometer (FT-IR)....	66
5.5.3 Iron content in NtEP composite.....	67
5.5.4 Cu adsorption on NtEP composite.....	68
5.5.5 Pb adsorption on NtEP composite.....	69
5.5.6 Filtration quatity.....	71
CHAPTER VI CONCLUSIONS AND SUGGESTIONS.....	72
REFERENCES.....	74
APPENDICES.....	82
VITAE.....	90

LIST OF FIGURES

Figure	Page	
3.1	Illustration showing the adsorption of positively charged ions in solution to a negatively charged surface.....	12
3.2	Illustration of the iron oxyhydroxide structures.....	14
3.3	Examples of the chain/tunnel (todorokite, hollandite, and ramsdellite) and layer (birnessite) typed crystal structures of manganese oxides.....	15
3.4	Illustration of the birnessite structure with alkali metal cations (A^+) and water molecules in the interlayer region.....	16
3.5	Schematic representation of the intercalation, swelling, exfoliation, and reflocculation processes in layered structure compound.....	18
3.6	Diffraction of X-ray by a crystal.....	19
3.7	Crystal structure and interplanar spacing between atoms of birnessite.....	20
3.8	The IUPAC classification of adsorption isotherms.....	22
5.1	XRD patterns of goethite prepared by the hydrolysis of ferric chloride, using different precipitating agents: (a) KOH, (b) TBAOH, and (c) TMAOH.....	34
5.2	Infrared spectrum of synthetic goethite.....	36
5.3	XRD patterns of potassium birnessite via (a) hydrothermal and (c) solid state methods, and their proton birnessite (b), (d) respectively..	37
5.4	Infrared spectra of (a) $HMnO_2$ ss, (b) $HMnO_2$ ht, (c) $KMnO_2$ ss, and (d) $KMnO_2$ ht	39
5.5	XRD patterns of (a) $HMnO_2$ ht, the product from PS method: (b) PS 70% Fe, and (c) goethite	41

Figure	Page
5.6 Infrared spectra of (a) goethite, (b) PS 70% Fe, and (c) HMnO ₂ ht ...	42
5.7 XRD patterns of (a) HMnO ₂ ht, and its exfoliated products: (b) TBA-HMnO ₂ bottom and (c) TBA-HMnO ₂ top	44
5.8 Simple structural models for the TBA intercalated manganese oxide phase based on zero, and one layer of water. The large empty spheres represents TBA cations and the small gray sphere represents water products	45
5.9 XRD patterns of (a) HMnO ₂ ht, the product from EP method: (b) CIEP and (c) NtEP, (d) akaganeite, and (e) goethite	46
5.10 Infrared spectra of (a) HMnO ₂ ht, the product from EP method: (b) CIEP and (c) NtEP, (d) akaganeite, and (e) goethite	48
5.11 XRD patterns of (a) HMnO ₂ ht, the product from CT method: (b) CICT and (c) NtCT, (d) akaganeite, and (e) goethite	50
5.12 Infrared spectra of (a) HMnO ₂ ht, the product from CT method: (b) CICT and (c) NtCT, (d) akaganeite, and (e) goethite.....	51
5.13 XRD pattern of (a) goethite and the composite CP method: (b) CP 70% Fe.....	53
5.14 Infrared spectra of (a) goethite and the product from CP method: (b) CP 70% Fe.....	53
5.15 XRD patterns of Mn-FeO _x composites from EP method: (a) CIEP and (c) NtEP, CT method: (b) CICT and (d) NtCT, PS method: (e) PS 70% Fe, and CP method: (f) CP 70% Fe	55
5.16 Infrared spectra of Mn-FeO _x composite from CP method: (a) CP 70% Fe, EP method: (b) CIEP and (d) NtEP, CT method: (c) CICT and (e) NtCT, and PS method: (f) PS 70% Fe	56

Figure	Page
5.17 EDX mapping of Mn and Fe on Mn-FeO _x composites from PS method: (a) PS 70% Fe, EP method: (c) ClEP and (e) NtEP, CT method: (b) NtCT and (d) ClCT, and CP method: (f) CP 70% Fe.....	58
5.18 Calibration curve for iron content determination by redox titration....	60
5.19 XRD patterns of NtEP composites at different % wt Mn loading: (a) 5%, (b) 10%, (c) 20%, and (d) 30%.....	65
5.20 Infrared spectra of NtEP composites at different % wt Mn loading: (a) 0%, (b) 5%, (c) 10%, and (d) 20% and (e) 30%.....	66
5.21 Effect of birnessite loading on Cu ²⁺ ions adsorption onto NtEP composites	69
5.22 Effect of birnessite loading on Pb ²⁺ ions adsorption onto NtEP composites.....	70
A-1 N ₂ adsorption-desorption isotherm and pore sizes distribution of HMnO ₂ ht.....	83
A-2 N ₂ adsorption-desorption isotherm and pore sizes distribution of Goethite.....	84
A-3 N ₂ adsorption-desorption isotherm and pore sizes distribution of PS sample.....	85
A-4 N ₂ adsorption-desorption isotherm and pore sizes distribution of NtEP composite.....	86
A-5 N ₂ adsorption-desorption isotherm and pore sizes distribution of ClEP composite.....	87
A-6 N ₂ adsorption-desorption isotherm and pore sizes distribution of NtCT composite.....	88
A-7 N ₂ adsorption-desorption isotherm and pore sizes distribution of ClCT composite.....	89

LIST OF TABLES

Table		Page
2.1	Metal adsorption onto iron oxide surface reported from literature.....	5
2.2	Metal adsorption onto manganese oxide surface reported from literature.....	6
5.1	Crystallite sizes of α -FeOOH samples, as estimated by using the Scherrer method.....	35
5.2	d spacing of birnessite samples	38
5.3	Crystallite sizes of birnessite samples	39
5.4	Crystallite sizes of PS sample	41
5.5	d spacing of exfoliated birnessite samples.....	45
5.6	The result of phase analysis and crystallite sizes, as determined by the strongest line in XRD patterns, of EP composites	47
5.7	The result of phase analysis and crystallite sizes, as determined by the strongest line in XRD pattern, of CT composites	50
5.8	The result of phase analysis and crystallite sizes, as determined by the strongest line in XRD pattern, of all Mn-FeO _x composites.....	54
5.9	Iron contents in Mn-FeO _x composites.....	60
5.10	Specific surface area and pore size distribution for birnessite, goethite and various Mn-FeO _x composites	61
5.11	The adsorption capacities of Cu ²⁺ ions onto birnessite samples	63
5.12	Iron contents, Cu adsorption capacities, and specific surface areas for birnessite, goethite and various Mn-FeO _x composites	64
5.13	Iron contents in PS samples using permanganate titration	67
5.14	Iron contents in NtEP samples using permanganate titration	68
5.15	Adsorption capacities of Cu ²⁺ ions onto PS samples	68
5.16	Adsorption capacities of Cu ²⁺ ions onto NtEP samples	68

LIST OF ABBREVIATIONS

Å	=	Angstrom unit
AAS	=	Atomic absorption spectroscopy
BET	=	Brunauer-Emmett-Teller
°C	=	Degree celsius
cm ⁻¹	=	Unit of wave number
CT	=	Coating
CP	=	Coprecipitation
EDX	=	Energy dispersive X-ray analysis
EP	=	Exfoliation-Precipitation
FeOOH	=	Iron oxyhydroxide
FT-IR	=	Fourier transform infrared spectroscopy
HMnO ₂	=	H-birnessite
ht	=	hydrothermal
KMnO ₂	=	K-birnessite
PS	=	Physical mixture
SEM	=	Scanning electron microscope
ss	=	Solid state
TBAOH	=	Tetrabutylammonium hydroxide
TMAOH	=	Tetramethylammonium hydroxide
XRD	=	X-ray diffraction

CHAPTER I

INTRODUCTION

1.1 Background

Water is needed for all life on earth. It may seem that we have it in abundance with two thirds of the planet covered by oceans. Unfortunately, in recent years, contamination of ground and surface water with heavy metals is becoming a major concern. Local industries such as batteries manufacturing, printing, ceramic, coatings for iron and steel industries use heavy metals in the processing of raw materials, and consequently discharge of such metals into sources of drinking water. Lead, cadmium, copper and zinc are regarded as major contaminants. These heavy metals are not biodegradable and tend to accumulate in living organisms causing various diseases and disorder. Within literatures, many treatment processes have been proposed for the removal of heavy metals [1-4]. Chemical precipitation, membrane filtration, ion exchange and adsorption are some of the most commonly used methods for the treatments. Adsorption is often the last stage of water treatment section because it is more effective when concentration is low. The material most used as adsorbent is activated carbon (AC) [5-7]. It is made from peat, wood, coal or synthetic high polymer by heating them under controlled conditions, however, the use of AC is not suitable in developing countries due to the high cost associated with the production and regeneration of spent carbon [8]. Due to the problems mentioned above, the use of alternative materials as potential sorbent for the removal of heavy metals has been growing interested. Attention has been focused on the various adsorbents which range from industrial by-product or waste to natural and synthetic materials such as clay, zeolite, manganese oxide, iron oxide and sand particles [9-12].

Iron oxides are abundant in soil and water environments. In comparison with other minerals existing in soil, they have relatively high surface areas and surface charges, and they often regulate free metal concentrations in soil through adsorption reactions. Many researchers have studied the adsorption characteristics of anions

[13-15], cations [16-20], and organics [21-22] onto the iron oxide surface such as ferrihydrite, hematite, goethite and magnetite at different candidates of pH, metal ion, solid/liquid ratio and temperature. Their adsorption is capable of removing metals over a wider pH range with high affinity. Among these iron oxides, goethite most efficient, therefore it is chosen as a representative iron oxide phase in this thesis. However, most high surface area iron oxides are available only as fine powders or are generated in aqueous suspension as hydroxide gel. In such forms, these oxides retain their desirable adsorptive properties for trace metals but are limited to reactor configurations incorporating large sedimentation basins or filtration units, which causes solid/liquid separation to become fairly difficult. Furthermore, iron oxides alone are not suitable as a filter medium because of its fine particles. Recently, several researchers have developed techniques for coating iron oxide onto the surface of sand to overcome the problem of using iron oxide powders in water treatment [23-28]. Iron oxide-coated sand has been tested for removal of heavy metals from synthetic and real waste. The results from these studies confirm that the utilization of iron oxide-coated sand for trace element removal from water is worth developing.

Besides, the increase of the sorption efficiency and potential for separation of heavy metal from aqueous solution, organic and/or inorganic coatings such as manganese oxides have been studied for a variety of metal-bearing wastewaters [29-32]. Lee et al. showed that manganese-coated sand is effective for removing copper ion from synthetic wastewater in a liquid fluidized-bed reactor [29]. Hu et al. also reported that manganese-coated sand is potential for removal of Mn^{2+} from raw water and suitable for application as a packed bed for engineering design [30]. Khraishes et al. prepared the impregnation of diatomite surface with manganese oxide that resulted in high removal efficiency of Cu^{2+} , Pb^{2+} , and Cd^{2+} ions from aqueous solutions [31]. Liu et al. found manganese oxide coated cementitious media provided surface characteristics that can significantly enhance adsorption of heavy metal in storm water, in comparison to manganese oxide coated sand [32]. In natural soils, manganese oxides are often associated with large amounts of iron oxide. A number of studies showed that accumulations manganese oxides have shown an affinity for heavy metals, including Pb^{2+} , Cu^{2+} , Cd^{2+} , and Zn^{2+} [33-34]. The negative charge on the structure, high surface area and exchange capacities of manganese oxide give it the capability to attract metal ions.

Although iron or manganese oxide coated media may offer potential for heavy metal removal, no manganese and iron oxide combination related research has been carried out. Therefore, the aim of this study is to prepare iron and manganese oxide composites used as adsorbents for the removal of heavy metal ions with a high adsorption capacity and good filtration quality. The method for synthesis is an alternative route for the preparation of composite, calling the exfoliation-precipitation process. Because the exfoliated or delaminated inorganic sheets have a higher degree of freedom than the stacked sheets, they are potentially used as the precursors for new materials, especially the high surface products. For example, Choy et al. showed hybridizing the exfoliated titanate with the anatase TiO_2 nanosol with enhanced photocatalytic activity [35]. Kooli et al. found that alumina-pillared titanates, prepared through exfoliation process, showed the presence of Bronsted and Lewis acid sites [36]. Ooi et al. prepared polycation intercalated layered manganese oxide nanocomposite with a higher stability against extraction by acid treatment [37]. Sasaki et al. found multilayered films of manganese oxide nanosheets and aluminum polyoxocations provide a new potentially electrodes for electrochemical applications [38].

1.2 Objectives

In the present study, there are four objectives. The first objective is to develop method for combined manganese oxide and iron oxide phases by exfoliation-precipitation method to generate new oxide composites with a higher specific surface area. The second objective is to characterize the physical structure of synthetic manganese-iron oxide composites using the fundamental analytical techniques, including scanning electron microscopy, energy dispersive X-ray analysis, specific surface area, fourier transform infra-red spectroscopy and powder X-ray diffraction. The third objective is to evaluate the different adsorption capacity for copper and lead through batch scale adsorption experiments at pH about 5.5 between the single and combined oxide phases. The fourth objective is to compare the filtration quality of obtained composites and goethite. The goal of this study is to prepare new manganese-iron oxide composites by potentially exfoliation-precipitation method, which disperses manganese oxide within iron oxide particles, for the removal of heavy metal with a high adsorption capacity and good filtration quality.

1.3 Approach and thesis outline

In this thesis we investigate the adsorption of heavy metals to several MnO_x - FeO_x composite, H-birnessite and iron oxyhydroxide. This thesis is divided into six chapters. Introduction of this work is described in the first chapter. Reviews of literature and theory data are summarized in chapter II and III, respectively. Chapter IV focuses on the procedures and instruments. Next, details and discussion over obtained results are presented in chapter V. Finally, in chapter VI the concluding remark and suggestion for further work can be found.



สถาบันวิทยบริการ
จุฬาลงกรณ์มหาวิทยาลัย

CHAPTER II

LITERATURE REVIEWS

2.1 Adsorption of cations on manganese oxide and iron oxide

Many researchers have studied the adsorption characteristics of Pb^{2+} , Cu^{2+} , Cd^{2+} , and Zn^{2+} ions onto the iron oxide and manganese oxide. Their adsorption is capable of removing metals over a wider pH range with high affinity. It is given by the surface charge on structure, and the relatively high surface area. For removal studies, the adsorption capacity of heavy metal ions on iron oxide and/or manganese oxide surface is summarized in Table 2.1.

Table 2.1 Metal cation adsorption onto iron oxide surface reported from literature.

Ref.	Oxide phases	Surface area (m^2/g)	Adsorbate	pH	sorption capacity ($mmol/g$)
[16]	goethite	20	Cu	4.7	0.042
			Cd	5.1	0.053
	lepidocrocite	70-80	Cu	5.5	0.048
			Cd	5.5	0.022
[39]	goethite	-	Cu	4	0.040
			Zn	4	0.010
[40]	goethite	55	Zn	6.5	0.016
			Pb	5.5	0.007
[41]	goethite	33	Cu	5.5	0.114
[42]	goethite	27	Zn	7	0.022
			Ni	7	0.130

Table 2.2 Metal cation adsorption onto manganese oxide surface reported from literature.

Ref.	Oxide phases	Surface area (m ² /g)	Adsorbate	pH	sorption capacity (mmol/g)
[12]	δ -MnO ₂ (amorphous)	-	Cu	6.05	0.760
			Ni	6.05	0.361
			Zn	6.05	0.665
[43]	δ -MnO ₂	-	Cu	7.25	0.577
[44]	δ -MnO ₂	-	Cu	5	0.720
			Zn	5	0.600
[45]	δ -MnO ₂	175	Zn	5.5	0.535

2.2 Adsorption of cations on modified surface oxide

The preparation, characterization, and sorption properties of single oxide phases have been the topic of several literatures. In recent years, some researchers have developed the techniques for coating iron oxide or manganese oxide on media surface such as sand for the treatment of heavy metal in water.

Lai et al. [46] prepared iron oxide-coated sand by hydrolysis of ferric nitrate in the presence of sand. The characterization by XRD was found that the crystalline phases of sand and iron oxide in coating were identified as quartz and goethite, respectively. BET and SEM analysis were used to investigate the surface properties of the coated sand. This result indicated that the iron-coated sand had a higher specific surface area than the uncoated sand because of the attachment of iron oxide. Equilibrium adsorption studies (pH 6 and initial concentration 62.43 mg/l of Cu) demonstrated that the adsorbed density of copper per mass of sand is 220 μ g Cu/g sand. The regeneration of the iron-coated sand could be achieved by soaking with acid solution of pH 3. Besides, the result of EDX analysis showed that copper was spread over the surface of iron oxide-coated sand.

Hu et al. [30] collected manganese oxide-coated sand from commercial product W-32. It was prepared under acidic conditions by impregnation process. XRD analysis showed that the pattern of sand turned out to be quartz. The mineral

constituents of manganese oxide coating were verified as corresponding to pyrolusite (MnO_2), $\gamma\text{-Mn}_2\text{O}_3$, and $\text{Mn}(\text{OH})_4$. The surface properties were analyzed by using gas adsorption porosimetry, SEM, and EDX. They were found that the manganese oxide-coated sand had high specific surface area, owing to attachment of manganese oxide. The removal study of Mn^{2+} ion from water by this sample was found to be the adsorption capacity (0.38 mg Mn/ g sample) for pH value of 5 at room temperature. In addition, the adsorption capacity was raised as the temperature increased. Furthermore, the regeneration of manganese-coated sand could be achieved by soaking in the solution of $\text{pH} < 2.0$.

Henric et al. [47] prepared and characterized the combined phases of iron oxyhydroxide and montmorillonite. Two different preparation procedures were employed. In the first method, Fe(III) was in contact with montmorillonite at pH 2.5. A coating of ferrihydrite on montmorillonite surface was created by slowly raising pH to 8.0 (Fe–mont). The characterization by TEM was found that Fe–mont appeared much like the pattern of pure montmorillonite and ferrihydrite. Moreover, the obtained product had the higher specific surface area and higher sorption capacity for Ni^{2+} ion (per g Fe) compared to the pure solids. In the second method, the oxygen was bubbled through the aqueous solution (pH 7.0) of Fe(II) ion in the presence of montmorillonite. This resulting precipitate is comprised of the predominant separated phases of lepidocrocite ($\gamma\text{-FeOOH}$) and montmorillonite. Its specific surface area and sorption data were higher than the mixture of both pure phases.

Axe et al. [48] investigated the formation and surface properties of manganese oxide in the presence of clay. Under the heterogeneous systems, amorphous hydrous manganese oxide (HMO) and crystalline manganese oxides such as birnessite and pyrolusite were coated on montmorillonite surface through a reduction and/or oxidation method. The presence of montmorillonite substrate potentially inhibited not only the crystallization of pyrolusite coating but also the formation of crystalline birnessite. Surface area of the coated systems increased while the pore size distribution decreased as compared to the external surface area and pores of montmorillonite. For both HMO- and birnessite-coated montmorillonite, the overall of systems were consistent with their discrete oxide counterparts. Moreover, the XAS

studies also suggested that the local structure of Mn in the HMO coating was similar to that in the discrete phase.

Khraishes et al. [31] modified the surface of diatomite (72% SiO₂) with manganese oxide so called Mn-diatomite, and examined its removal of Pb²⁺, Cu²⁺, and Cd²⁺ ions from wastewater. The modifying manganese oxide phases was birnessite, characterized by SEM. Adsorption studies demonstrated that diatomite and Mn-diatomite were the effective adsorbents for removal of metal ions at pH 4. The adsorption capacities for diatomite were 24.9, 27.6 and 16.1 mg/g adsorbent for Pb, Cu and Cd, respectively, while the values of 99.0, 57.6 and 27.9 mg/g adsorbent were obtained for Mn-diatomite. This improvement in diatomite performance was attributed to an increase in surface area after coating, as well as the resulting surface charge due to the formation of birnessite on the diatomite surface. Furthermore, this modification resulted in significantly improve of the filtration quality of diatomite.

Lee et al. [29] intended to remove Cu²⁺ ion from wastewater by using a fluidized-bed reactor (FBR) filled with manganese-coated sand (MCS) as adsorbent. It was found that the removal efficiency was highly dependent on pH. The capacity increased with increasing pH from 2 to 8. In addition, it reached 0.97 Cu mg/ g MCS at pH 6.

Axe and Xu [28] focused on the synthesis and characterization of iron oxide-coated silica. Two different synthetic methods, a modified adsorption and a modified precipitation, were employed. Goethite coatings on silica surface were observed to be non-uniform. A band shift and new band from FT-IR suggested that the goethite-silica interaction might involve with chemical forces. Besides, deposited goethite was composed of nanometer sized crystals, resulting in the increase of surface area and the change of surface charge distribution of silica. Ni²⁺ ion adsorption on the coated silica was greater than that for pure silica.

Benjamin et al. [49] synthesized iron oxide-coated sand (IOCS) by two methods. Both types of IOCS were coated in two rounds. In the first round, hematite (α -Fe₂O₃) was coated on the sand grains. In the second round, the obtained sample was mixed with a solution of ferric nitrate (IOCS-1) or ferric chloride (IOCS-2) and

precipitated with NaOH. IOCS samples were used for removal of various cations from simulated and actual waste streams. Compared to sand, both IOCS samples had dramatically increased surface area, and significantly greater tendency to adsorb both cationic and anionic metals.

Al-Sewailem et al. [50] prepared iron oxide-coated sand by coating partially hydroxylated ferric hydroxides on sand particles. The different fractions of iron oxide coating derived from various OH/Fe molar ratios of 1.00, 1.50, 2.00, and 2.84. Adsorption studies showed that the amount of adsorbed Cu^{2+} ion was higher for ferric hydroxide coated sand than for the uncoated one. Considering the effect of OH/Fe molar ratio, the higher of OH/Fe of ferric sols resulted in the lower of Cu adsorption capacity. This could suggest that ferric oxide polymers with higher OH/Fe ratio tended to have bigger particles than those with lower OH/Fe ratios. Therefore, the average size of particles increased with increasing OH/Fe ratio.

Liu et al. [32] developed the method for coating manganese oxide onto sand and cementitious media surfaces. Manganese oxide coating method (MOC) was used to prepare coating surface of dry media in a reaction column. Crystal morphology analysis indicated that the manganese oxide of MOC method was mainly ramsdellite. In case of birnessite coating method (BCM), a procedure was modified for the precipitation of colloidal birnessite on the media surfaces. The manganese oxide phase of BCM was the mixture of birnessite and cryptomelane. Both MOC and BCM samples had a significantly rougher surface than plain media resulting to the much larger specific surface area.

2.3 Synthesis route for modification surface oxide

The delamination or exfoliation of layered compound is used as a suitable starting material for the preparation of nanocomposites. The layered host undergoes exfoliation upon interaction with bulky guests, for example, quaternary ammonium ions. The obtained unilamellar crystallites can be described as nanosheets. The colloidal nanosheets undergo flocculation to form a restacking product by changing the ionic strength or pH of suspensions. In addition, the restacking sequence is usually disordered, resulting to the increase in surface area of host materials.

Ooi et al. [37] synthesized diallyldimethylammonium chloride, PDDA, incorporated between birnessite sheets by a delamination/reassembling process. Delamination of birnessite was obtained by mixing with an aqueous solution of tetramethylammonium hydroxide (TMAOH) for 7 days at room temperature. The amount of TMAOH added was 25-folds that of the exchangeable capacity of H-birnessite. The combination of delaminated birnessite and aqueous solution of PDDA resulted to the reassembling of composites. The prepared product was comprised of the PDDA polymer existing in a polycation form. The expansion of interlayer distance depended on the amount of intercalated PDDA. Moreover, this nanocomposite had a higher stability against to extraction acid treatment, probably due to the strong electrostatic attraction between birnessite sheets and PDDA chains.

Sasaki et al. [51] prepared colloidal perovskite nanosheets of $[\text{Ca}_2\text{Nb}_3\text{O}_{10}]$ by mixing the perovskite in an aqueous solution of tetrabutylammonium hydroxide (TBAOH). Then, perovskite nanosheets were loaded with Pt before flocculation with alkali metal ions. This exfoliation-restacking process resulted in porous aggregates of fine crystallites with high specific surface areas compared to the original layered perovskite. The aggregates showed high photocatalytic activity for hydrogen gas generation from an aqueous methanol solution.

Vicente et al. [52] studied the NO_x reduction with propene over Fe-saponite clay catalysts. The catalysts were prepared by mixing the clay suspension in water with polymerised Fe solutions. The samples showed significant activity in the NO_x reduction in the absence of oxygen with a maximum activity for Fe content close to 10 wt.%.

Choy et al. [35] prepared a new microporous TiO_2 -pillared layered titanate by hybridizing the exfoliated titanate with anatase TiO_2 nanosol. The colloidal nanosheet was obtained by intercalating tetrabutylamine into the layered titanate. The exfoliated titanate was mixed with the monodispersed anatase TiO_2 nanosol solution. It was found that the TiO_2 -pillared layered titanate showed the high surface area of $460 \text{ m}^2/\text{g}$, and the pore size of 0.95 nm, indicating the formation of microporous pillar structure. Its photocatalytic activity increased as compare to the parent titanate.

Sasaki et al. [36] studied the porosity and acidity of alumina-pillared titanates. A layered titanate had been exfoliated by TBA cations, followed by subsequent restacking with aluminum-polyoxocations (Al_{13} cations). The pillared structure of these materials was found to be stable up to 500 °C without changing of layered structure. In addition, it showed the presence of lewis acid sites, and Brønsted acid sites upon incorporation of the alumina pillars.

Sasaki et al. [53] synthesized a mesoporous alumina-pillared titanate with the large basal spacing of 2.6 nm. Pillared compound was achieved by exfoliation of layered titanate and subsequent restacking in the presence of Al_{13} cations. Heat treatment at 500°C resulted in the mesoporous product with specific surface area of 300 m^2/g and the predominant pores diameter of 4.0 nm. The acidity of obtained product was *ca.* 0.60 mmol of proton/g, which enhanced in comparison to that of the parent titanate.

Sasaki et al. [54] prepared a layered Li-Mn-oxide via flocculation of delaminated manganese oxide nanosheets with Li ions. The restacked product produced a lamellar material with the basal spacing of 7.2 Å. Its specific surface area (65 m^2/g) was significantly higher than that of its parent material (2 m^2/g). A dehydrated sample of layered Li-Mn-oxide underwent electrochemical Li^+ insertion/extraction, which showed its smooth cycling curves as a cathode material.

Feng et al. [55] prepared and characterized a mixed compound of $\text{Ni}(\text{OH})_2$ and manganese oxide with a high nickel contents. Birnessite was exfoliated in TMAOH solution into colloidal nanosheets and then restacked with Ni ions. The electrochemical properties of samples were dependent on the chemical composition and oxidation states of Ni and Mn.

Sasaki et al. [38] prepared inorganic multilayer films of manganese oxide nanosheets and Al_{13} cations. Multilayer films were fabricated by sequential deposition of Al_{13} cations and MnO_2 nanosheets onto a substrate. MnO_2 nanosheets in the multilayer films predominantly underwent electrochemical redox processes of $\text{Mn}^{\text{III}}/\text{Mn}^{\text{IV}}$, giving very stable voltammogram cycling.

CHAPTER III

THEORY

3.1 Adsorption of metal onto mineral surfaces

Adsorption is the removal of a metal from solution by the electrostatic forces of a mineral surface, forming a mono-molecular layer on the mineral surface [56]. It is well known that metal solutes exhibit a charge when dissolved in a solution and like these dissolved species, mineral surfaces may also exhibit charge properties. Therefore, if a dissolved ion approaches within a given distance of a mineral surface, it may be attracted to and stuck on the mineral surface (Figure 3.1).

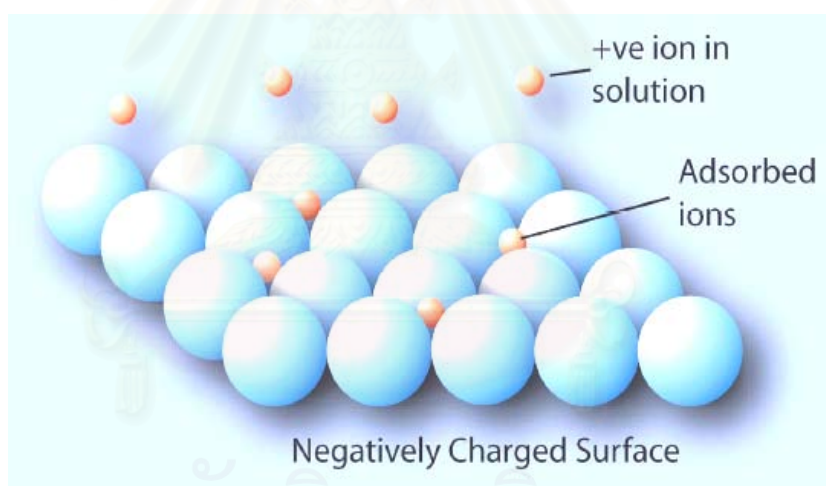


Figure 3.1 Illustration showing the adsorption of positively charged ions in solution to a negatively charged surface [56].

There are three major factors that must be considered when examining the adsorption of metals onto mineral surfaces *i.e.* type of mineral and its surface properties, metal species in solution, and a chemistry of the surrounding solution. Each of these components plays an important part in determining the adsorptive capacity of a system.

3.2 Mineral properties

There are a number of important properties that make minerals ideal for adsorbing metals, but two of the more important factors are surface area or site density and charge properties. Other factors that control adsorption, such as crystal morphology, chemical composition and particle size distribution, are not described here. The ability of a mineral to adsorb metals is strongly dependent upon the surface area per unit mass of the mineral. Minerals with a high surface area are able to adsorb higher concentrations of metals. Whereas the charge properties of mineral are determined the effectively adsorbed metal ions from solution.

Most mineral surfaces have one of two main surface charge types, either a permanent structural charge or a non-permanent surface charge [57]. Minerals with a permanent structural charge normally obtain a charge due to the isomorphous substitution of elements in their structure. For example, Al^{3+} is substituted by Si^{4+} in smectite clay, creating a net positive charge due to the surplus of protons. The opposite may also occur if Al^{3+} site is occupied with Mg^{2+} , producing a surplus of electrons and a net negative charge. In general, the adsorption property minerals that have a permanent structural charge is not affected by changes in pH. On the other hand, minerals with a non-permanent surface charge acquire their charges based on surface hydroxyl reactions, as a result, they are highly dependent on pH. In solutions with a low pH, charge is predominantly positive due to adsorption of protons from solution and consequently the anion exchange capacity is high. When the pH of the solution is increased, the charge becomes negative due to the adsorption of OH^- or loss of H^+ , producing cation exchange capacity.

Examples of non-permanently charged minerals include iron oxides and oxyhydroxides such as ferrihydrite, goethite and hematite [58]. Manganese (oxyhydr)oxides are also important non-permanently charged mineral commonly found in natural environment. Goethite is the most commonly mineral used for adsorption studies due to its ideal adsorption properties and high abundance in natural systems.

3.3 Structural features of iron oxyhydroxides

Iron oxyhydroxides (FeOOH) has several polymorphs as seen in Figure 3.2. The chemical and physical conditions of the soil environment determine which polymorph will form.

Goethite (α -FeOOH) is the most common iron oxide in soils. The goethite crystal structure consists of double rows of $\text{FeO}_3(\text{OH})_3$ octahedra, which share edges and corners to form 2x1 octahedra tunnels partially bonds by hydrogen bonds.

Akaganeite (β -FeOOH) has a crystal structure containing double chains of edge-linked $\text{FeO}_3(\text{OH})_3$ octahedra that share corners to form large 2x2 octahedra tunnels framework. The tunnels are partially filled with Cl^- ions. It has been pointed out that large ions, such as chloride, are necessary for the formation of this tunnel structure. Thus, akaganeite is often observed as a corrosion product of iron in marine (i.e. chloride containing environment).

Lepidocrocite (γ -FeOOH) is a relatively uncommon mineral and appears to form only from the relatively rapid oxidation of Fe^{2+} . Its structure is comprised of layers of FeO_6 octahedra linked by hydrogen bond.

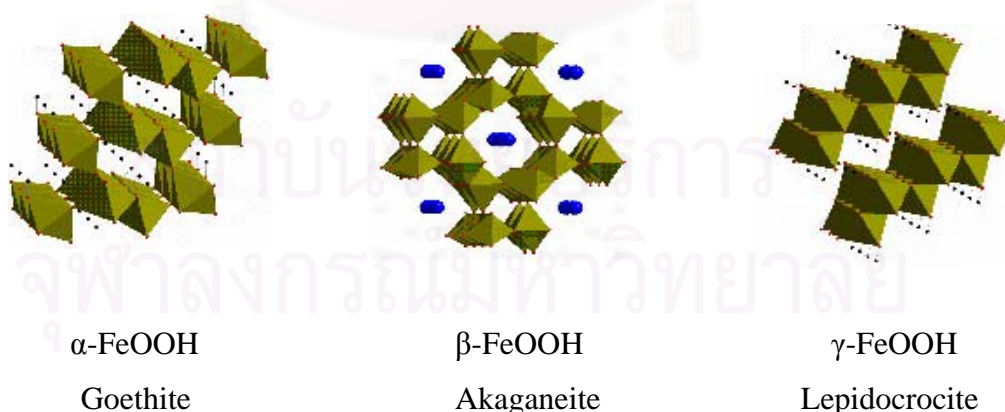


Figure 3.2 Illustration of the iron oxyhydroxide structures [59].

Iron oxyhydroxides are often highly hydrated, and usually have very high specific surface areas. They play a major role in the retention of anions, and trace

elements such as Cu, Pb, Zn, Co, Cr, and Ni. Especially, goethite has been shown never both adsorption properties towards Cu and Zn ions [41-42].

3.4 Structural features of manganese oxide

The manganese (IV) oxides and the mixed manganese (III,IV) (hydroxy)-oxides are termed manganates [57]. Manganates have characteristically open crystal structures, large surface areas with high negative charges, and exchangeable charge-balancing cations. The basic unit of most manganese oxide minerals is the MnO_6 octahedron, which is generally arranged into either layer structures or chain/tunnel structures. The tunnel structures have single, double, or triple chains of edge-sharing MnO_6 octahedra in which the chains share corners to form tunnels of square or rectangular cross section (Figure 3.3). The layered manganese oxide consists of stacks of sheets, or layers, of edge-sharing MnO_6 octahedra.

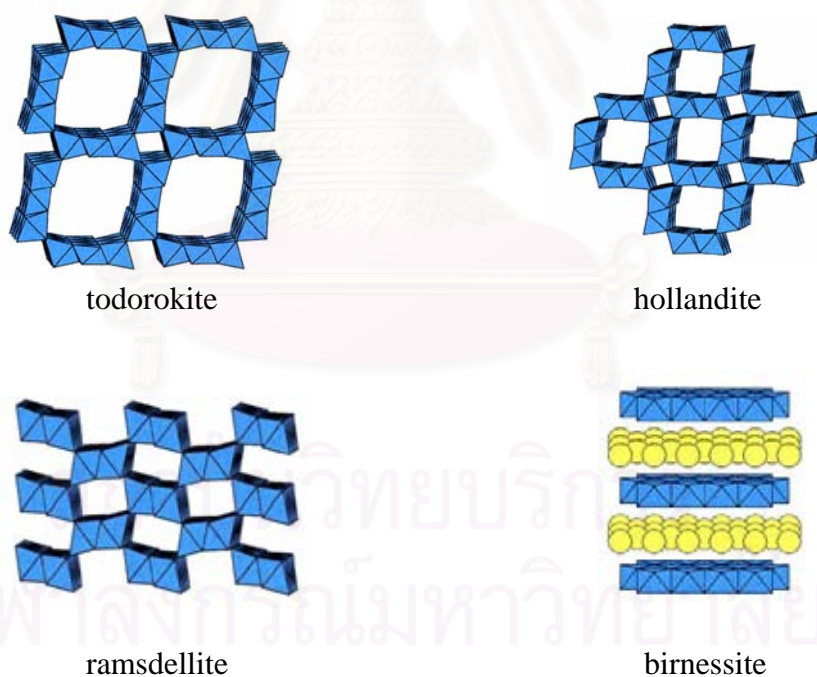


Figure 3.3 Examples of the chain/tunnel (todorokite, hollandite, and ramsdellite) and layer (birnessite) typed crystal structures of manganese oxides [60].

3.4.1 Structural features of birnessite

The interesting thing about manganese oxide structures is that they have cavities and tunnels. These cavities and tunnels allow the penetration of water and cations into their frameworks. Birnessite is a common manganese oxide mineral, existing in a variety of geological settings. It is also a significant component of soil and involved in ion-exchange processes and redox reactions related to groundwater chemistry.

Birnessite has a two-dimensional structure that consists of edge-shared MnO_6 octahedra forming the layers, as depicted in Figure 3.4 [61]. Various cations and water molecules are incorporated into the interlayer region between the octahedral sheets such that the distance between sheets is affected by the number of water layers and by the size of counter ion. The interlayer distance in birnessite is typically 7 \AA , but further hydration can increase this spacing to produce a closely related 10 \AA , called busserite. A dehydrated form of birnessite with a layer spacing of about $5.5 - 5.6 \text{ \AA}$ has also been identified.

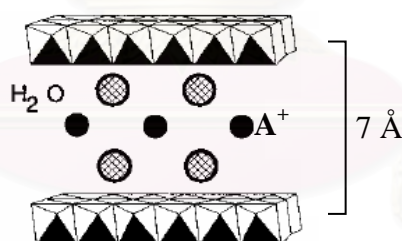


Figure 3.4 Illustration of the birnessite structure with alkali metal cations (A^+) and water molecules in the interlayer region [61].

Although the exact formula of layered manganese oxide varies depending on the reaction conditions employed. The A-birnessite is generally expressed as $\text{A}_x\text{MnO}_{2-y} \cdot z(\text{H}_2\text{O})$, in which A typically represents an alkali metal cation, $x = 0.2-0.7$, $y = -0.16-0.16$, and $z = 0.4-0.8$. The average oxidation state of the mixed valence manganese normally falls between 3.6 and 3.8, which represents a predominance of Mn(IV) with minor amounts of Mn(III).

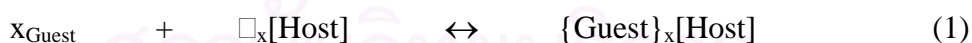
3.4.2 Properties of birnessite

It is known about the amount of permanent charge produced by isomorphous substitutions. In case of birnessite, this charge induces by the replacement of Mn^{4+} with Mn^{3+} in octahedral layers, but it is assumed to be small. However, the porous structures of layered birnessite are suitable locations for exchangeable cations to balance permanent charges that might result from such substitutions.

In addition, the hydrated layer structure of birnessite allows for facile mobility of the interlayer cations with a little structural rearrangement. The structural flexibility of the layer structures, with their ability to adapt to the geometry of the inserted guest species by free adjustment of the interlayer separation, is presumably responsible for the occurrence of intercalation compounds for this structure type. Consequently, this result makes it an attractive candidate for the ion-exchanged, intercalation, and exfoliation applications.

3.4.2.1 Intercalation

Intercalation reaction, generally reversible, involves the introduction of a guest species into a host structure without a major structural modification of the host materials [62]. In this research, intercalation refers to the insertion of a guest into a two-dimensional host structures. The reaction can be generalized by equation (1).



Intercalation is typically involved breaking interaction in the host structure and the forming new interaction between the guest and host. The final product of this reaction has a host structure, which is slightly expanded in the direction perpendicular to the layers. Layered host lattice that have stronger interlayer bonding appear to be more difficult for intercalation process.

3.4.2.2 Swelling, exfoliation/delamination and reflocculation

Intercalation of guest molecules brings about the increase in the basal spacing, which depends on the host structure as well as the nature of guest species. Expansion of the interlayer involving the intercalation of a solvent is called swelling, as shown in Figure 3.5. The interlayer distance expands in a stepwise fashion, as the number of molecular layers of water increase.

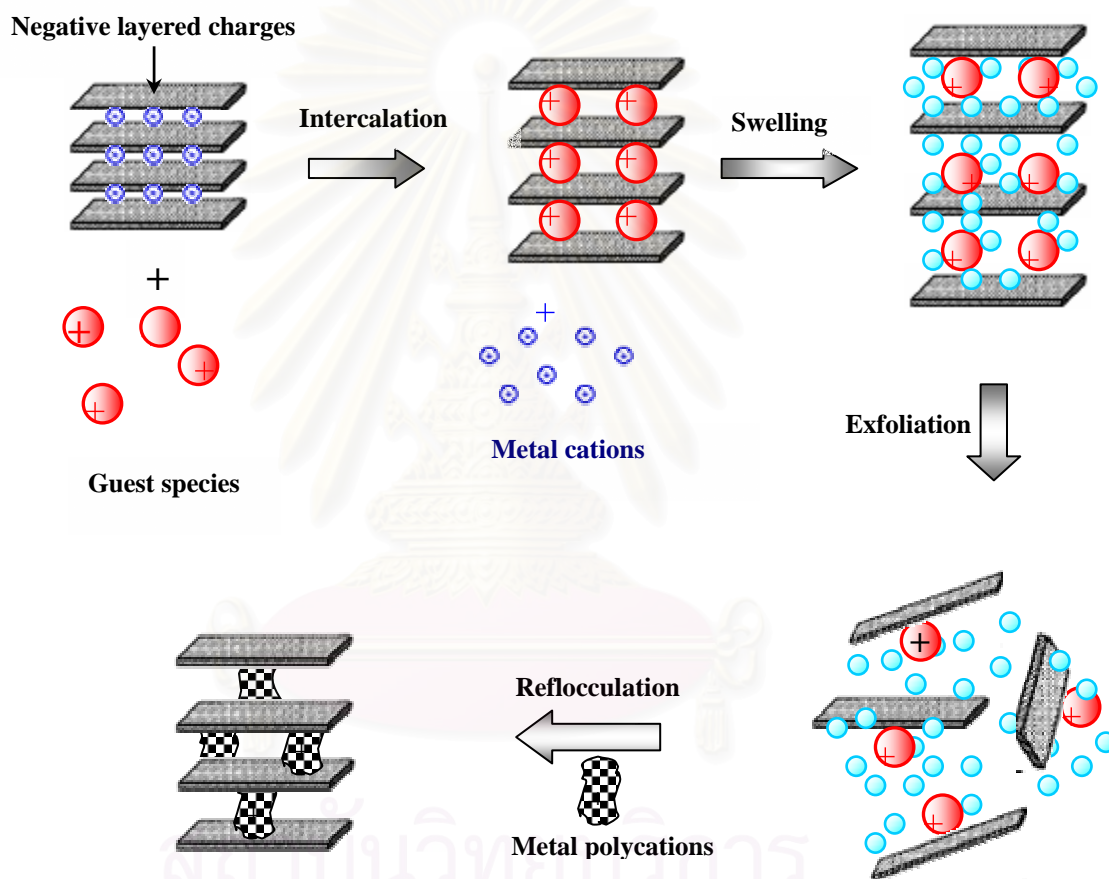


Figure 3.5 Schematic representation of the intercalation, swelling, exfoliation, and reflocculation processes in layered structure compound.

In addition to swelling, the high activation energies associated with the deformation of a layer to accommodate the incoming guests can be largely overcome to the point where the interlayer spacing is comparable to the diameter of the reactant molecule. If this process is taken to its extreme, then the host structure is completely dispersed or exfoliated (Figure 3.5). The delamination (exfoliation) of layered oxides

into their elementary host sheets is typically observed for some of the clay minerals such as montmorillonite and smectite and other layered compound such as birnessite and titanate [53-55].

The delaminated colloidal nanosheets have attracted much attention due to their unique chemical and physical properties distinctive from those in the stacked state. From the fundamental standpoint, they are expected to function as precursors for preparing mesoporous materials.

The colloidal dispersions can be reflocculate or restructure the layers by addition of electrolyte solution of other cations (Figure 3.5). The resulting products consisting of a restacked nanosheets often exhibit a disordered layered structure involving irregular orientation and lateral displacement of the nanosheets.

3.5 Characterization of materials

Measurements for obtained composites are divided into two major parts, in which physical measurement characterizes the structure of the material, while chemical measurement determines the iron content in samples.

3.5.1 Powder X-ray diffraction (XRD)

X-ray diffraction (XRD) is a non-destructive analytical tool for characterization of crystalline materials. XRD is a technique in which a collimated beam of nearly monochromatic X-rays is directed onto the flat surface of a relatively thin layer of finely ground material. Figure 3.6 shows a monochromatic beam of X-ray incident on the surface of crystal at an angle θ . The scattered intensity can be measured as a function of scattering angle 2θ . The resulting XRD pattern efficiently determines the different phases present in the sample.

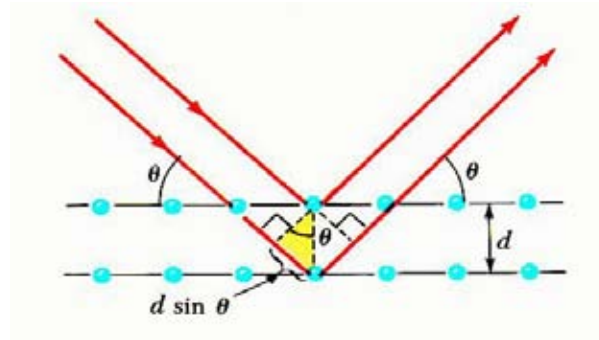


Figure 3.6 Diffraction of X-ray by a crystal [63].

Using this method, Bragg's law are able to determine the interplanar spacing of birnessite studied in this thesis, from diffraction peak according to Bragg angle.

$$n\lambda = 2 d \sin\theta \quad (2)$$

Where d is the distance between equivalent atomic planes, θ is the angle between the incident beam and these planes, n is an integer and λ is the wavelength. The crystal structure of birnessite is shown in figure 3.7. Focusing on the layered structure of the incident beam the set of d_{00l} values is observed from calculating their corresponding peak angle, where $00l$ is the Miller indices of the measured planes. The $d_{\text{basal spacing}}$ which is the spacing of the crystal planes is obtained from the below equation.

$$d_{\text{basal spacing}} = d_{001} = 2 \times d_{002} = 3 \times d_{003} = 1 \times d_{001} \quad (3)$$

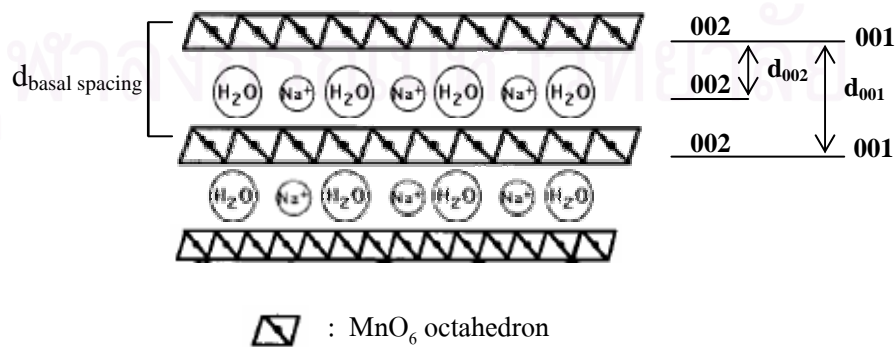


Figure 3.7 Crystal structure and interplanar spacing between atoms of birnessite.

The study of intercalation and exfoliation processes in birnessite has been investigated by monitoring basal spacing changes in the structure.

A characteristic of layered compound is that size of their coherent scattering domains is typically small and there are imperfections or stacking defects between adjacent domains. The result of numerous stacking faults or small domain sizes is known as particle size broadening and can be inferred from the peak widths. Peak widths are measured by their full widths at maximum half-height (FWMH). Under certain conditions the FWMH can be used to estimate the distribution of particle sizes.

This is expressed by the Scherrer equation, which assumes all reflections along a line normal to the reflecting plane.

$$L = \lambda K / \beta \cos\theta \quad (4)$$

Where L is mean crystallite dimension (\AA). K is the shape factor, which typically has a value of about 0.9. β is the FWMH of the peak in radians of 2θ .

3.5.2 Scanning electron microscopy and energy dispersive X-ray analysis (SEM-EDX)

Scanning electron microscope combined energy dispersive X-Ray analysis, (SEM-EDX), is a suitable instrument in order to investigate the relationship between the physical and chemical structure of the composite samples.

The basic function of SEM is to produce a highly magnified image of three-dimensional appearance, derived from the action of an electron beam scanning across the surface of a specimen. The size and shape of features on the surface of solid bulk samples can be examined. The SEM can have a magnification range of between ten to several hundred thousand, the higher magnification range being limited only by image resolution.

An additional feature of SEM is the ability to derive chemical information of the samples through the use of EDX. The technique of EDX makes use of the fact that

X-rays are produced whenever an electron beam interacts with matter, as in the SEM, and can be used to provide information about the elemental composition of samples. On bombardment of a sample with an electron beam in vacua, the amount of energy released by excited electrons in the sample is characteristic of the atomic number of the element exposed to the beam. The method is a non-destructive technique.

3.5.3 Nitrogen adsorption-desorption isotherm

The N₂ adsorption is a valuable technique for determining the physical properties of mesoporous molecular sieves. It is widely used to determine the surface area, pore volume, pore diameter and to characterize the pore-size distribution of solid catalysts.

Adsorption of a gas by a porous material is described by an adsorption isotherm, the amount of adsorbed gas by the material at a fixed temperature as a function of pressure. Porous materials are frequently characterized in terms of pore sizes derived from gas sorption data. IUPAC conventions have been proposed for classifying pore sizes and gas sorption isotherms that reflect the relationship between porosity and sorption. The IUPAC classification of adsorption isotherms is illustrated in Figure 3.8. The six types of isotherm are characteristic of adsorbents that are microporous (type I), nonporous or macroporous (types II, III, and VI) or mesoporous (types IV and V) [64].

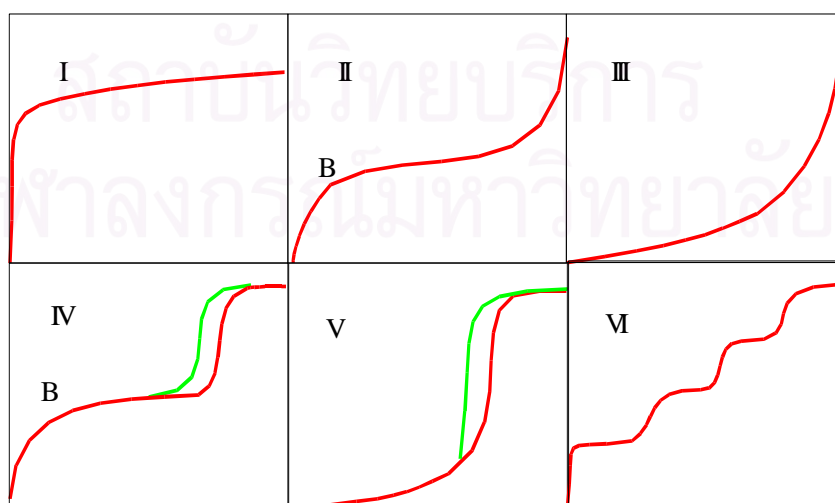


Figure 3.8 The IUPAC classification of adsorption isotherms [64].

Pore size distribution is measured by the use of nitrogen adsorption/desorption isotherms at liquid nitrogen temperature and relative pressures (P/P_0) ranging from 0.05 - 1.0. The large uptake of nitrogen at low P/P_0 indicates filling of the micropores ($< 20 \text{ \AA}$) in the adsorbent. The linear portion of the curve represents multilayer adsorption of nitrogen on the surface of the sample, and the concave upward portion of the curve represents filling of mesopores ($20 - 500 \text{ \AA}$) and macropores ($>500 \text{ \AA}$).

There are different methods used to measure surface area and each method can yield different results. Most methods are based on the isothermal adsorption of nitrogen. The multipoint Brunauer, Emmett and Teller (BET) method is commonly used to measure total surface area.

$$\frac{1}{W[(P_0/P)-1]} = \frac{1}{W_m C} + \frac{C-1}{W_m C} (P/P_0) \quad (5)$$

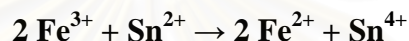
Where W is the weight of nitrogen adsorbed at a given P/P_0 , and W_m the weight of gas to give monolayer coverage and C , a constant that is related to the heat of adsorption. A linear relationship between $1/W[(P_0/P)-1]$ and P/P_0 is required to obtain the quantity of nitrogen adsorbed. This linear portion of the curve is restricted to a limited portion of the isotherm, generally between 0.05-0.30. The slope and intercept are used to determine the quantity of nitrogen adsorbed in the monolayer and used to calculate the surface area. For a single point method, the intercept is taken as zero or a small positive value, and the slope from the BET plot used to calculate the surface area. The surface area reported depend upon the method used, as well as the partial pressures at which the data are collected.

3.5.4 Determination of iron content in sample

Analysis of iron compound by the Zimmermann-Reinhardt method is discussed below in some details [65]. Steps in the analysis of sample is (1) dissolution of the sample, (2) reduction of iron to the divalent state, (3) removal of excess reductant, and (4) titration of iron(II) with a standard oxidant.

Dissolution of the sample. Iron oxides are often decomposed completely in hot concentrated hydrochloric acid. The rate of attack by this reagent is increased by the presence of a small amount of tin(II) chloride which probably acts by reducing soluble iron(III) oxides.

Reduction of iron. Because part of all of the iron is in the trivalent state after decomposition of the sample, reduce iron(III) to iron(II) must precede titration with the oxidant. The Zimmermann-Reinhardt method uses tin(II) chloride as a prereductant for iron. Tin(II) chloride is added dropwise to the disappearance of the yellow color of Fe(III).



The other common species reduced by this reagent are the high oxidation states of arsenic, copper, mercury, molybdenum, tungsten, and vanadium.

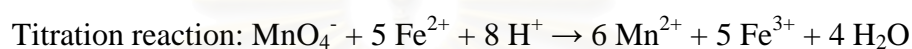
Removal of excess reductant. The slight excess of tin(II) chloride is eliminated by the addition of mercury(II) chloride:



Elemental mercury reacts with permanganate and causes the results of the analysis to be high. The formation of mercury, which is favored by an appreciable excess of tin(II), is prevented by careful control of this excess and by the rapid addition of excess mercury(II) chloride. A proper reduction is indicated by the appearance of a small amount of a silky white precipitate after the addition of mercury(II). Formation of a gray precipitate at this juncture indicates the presence of metallic mercury or the total absence of a precipitate indicates that an insufficient amount of tin(II) chloride was used. In either event, the sample must be discarded.

The titration of iron(II). The iron(II) solution from above is added with the Zimmermann-Reinhardt reagent, which contains manganese(II) in a fairly concentrated mixture of sulfuric and phosphoric acids. The reaction of iron(II) with permanganate should be added slowly and with good mixing.

The oxidation of chloride ion during a titration is believed to involve a direct reaction between this species and the manganese(III) ions that form as an intermediate in the reduction of permanganate ion by iron(II). The presence of manganese(II) in the Zimmermann-Reinhardt reagent is believed to inhibit the formation of chlorine by decreasing the potential of the manganese(III)/ manganese(II) couple. Phosphate ion is believed to give a similar effect by forming stable manganese(III) complexes. Moreover, phosphate ions react with iron(III) to form nearly colorless complexes of $\text{Fe}(\text{PO}_4)_2^{3-}$ so that the yellow color of the iron(II)/chloro complexes does not interfere with the end point. Sulfuric acid provides the necessary hydrogen ion.



สถาบันวิทยบริการ
จุฬาลงกรณ์มหาวิทยาลัย

CHAPTER IV

EXPERIMENTS

4.1 Instrument and apparatus

4.1.1 Powder X-ray diffraction (XRD)

A Rigaku, Dmax 2200/Ultima⁺ diffractometer is used with a monochromator and Cu K α radiation (1.54060 Å). The tube voltage and current are set at 40 kV and 30 mA, respectively. The scanning rate is 2 degree per minute. The diffraction is recorded in the 2 θ range of 5 to 60 degree. In the case that preferred orientation is in concern, the sample is prepared by dropping the solid colloidal sample glass slides, and allowing the solvent to evaporate for a certain time at ambient temperature.

4.1.2 Scanning electron microscopy and energy dispersive X-ray analysis (SEM-EDX)

Samples for SEM/EDX (JEOL JSM-5800LV SEM with an EDX Oxford link ISIS Series 300) analysis are coated with gold. Elemental micro-probe and elemental distribution mapping techniques are used for analysis of the elemental constitution of solid samples.

4.1.3 Fourier transform infrared (FTIR)

Fourier transform infrared (FTIR) spectra are recorded on a Nicolet Impact 410 FTIR spectrometer. Sample powder are prepare as a KBr pellet, by grinding a small amount of sample with dried KBr and pressing to 6000 psi in a pellet press. IR data are collected from 4000 to 400 cm⁻¹.

4.1.4 Centrifuge

A centaur 2, Sanyo centrifuge is used to separate and collect the iron oxide or/and manganese oxide in all steps. In addition, this equipment was used to separate adsorbate solution from the adsorbent.

4.1.5 Oven and furnace

Mamert UM-500 oven at 80°C is used for synthesis of birnessite sample under hydrothermal condition, whereas Carbolite RHF 1600 muffer furnace setting at 750°C for 30 h with the heating rate of 5°C per min is used for heat treatment for synthesis of birnessite by solid state method.

4.1.6 Atomic absorption spectroscopy (AAS)

The concentration of metal ios after adsorption experiment is measured on a PE-Analyst 100 (Perkin Elmer) using air-acetylene flame.

4.1.7 Nitrogen adsorptometer

A Quantachrome Autosorb-1 nitrogen adsorptometer accelerated surface area and porosity system is employed for the specific surface area measurement. Nitrogen gas is used as an adsorbate at 77 K. The samples are pre-degassed at 200°C. The specific surface areas of samples are measured using a BET method.

4.2 Chemicals

1. Potassium permanganate, KMnO_4 (Aldrich, 99+%)
2. Iron(III) chloride anhydrous, FeCl_3 (Riedel-de Haën, reagent grade)
3. Manganese(III) oxide, Mn_2O_3 (Aldrich, 99 %)
4. Potassium hydroxide, KOH (Merck, reagent grade)
5. Potassium carbonate anhydrous, K_2CO_3 (Fisher Chem, 100.2%)
6. Tetrabutyl ammonium hydroxide 40% in water, TBAOH (Fluka, reagent grade)
7. Tetramethyl ammonium hydroxide 25% in water, TMAOH (Fluka, reagent grade)
8. Ammonium acetate, NH_4COOH (Univar, 97%)
9. Tin chloride, SnCl_2 (reagent grade)
10. Mercury chloride, HgCl_2 (reagent grade)
11. Manganese sulfate monohydrate, $\text{MnSO}_4 \cdot \text{H}_2\text{O}$ (Univar, 98%)
12. Potassium bromide, KBr (Fluka, reagent grade)
13. Acetone, CH_3COCH_3 (commercial grade)
14. Acetic acid glacial, CH_3COOH (Merck, reagent grade)
15. Hydrochloric acid S.G. 37%, HCl (Fisher Chem, reagent grade)
16. Sulfuric acid 95-97%, H_2SO_4 (Merck, reagent grade)
17. Nitric acid 65 %, HNO_3 (Merck, reagent grade)
18. Orthophosphoric acid 85%, H_3PO_4 (Univar, reagent grade)
19. Ethanol, $\text{C}_2\text{H}_5\text{OH}$ (Merck, reagent grade)
20. Cu standard solution 1000 ppm, Cu (Fisher Scientific)
21. Pb standard solution 1000 ppm, Pb (Fisher Scientific)

4.3 Synthesis of goethite

The synthesis of goethite was adapted from the procedure reported by Kosmulski et al. [66]. Under stirring, 50 mL of 2.5 M KOH solution was added to an aqueous solution of 250 mL of 0.15 M $\text{Fe}(\text{NO}_3)_3$. The resulting suspension was heated in oil bath at 65°C for 48 h to convert the ferrihydrite precipitate to goethite. The goethite precipitate was then centrifuged out and re-dispersed in 0.01 M HNO_3 solution, and re-dispersing/centrifugation procedure was repeated 3 times, and another three times using DI water instead of HNO_3 solution. Finally, a few portions of the yellow brownish precipitate were mixed together and air-dried.

4.4 Synthesis of birnessite

Birnessite materials were prepared using two distinguished approaches. One is solid state method, denoted as ss, according to the procedure stated by Sasaki et al. [55]. Another is hydrothermal method, denoted as ht, described by Suib et al [67].

4.4.1 Solid state method

The layered manganese oxide with K^+ ions occupied in an interlayer, KMnO_2 ss, was prepared by repeating twice heat treatment of a stoichiometric mixture of KOH and Mn_2O_3 at 750 °C for 15 h. The interlayer K^+ ions were extracted by stirring 10 g of obtained compound in a 1 L of HCl solution (1 M). The acid solution was replaced with a new one every 24 h. Repetition of this acid exchanged procedure for 10 days achieved nearly complete removal of K^+ ions. The resulting protonic oxide, HMnO_2 ss, was washed with DI water to remove excess acid, filtered, and then dried in air.

4.4.2 Hydrothermal method

Potassium type birnessite, KMnO_2 ht, was synthesized by reduction method. The 200 mL aqueous solution of the mixture of 92 mL of ethanol and 33.6 g of potassium hydroxide was added slowly to a beaker containing a 150 mL aqueous

solution of 9.48 g of potassium permanganate with vigorous stirring for 1 h. The obtained mixture was transferred to the sealed bottle and aged at 80 °C for 48 h. The product was washed with water to a pH lower than 9. The protonic birnessite was prepared by an overnight acid exchange of still-wet KMnO_2ht in an aqueous HNO_3 solution (200 mL, 1.0 M) at ambient temperature. The acid-treatment was repeated three times. The obtained product was washed with DI water to a pH higher than 6, filtered, and air-dried at room temperature. Kept wet, the HMnO_2ht sample was used for further intercalation reactions.

4.5 Synthesis of manganese-iron oxide composites

There are four different methods to synthesize manganese-iron oxide composites, abbreviated as Mn-FeO_x composites. The first method is to prepare by using physical mixture of both oxides. The second method, so called exfoliation/precipitation, is an alternative route for synthesis. The third method is to obtain by iron coating performed birnessite. Last method is co-precipitation of iron and manganese in solution.

4.5.1 Physical mixture

The two crystalline oxides, birnessite and goethite, were mixed mechanically in different weight proportions (of 5-40 % Mn to total metal). Materials were grinded heavily in an agate mortar about 20 min.

4.5.2 Co-precipitation

The preparation of MnFeO_x co-precipitate was carried out by titration the various proportion of the mixtures between 0.2 M MnCl_2 and 0.2 M FeCl_3 with 2.5 M KOH, following by ageing at 65°C for 2 days, filtering, washing and drying. The molar ratio of OH/metal equal to 4 and the amount of Mn in the sample was 30% of total metal.

4.5.3 Coating

The composites were prepared by the deposition of iron oxide on the performed birnessite, so called coating method. First, Fe-polycation solution was prepared by addition of KOH solution to solution of 0.2 M FeCl_3 with the OH/Fe molar ratio of 2, and stirred overnight at room temperature. Then HMnO_2 ht was soaked in the prepared Fe-polycation solution. The solution of 0.2 M KOH was added to the mixture with the OH/Fe molar ratio of 4. The suspension was placed in an oil bath at 65°C for 48 h, which stirred during the first 24 h. After that, the obtained precipitation, iron-coated birnessite, washed with DI water, filtered and air-dried.

4.5.4 Exfoliation-precipitation

The Mn-FeO_x oxide solid was prepared by two steps process. Firstly, Birnessite was exfoliated in the solution of tetrabutylammonium hydroxide (TBAOH). Next, the mixture of exfoliated birnessite and Fe-polycations produced the precipitating oxide composite, which were subsequently converted the intercalated Fe-precursor to iron oxides by thermal treatment.

The exfoliated birnessite was prepared by modifying the method used by Sasaki et al. [68]. Weighed HMnO_2 ht was soaked in TBAOH solutions under stirring for 10 days at room temperature. The molar ratio of TBA cations to exchangeable protons in the HMnO_2 ht (referred as TBA/H^+) was adjusted to 10, 25 and 50 folds. After soaking, the suspension was centrifuged at 6000 rpm for 15 min. The supernatant colloids, so called exfoliated birnessite, and solid at bottom, so called intercalated birnessite, were subjected to XRD analysis in their wet state.

The Fe-polycation was prepared by hydrolysis a solution of 0.2 M ferric chloride with tetramethylammonium hydroxide (TMAOH, 0.2 M) and aging overnight, all at room temperature. The OH/Fe molar ratio was adjusted to 2, at this value the Fe-polycations were predominant [69]. TMAOH base was used instead of NaOH/KOH in order to avoid competition for intercalation between Na^+ ions and the Fe-polycations.

The suspension of exfoliated birnessite was poured into Fe-precursor solution and then added 0.2 M TMAOH solution to adjust the OH/Fe to 4. The mixture was maintained over night under stirring at 65 °C, and subsequently aged in the mother liquor at the same temperature for 24 h. The ratio of metal in sample was ranged from 10-40 wt % of Mn to total metals in composites. The product was collected by centrifugation, washed with DI water, and then air-dried.

To study the effect of ferric source to phase of FeOOH in Mn-FeO_x composite, ferric nitrate was used instead of ferric chloride.

4.6 Determination of iron content by redox titration

Iron content of composite samples was analyzed by Zimmermann-Reinhardt method following the recommended by Gilbert [63].

Accurately weigh two 0.1 g samples of the composite into two 250 mL beakers. To each beaker add 8 mL of concentrated HCl and 2 mL of 0.25 M SnCl₂; cover with a watch glass. Heat the beakers in a hood at just below the boiling point until the samples are dissolved. Add an additional 1-2 mL of 0.25 M SnCl₂ to eliminate any yellow color that may develop during heating. If the final solution is colorless because of an excess of Sn(II), add 0.02 M KMnO₄ just to restore the yellow color. Heat the sample solution nearly to boiling and add 0.25 M SnCl₂ solution dropwise until the yellow color just disappears. Rinse down the sides of the flask with a very small amount of water and then add not more than 2 drops of excess SnCl₂.

Cool the sample to room temperature and rapidly add 10 mL of 5% HgCl₂ solution, and mix well. A small amount of a silky-white precipitate (Hg₂Cl₂) should occur.

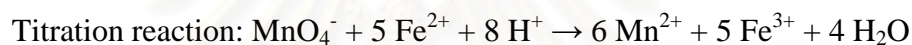
(1) If no precipitate forms, the amount of SnCl₂ is insufficient, and reduction of Fe(III) is incomplete. Discard the sample.

(2) If a gray precipitate the formation, this indicates formation of elemental mercury occur discard the sample.

Wait 2-3 minutes after addition of the HgCl_2 solution, then added 25 mL of Zimmermann-Reinhardt reagent and 150 mL of water. Titrate the solution immediately with the freshly standardized 0.02 M KMnO_4 solution to the first detectable pink tinge that persists for at least 30 seconds.

Determine the blank as follow: In a flask contain 8 mL conc. HCl and 10 mL of water, add two drops of the SnCl_2 solution and 10 mL of 5 % Hg_2Cl_2 solution. Then proceed all steps as in the determination above.

Subtract the volume used for the blank solution used from the volume for the sample. Calculate % Fe by mass in the unknown. To minimize air oxidation of Fe(II), carry out the above steps one sample at a time.



4.7 Adsorption experiment

The adsorption capacity for birnessite, goethite and $\text{MnO}_x\text{-FeO}_x$ composites were determined by adding 30 mg of adsorbent to 25 ml of the heavy metal solution of $300 \text{ mg dm}^{-3} \text{Pb}^{2+}$ (aq), and $100 \text{ mg dm}^{-3} \text{Cu}^{2+}$ (aq) ions (Pb^{2+} ion adsorption was studied at increased concentration due to the high capacity of birnessite and Mn- FeO_x composites for the ion). The adsorbate solution was adjusted around pH 5.5 using potassium hydroxide and carried out in 0.2 M acetate buffer solution at pH 5.5. The suspensions of adsorbent and solution were sealed, stirred and equilibrated for 24 h at room temperature. Afterwards, the suspensions were centrifuged and the supernatants were analyzed for metal ions concentration using AAS. The quantity of metal ion adsorbed was estimated from the difference between the amount added and the amount remaining in the supernatant solution.

The filtration quality of obtained composites was investigated, using centrifugal speed of 3000 rpm at 10, 20, and 30 min, and compared the clear solution of them.

CHAPTER V

RESULTS AND DISCUSSIONS

5.1 Synthesis and characterization of goethite (α -FeOOH)

Goethite is prepared using the method described by Kosmulksi [66]. Ferrihydrite was initially precipitated, by adding precipitating agents to aqueous solution of ferric chloride. The formation of goethite is produced by crystallization from ferrihydrite in an alkaline pH medium after thermal treatment at 65 °C.

5.1.1 X-ray diffraction (XRD)

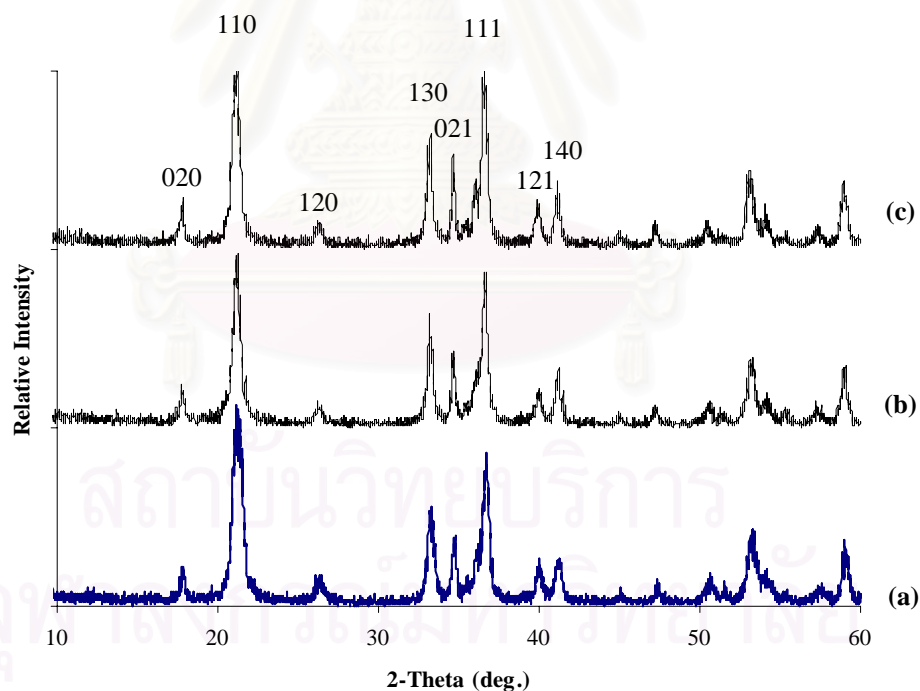


Figure 5.1 XRD patterns of goethite prepared by the hydrolysis of ferric chloride, using different precipitating agents: (a) KOH, (b) TBAOH, and (c) TMAOH.

Figure 5.1 shows XRD characteristic patterns of samples, prepared by the hydrolysis of ferric chloride by using different precipitating agents. XRD analysis shows that goethite is formed as a single phase in all synthetic samples. The d spacing values of strong peaks match the values for goethite in JCPDS card 29-0713 that is: 4.98, 4.18, 3.38, 2.69, 2.58, 2.49, 2.45, 2.25, and 2.18 Å.

The crystallite size of goethite particles is estimated from the widths of the diffraction lines of 111 and 110 planes, by using the Scherrer method. Table 5.1 shows the crystallite sizes of goethite samples. The data indicates as the representatives that the sizes of synthetic α -FeOOH crystallites are in nanosize range. Therefore in this alkaline system, a change in the precipitating agents does not affect the crystallinity of α -FeOOH particles much. However, the larger crystallite size obtained from TBAOH may result from the slow rate of hydrolysis /polymerization of iron complexes because of bulky shape.

Table 5.1 Crystallite sizes of α -FeOOH samples, as estimated by using the Scherrer method.

Precipitating agent	Crystallite size (Å)		
	L_{111}	L_{110}	L_{average}
KOH	171	144	157.5
TMAOH	175	139	157.5
TBAOH	186	163	174.5

5.1.2 Fourier transform infra-red spectrometer (FT-IR)

All FT-IR spectra of the sample prepared in this work show typical features of α -FeOOH. Figure 5.2 shows the spectrum of goethite, using KOH as precipitating agent. In accordance with previous work [66,70] a very strong IR band at 3143 cm^{-1} is due to the presence of the OH stretching mode in goethite, whereas the IR band 3401 cm^{-1} can be ascribed to stretching modes of surface H_2O molecules or of hydrogen-bonded surface OH group. Two characteristic bands of goethite at 892 and 797 cm^{-1} can be assigned to Fe-O-H bending vibrations. The band observed at 641 cm^{-1} is ascribed to Fe-O stretching vibrations in goethite.

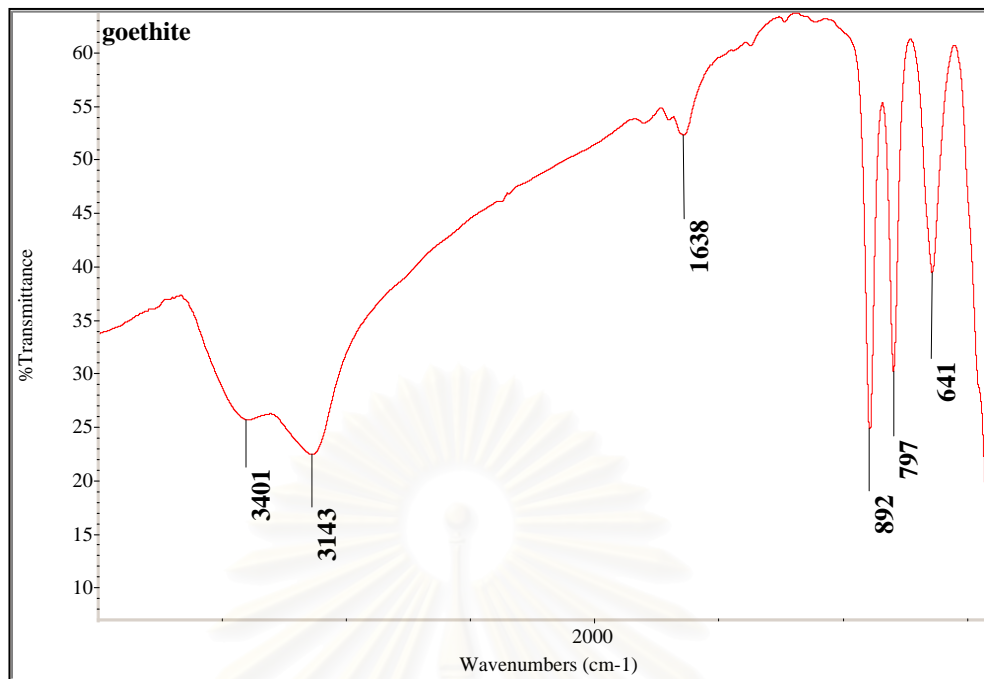


Figure 5.2 Infrared spectrum of synthetic goethite.

5.2 Synthesis and characterization of birnessite

Birnessite is important two-dimensional layered inorganic materials due to their unique cation-exchange, adsorptive and catalytic properties. The syntheses of potassium manganese oxide birnessite (KMnO_2) have been carried out by hydrothermal method, based on procedure used by Suib and Gao [67], and solid state method, modified from method described by Sasaki et al. [54]. Although structurally similar materials can be prepared by a variety of routes, the ion-exchange and physical properties highly depend on synthetic conditions. KMnO_2 is not active for ion-exchange reaction of organic ammonium ions or large intercalates. On the other hand, proton birnessite (HMnO_2) is more suitable for further reactions, since the proton allows easier access of the guest molecules into birnessite structure via water swelling process. Ion exchange reaction is chosen to prepare HMnO_2 , which is used as the starting birnessite for further process.

5.2.1 X-ray diffraction (XRD)

Figure 5.3 illustrates XRD patterns of potassium and proton birnessite prepared via hydrothermal method, denoted by ht, and solid state method, denoted by ss. The characteristic peaks of birnessite are presented in all patterns. From ht treatment, XRD pattern (Figure 5.3 (a)) shows only KMnO_2 phase without any amorphous or other kinds of crystalline phases, indicating that the single phase of KMnO_2 is obtained. Whereas pattern of KMnO_2 ss (Figure 5.3 (c)) presents mixtures of both birnessite and manganese oxide (MnO_2), which results from incomplete solid state reactions. MnO_2 exhibits strong XRD peaks at 6.93, 4.90 and 3.10 Å. In the Starting KMnO_2 ht, two peaks are observed at 2θ of 12.4 and 24.9°. According to Bragg's equation, these 2θ values correspond to d spacing of 7.14 and 3.55 Å, as summarized in Table 5.2, which can be indexed to (001) and (002) reflections of a

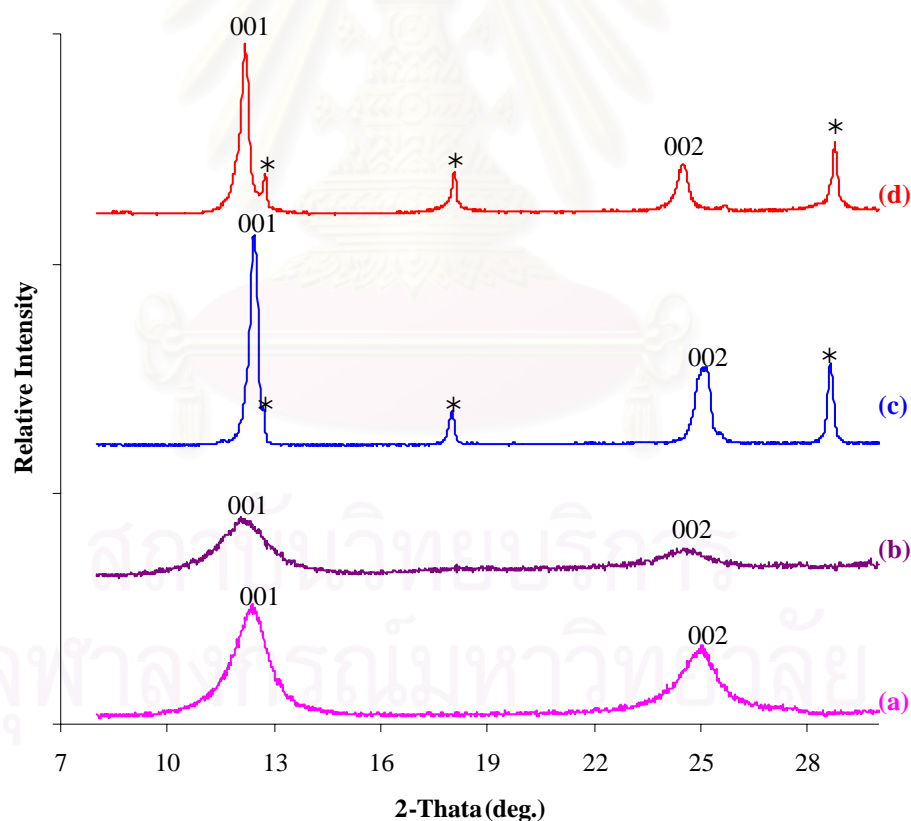


Figure 5.3 XRD patterns of potassium birnessite via (a) hydrothermal and (c) solid state methods, and their proton birnessite (b), (d) respectively. * indicates MnO_2 phase.

layered structure, respectively. This pattern with an interlayer distance of 7.12 Å is consistent with that typically observed for bulk birnessite with hydrated small cations. Similarly, KMnO_2 ss has interlayer spacing of 7.10 Å.

In addition, birnessite prepared from both methods can easily be converted to proton birnessite, HMnO_2 (Figure 5.3 (b) and (d)), by ion-exchange reaction. When the KMnO_2 sample is treated with acid solution, the basal spacing of both samples slightly increases to 7.26 Å, indicating H_3O^+ ions occupy the K^+ ion position of KMnO_2 . The radii of hydrated proton is slightly bigger than that the hydrated K^+ ion, so the interlayer distances of HMnO_2 is shifted to the larger d spacing. Unlike KMnO_2 ht, it is found that the proton exchange of KMnO_2 ss is not complete by the present of KMnO_2 peak in the pattern of HMnO_2 ss. This could results from the larger crystallite size of KMnO_2 ss.

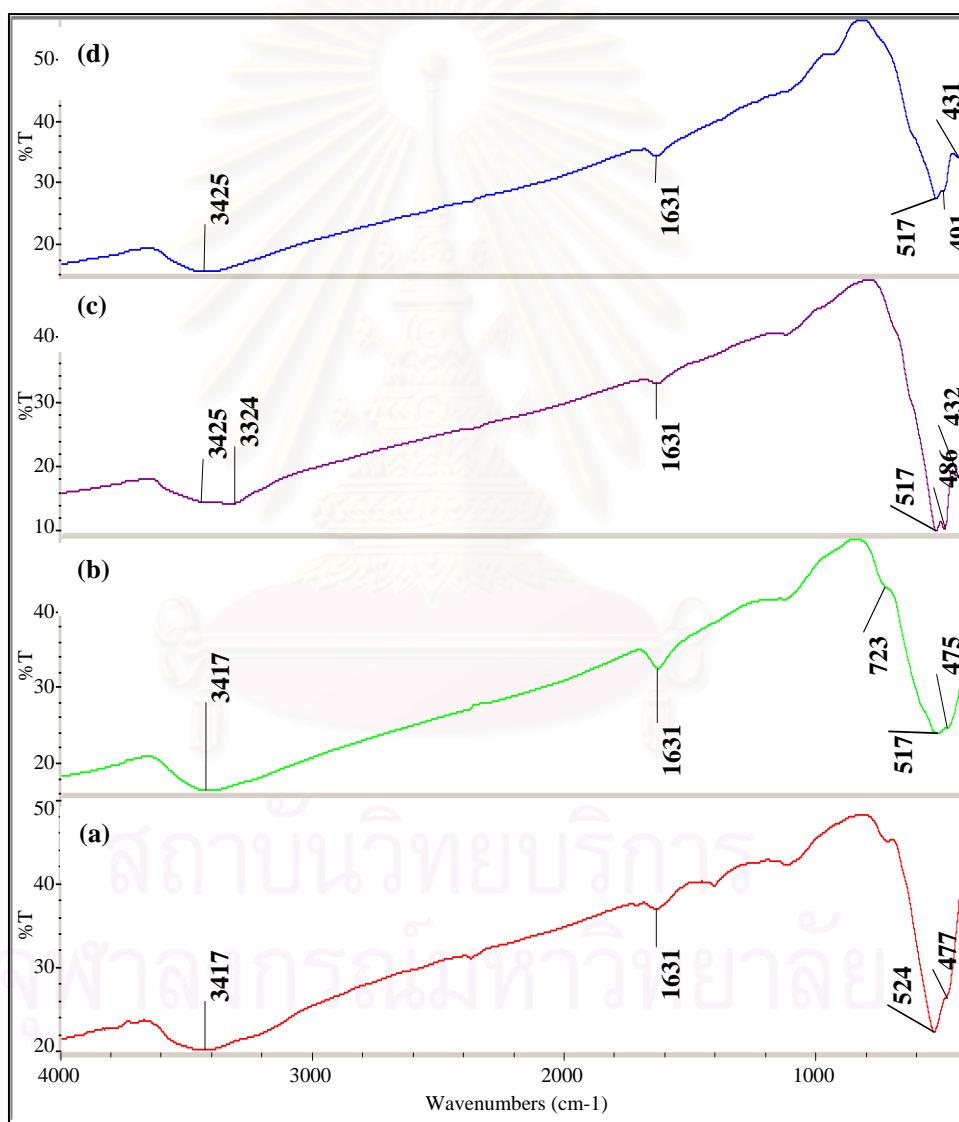
Table 5.2 d spacing of birnessite samples.

sample	d spacing (Å)		
	d_{001}	d_{002}	$d_{\text{basal spacing}}$
KMnO_2 ht	7.14	3.55	7.12
HMnO_2 ht	7.26	3.63	7.26
KMnO_2 ss	7.10	3.55	7.10
HMnO_2 ss	7.26	3.63	7.26

The patterns of hydrothermal treatment, synthesized samples show weak and broadening of the strong peaks indicating that samples are composed of small crystallites with a size in nanometer scale. The crystallite size of all samples is calculated from peaks (001) using the Scherrer equation, reported in Table 5.3. For ss method, the intensities of XRD peaks increase rapidly while the peak widths decrease considerably, corresponding to the large crystallites of a better layered order. This could be explained that, the high temperature and long processing time used in ss method allows the better atomic arrangement in the sample.

Table 5.3 Crystallite sizes of birnessite samples.

sample	Crystallite size (L_{001} , Å)
KMnO ₂ ht	106
HMnO ₂ ht	96
KMnO ₂ ss	307
HMnO ₂ ss	266

5.2.2 Fourier transform infrared spectrometer (FT-IR)**Figure 5.4** Infrared spectra of (a) HMnO₂ ss, (b) HMnO₂ ht, (c) KMnO₂ ss, and (d) KMnO₂ ht.

IR spectra of birnessite sample are presented in Figure 5.4. There is not much difference in the IR spectra of both methods and counter-ion of birnessite. In the range of less than 700 cm^{-1} , 517 , 491 and 431 cm^{-1} bands can be assigned to the Mn-O stretching vibrations, which are characteristic IR band in birnessite [71]. Two bands at 3425 and 1631 cm^{-1} are due to stretching and bending vibrations respectively of OH groups in adsorbed water molecules.

XRD and FT-IR analysis confirm that potassium birnessite remains layered structure after acid treatment.

5.3 Synthesis of manganese-iron oxide composites

In this part, HMnO_2 ht is chosen for the synthesis of manganese-iron oxide composites, Mn- FeO_x composites, because of its adsorption capacities for copper is higher than that of the HMnO_2 ss, directly resulting from very small particle size. This issue will be discussed in the next section, 5.4 adsorption capacities. The Mn- FeO_x composites have been synthesized by different methods.

5.3.1 Physical mixtures

Two oxides HMnO_2 ht and goethite are mixed mechanically in different proportion. Their structural features and adsorption behavior are compared composites prepared by other approaches in the further discussion.

5.3.1.1 X-ray diffraction (XRD)

XRD pattern of the physical mixture of 70% wt Fe (Figure 5.3 (b)), denoted as PS 70% Fe, is compared in Figure 5.5 with the patterns of HMnO_2 (a) and goethite (c). Its pattern is exactly the combination of HMnO_2 's and goethite's patterns based on d spacings and relative intensities, which reflect the amount of each loading.

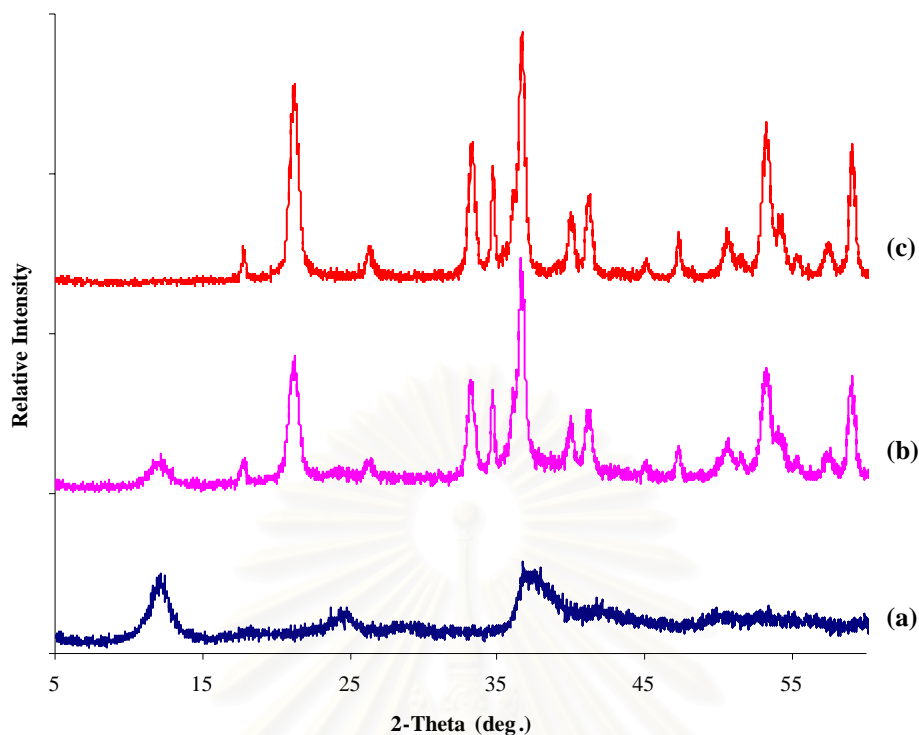


Figure 5.5 XRD patterns of (a) HMnO_2 ht, the product from PS method: (b) PS 70% Fe, and (c) goethite.

Table 5.4 gives the crystallite size PS 70% Fe, compared to those of starting materials. It is slightly decreased in crystallite size of goethite, resulting from heavily mechanical grinding. On the other hand, the size of HMnO_2 ht in the mixture may seem to be higher than usually observed for pure birnessite. However, this small proportion of HMnO_2 ht not exactly determines experimentally because of the very weak broad on peak of d_{001} .

Table 5.4 Crystallite sizes of PS sample.

sample	Crystallite sizes (\AA)		
	L_{001} (Birnessite)	L_{111} (Goethite)	L_{110} (Goethite)
HMnO_2 ht	96	-	-
PS 70% Fe	132	159	133
Goethite	-	171	144

5.3.1.2 Fourier transform infra-red spectrometer (FT-IR)

The IR data of composites from PS method are also in agreement with that observed in XRD data, as presented in Figure 5.6 (b). As previously mentioned, XRD shows that the sample has goethite as the dominant phase. The spectrum of PS 70% Fe gives the features of goethite with just a small effect of HMnO₂ phase at lower wavenumbers.

The wide band around 600-400 cm⁻¹ is due to weak signal of the small fraction of HMnO₂ in the mixture. On the basis of the XRD and IR, it can be concluded that the PS method does not change the structures and bonding of each strating materials.

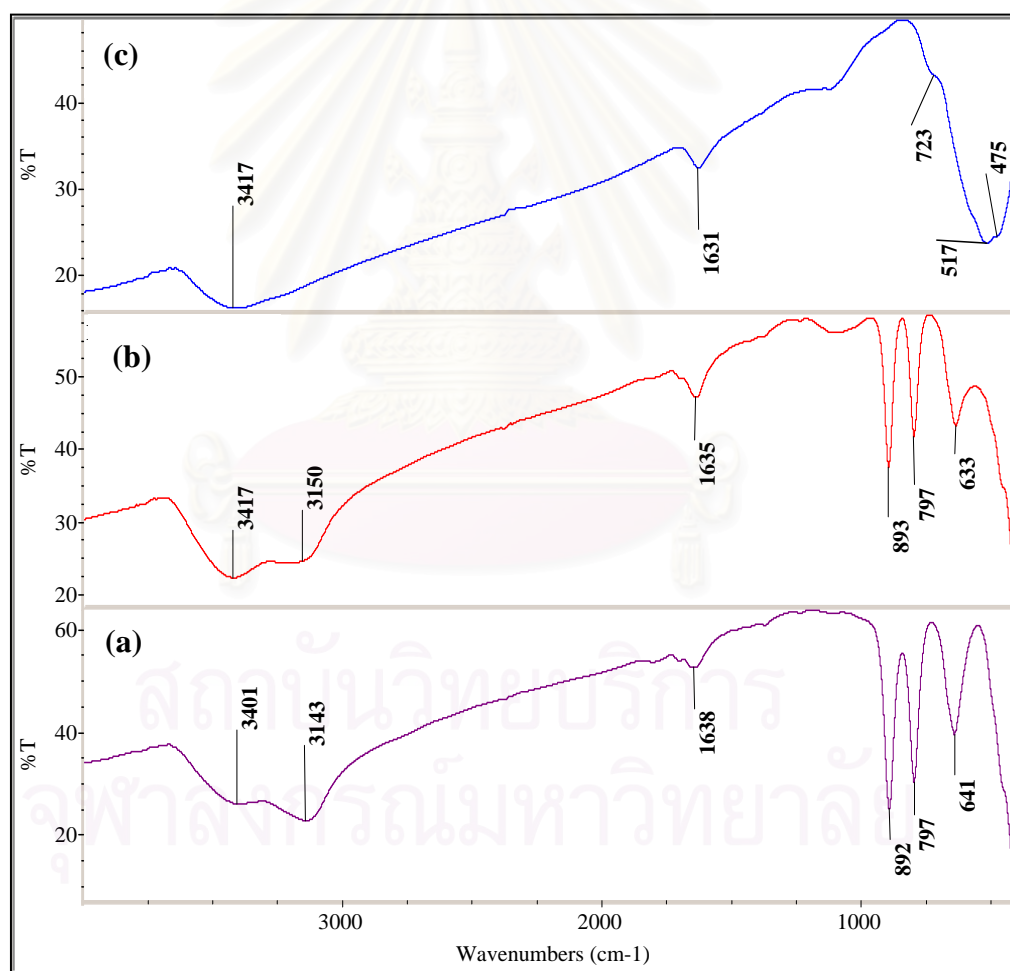


Figure 5.6 Infrared spectra of (a) goethite, (b) PS 70% Fe, and (c) HMnO₂ ht.

5.3.2 Exfoliation-precipitation

Various organic alkylammonium ions have been exchanged with interlayered H_3O^+ ions by an ion-exchange reaction, accompanied by the expansion of the spacing between adjacent layers. The expanded layered birnessite involving the intercalation of a solvent is called swelling. When the large of solvent or the electrolyte solution is introduced into the interlayered space, the exfoliation occurs, and each sheet is considered to be free from each other. The exfoliation of manganese oxide sheets has a higher degree of freedom than the stacked sheets, the bulky guest ions can be easily adsorbed onto their surface. Therefore, this exfoliation-precipitation method, denoted as EP, gives an alternative route to prepare manganese-iron oxide composites, Mn- FeO_x .

This procedure composes of two steps, first step concerns the expansion of layered manganese oxide using tetrabutylammonium hydroxide, TBAOH, as the resulting agent. The second step, Fe-precursor is mixed with exfoliated manganese oxide in order to precipitate the Mn- FeO_x composites.

5.3.2.1 X-ray diffraction (XRD)

The first step of this procedure is the exfoliation of birnessite with TBAOH solution. Colloidal suspensions are obtained by treating HMnO_2 with TBAOH solution at the molar ratio of TBA ions over exchangeable proton in birnessite, TBA^+/H^+ , is 10. This ratio is an important feature because it can be taken as the ratio that birnessite structure is exfoliated into individual manganese oxide sheet [68]. The mixtures are then centrifuged at 6000 rpm for 15 min and solid is recovered. The supernatant solution, dark brown colloidal as characteristic of manganese oxide sheets, is examined by XRD, as depicted in Figure 5.7.

The solid phase recovered by centrifugation, *TBA-HMnO₂ bottom*, shows the pattern (Figure 5.7 (b)) arising from a single phase consisting of the (00l) reflections, the set of diffraction lines is found to shift to lower angles and corresponding larger d spacing. Sharp diffraction lines up to the third order indicate a highly ordered structure similar to the patterns observed in all studies on the TBA intercalated

birnessite. The intercalation of TBA ions into birnessite structure gives layer with a d_{spacing} of 12.8 Å, as summarized in Table 5.5, that corresponds to the presence of one molecular layer of dehydrated TBA ions. The colloidal phases from centrifugation (Figure 5.3 (c)), *TBA-HMnO₂ top*, are casted on a glass slide and drying for XRD measurement. On drying, the exfoliated lamellar is restacked again. The peaks shifted to lower angles, with a d_{spacing} of 15 Å, showing that the degree of swelling is enhanced. The very broad (001) peak indicates that the casted sample is resulted from the restacking of well-dispersed birnessite sheets. A broad halo observed at 2θ of 15-30° (rising portion of the baseline as seen in *TBA-HMnO₂ top* sample) is attributed from X-ray scattering by non-ordered phase of water-swelling manganese oxide.

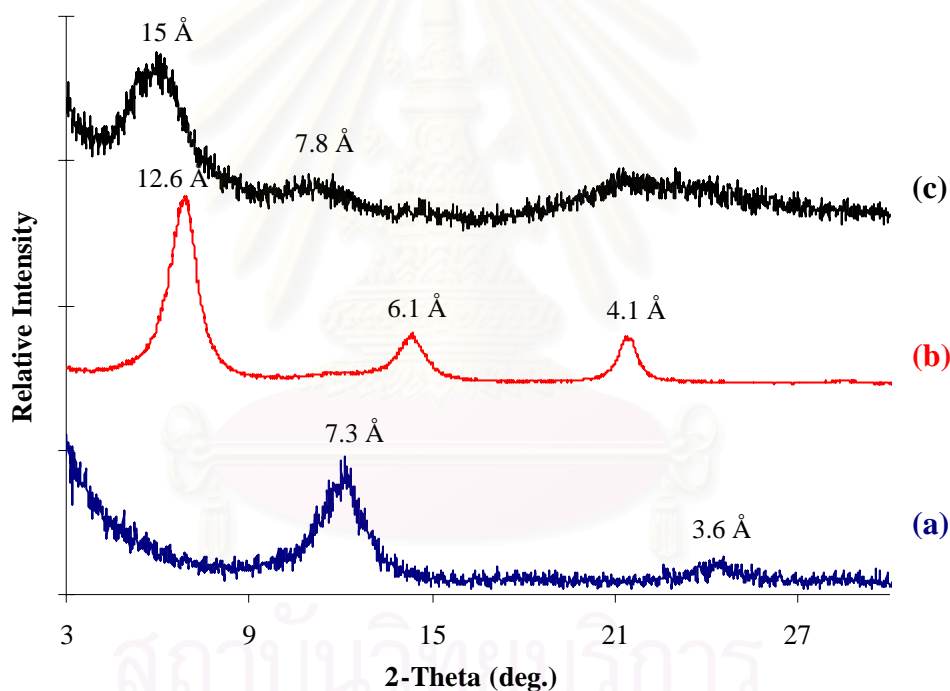


Figure 5.7 XRD patterns of (a) HMnO₂ ht, and its exfoliated products: (b) TBA-HMnO₂ bottom and (c) TBA-HMnO₂ top.

Table 5.5 d spacing of exfoliated birnessite samples.

sample	d spacing (Å)			
	d_{001}	d_{002}	d_{003}	$d_{\text{basal spacing}}$
HMnO ₂ ht	7.26	3.63	-	7.26
TBA-HMnO ₂ bottom	12.6	6.1	4.1	12.4
TBA-HMnO ₂ top	15.0	7.8	-	15.3

Proposed structural models related with the observed interlayer spacings are presented in Figure 5.8. Calculated interlayer spacings are based on the dimensions of the manganese oxide layer (thickness of 5.2 Å) [72], the van der Waals radius of water (2.8 Å), and the size of packed TBA cation (8.4 Å) [72]. Model I assumes the absence of a hydration layer between the TBA cation and manganese oxide layers, although water molecules may be present in the same plane as the TBA cations. Whereas the model II is corresponds to a total of one effective layer of water in addition to the layer of TBA cations.

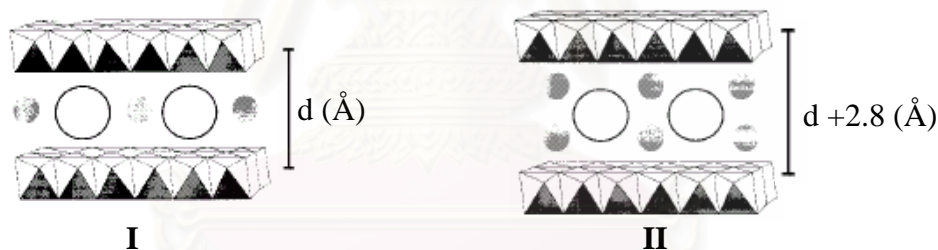


Figure 5.8 Simple structural models for the TBA intercalated manganese oxide phase based on zero, and one layer of water. The large empty spheres represents TBA cations and the small gray sphere represents water products [72].

In the second step of this synthesis, we study the restacking of the manganese oxide sheets by precipitation with Fe-precursor ions. Among the Fe-precursors, the hydrolysis of an aqueous solution of iron salt by a base produces the iron polyhydroxy oligomer, Fe-polycation. This process has been studied extensively [52,73] but the structure of the polynuclear complexes are not yet clearly known.

Addition of a suspension of exfoliated birnessite into Fe-polycation solution produces precipitation of ferrihydrite, which can be converted to composite of Mn-FeO_x by subsequent heat treatment. Figure 5.9 shows pattern of composites derived from EP method. In the case Fe-polycation is formed by the hydrolysis of ferric chloride solution, that its precipitated composite is denoted as CIEP. Its XRD peaks are weak and broad (Figure 5.9(b)), indicating that the crystallinity of the structure is poor. In the attempt of matching the pattern with known iron oxide phase, the closest matching is belongs to akaganeite, β -FeOOH. However the relative intensities of all peaks are not quite right. With the broadening feature of its XRD pattern, we can conclude that the iron oxide phase is poorly ordered FeOOH.

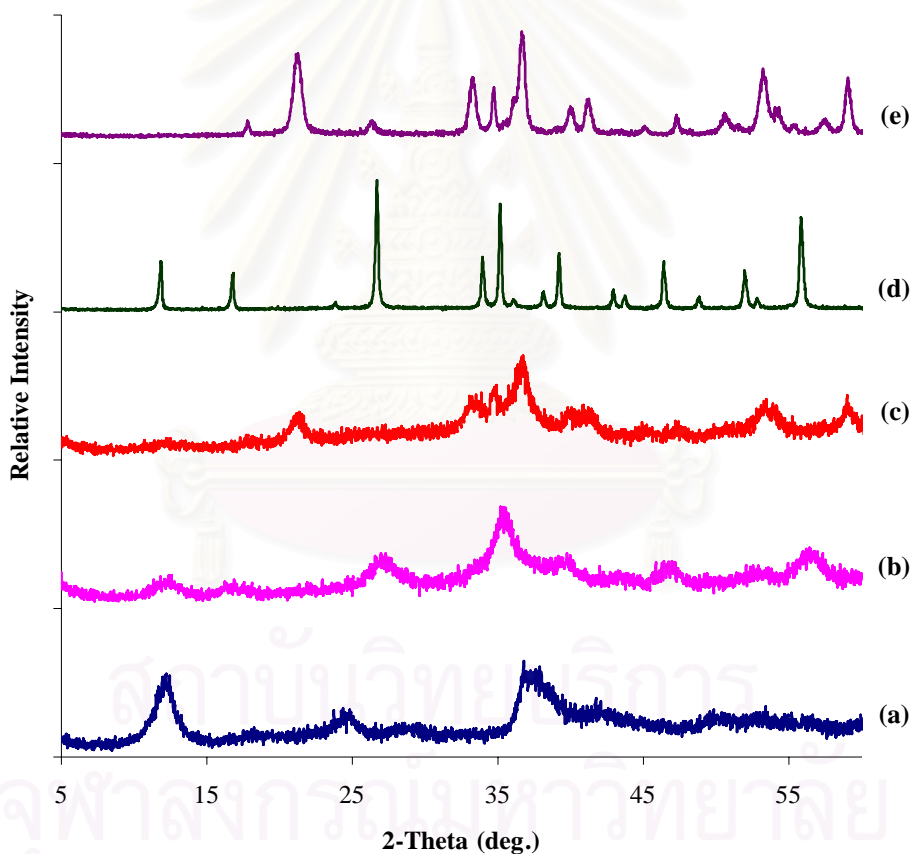


Figure 5.9 XRD patterns of (a) HMnO₂ ht, the product from EP method: (b) CIEP and (c) NtEP, (d) akaganeite, and (e) goethite.

As in Table 5.6, the crystallite size of the FeOOH phase in CIEP composites, is smaller than that prepared in absence of HMnO₂. The resulting less crystalline form of FeOOH may be due to the presence of the substrate as well as Cl⁻ ion, and has been observed others [28] to inhibit crystallization. Many previous studies show that Cl⁻ ions are important synthetic parameters in the preparation of akaganeite but only in acidic pH condition. To investigate further, ferric nitrate is used instead of ferric chloride to prepare Fe-polycation, in the next case.

To study the effect of different anions on the formation of Fe oxyhydroxide in composite phases, ferric nitrate is used instead of ferric chloride. The XRD pattern of composite from nitrate salt, NtEP, is presented in Figure 5.9 (c). Strange reflections from goethite (at $d = 4.94, 4.19, 2.70, 2.58, 2.44, 2.25,$ and 2.19 \AA) are observed in the pattern, which is perfectly matched with the JCPDS card no. 29-0713 of goethite. Therefore goethite is the dominant phase coexisting with other minor peaks due to HMnO₂ and no any other crystalline iron oxide phase is found in this product. The line broadening indicates a small crystallite size of approximately 112 Å in Table 5.6.

Table 5.6 The result of phase analysis and crystallite sizes, as determined by the strongest line in XRD patterns, of EP composites.

Iron source	FeOOH phase	Crystallite size(Å)
Chloride salt (CIEP)	Poorly ordered β -FeOOH (akaganeite)	122
Nitrate salt (NtEP)	α -FeOOH (goethite)	112

5.3.2.2 Fourier transform infra-red spectrometer (FT-IR)

Figure 5.10 presents the IR spectra of composites prepared by EP method. The spectrum of the composite produced from nitrate salt (Figure 5.10 (c)) appears almost identical to that pure goethite. Most likely, the strong Mn-O stretching vibrations bands around 400-700 cm⁻¹ from HMnO₂ masks the characteristic goethite peaks at 641 and 400 cm⁻¹. Whereas typical bands of goethite at 892 and 797 cm⁻¹, due to the

Fe-O-H bending vibrations, and the band at 3402 and 3149 cm^{-1} , due to OH stretching mode, are observed.

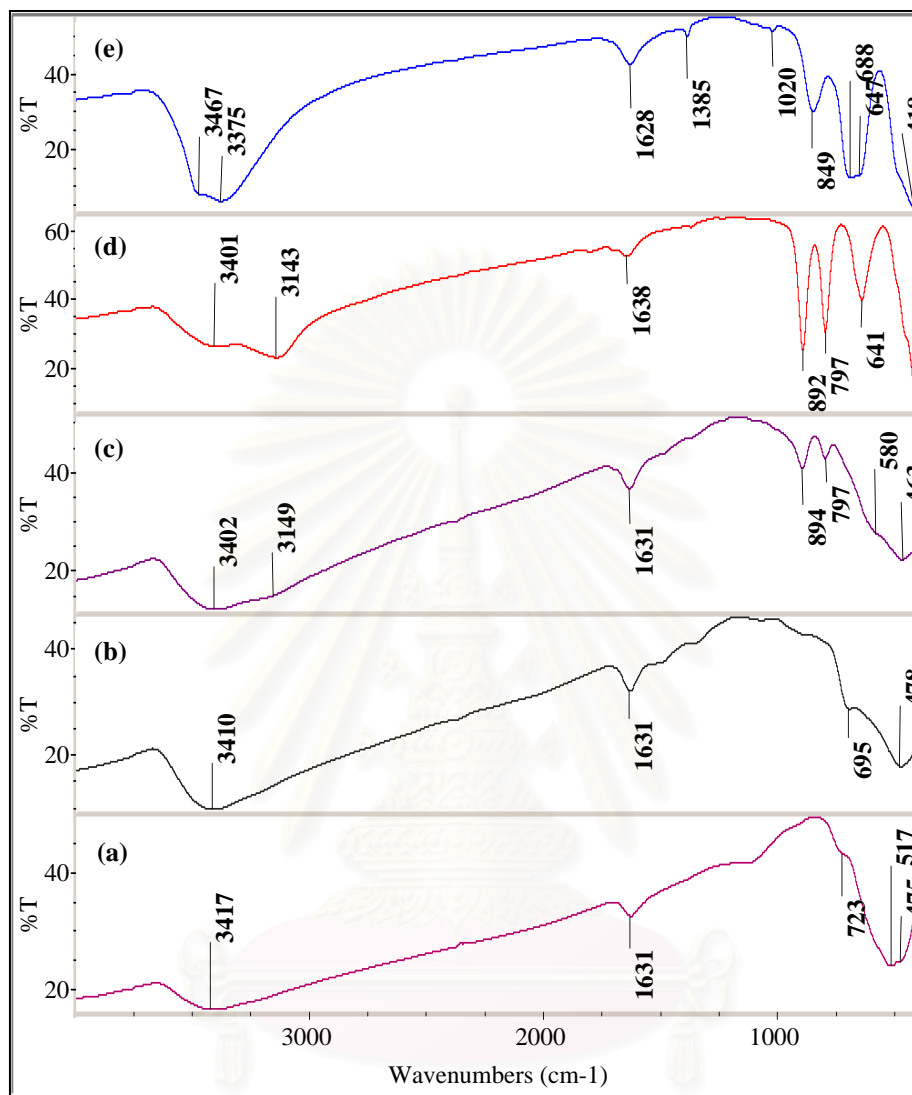


Figure 5.10 Infrared spectra of (a) HMnO_2 ht, the product from EP method: (b) CIEP and (c) NtEP, (d) akaganeite, and (e) goethite.

On the other hand, the spectrum of composite produced by chloride salt (Figure 5.10 (b)) does not much with those of goethite and NtEP but its absorption band is closed to that of HMnO_2 . The new band at 695 cm^{-1} may be related to O-H...Cl hydrogen bond that is characteristic of akaganeite [74-75]. But the absence of the band at 849 cm^{-1} may be due to the removal of the chloride ions, which reported by Bakoyannakis et al. [75]. It may be suggested that there is a poorly crystalline β -FeOOH in a CIEP composite.

Based on the XRD, and IR data, it is concluded that the phase of Mn-FeO_x composites, which prepared from chloride salt, are mixtures of poorly ordered β-FeOOH and HMnO₂. Whereas composites from nitrate salt give mixtures of goethite and HMnO₂.

This observation may support the conclusion that the Fe oxyhydroxide phase in Mn-FeO_x composites depend on the starting salt of ferric solution. Therefore, salts of ferric solution are one of the major determining factors in the synthesis of this system. Ferric chloride favors the nucleation and growth of β-FeOOH while ferric nitrate favors the crystallization of α-FeOOH.

5.3.3 Coating

To study the effect of substrate dispersion to formation of composite phases experiments without the dispersion of birnessite are carried out. The method is so called Fe-coating birnessite, denoted as CT method. In this section, the composites are compared in the same way as section 5.3.2 but using HMnO₂ ht as a substrate material instead of exfoliated birnessite.

5.3.3.1 X-ray diffraction (XRD)

In this method, the pattern of Mn-FeO_x composites are similar to those of the composites prepared by EP method in the number of peaks, the relative peak intensity, and the peak width. The XRD pattern of composite prepared from ferric chloride salt, ClCT, shows in Figure 5.11(b). Its pattern is composed of poorly ordered akaganeite and HMnO₂. In the case of ferric nitrate salt, NtCT (Figure 5.11 (c)), it can be conclude in the same way as EP method that the pattern matches with goethite with a small broad peak of HMnO₂.

The crystallite size of sample from CT method, reported in Table 5.7, is nearly similar to the value that observed in EP method, which is about 120-130 Å.

Table 5.7 The result of phase analysis and crystallite sizes, as determined by the strongest line in XRD pattern, of CT composites.

Iron source	FeOOH phase	Crystallite size (Å)
Chloride salt (ClCT)	Poorly ordered β -FeOOH (akaganeite)	129
Nitrate salt (NtCT)	α -FeOOH (goethite)	122

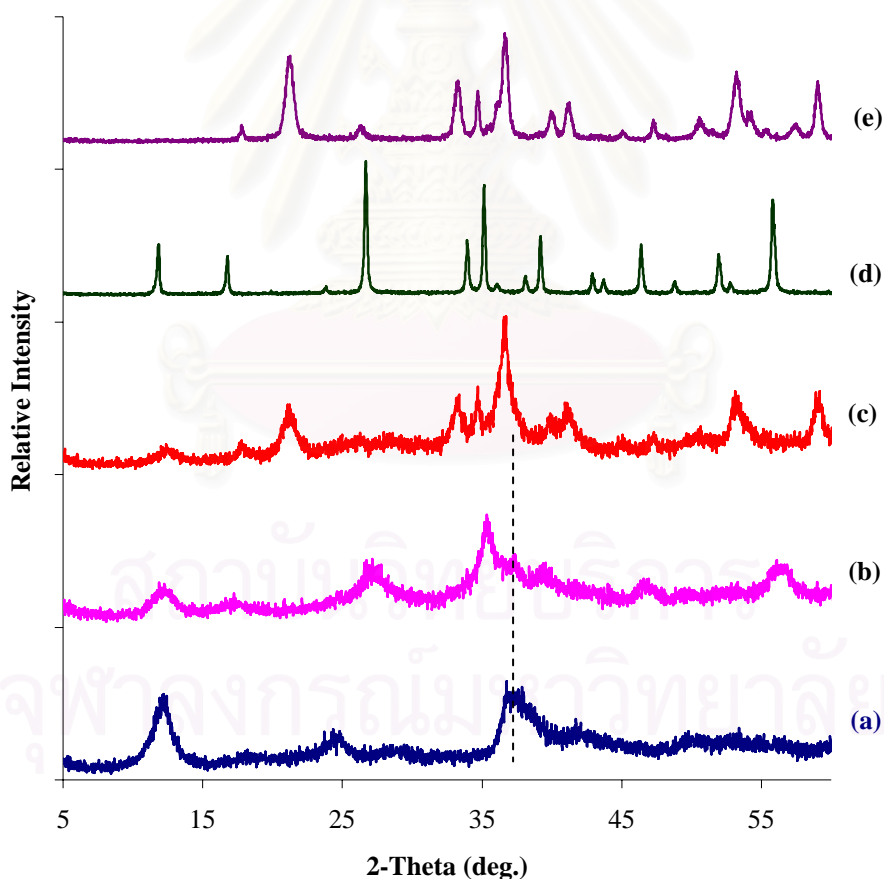


Figure 5.11 XRD patterns of (a) HMnO_2 ht, the product from CT method: (b) ClCT and (c) NtCT, (d) akaganeite, and (e) goethite.

5.3.3.2 Fourier transform infra-red spectrometer (FT-IR)

The IR spectra of composites from CT method are presented in Figure 5.12. Their absorption bands are similar to that observed in EP method. The spectrum of NtCT composite displays almost identical to that of pure goethite. It presents a characteristic band of goethite (892 and 797 cm^{-1}) and a wide band of HMnO_2 (400 – 700 cm^{-1}). Whereas the spectrum of ClCT sample is similar to those of ClEP, showing the absorption band close to that of HMnO_2 .

Now, it is able to conclude that the phase of FeOOH depends on the source of iron, but not on the dispersion of preformed birnessite.

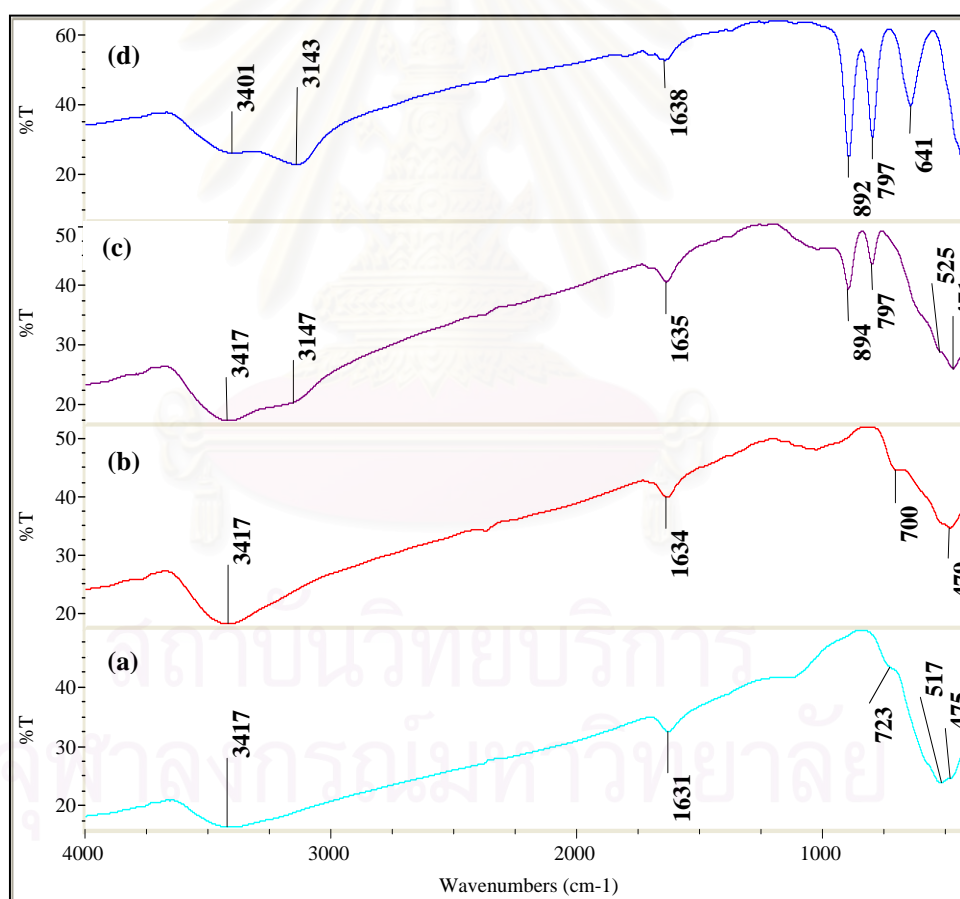


Figure 5.12 Infrared spectra of (a) HMnO_2 ht, the product from CT method: (b) ClCT and (c) NtCT, (d) akaganeite, and (e) goethite.

5.3.4 Coprecipitation

Under coprecipitation method, denoted as CP method, manganese chloride and iron chloride are mixed in aqueous solution with 70% wt Fe and 30% wt Mn. The hydrolysis by base and consequently condensation results to the co-precipitation oxide product.

5.3.4.1 X-ray diffraction (XRD)

The XRD pattern of the CP 70% Fe sample is shown in Figure 5.13 (b). The mixed oxide is identified as mixtures of MnFe_2O_4 , jacobsite, according to JCPDS card 74-2403, and goethite. No other peaks corresponding to crystalline manganese oxide and iron oxide are observed. The crystallite size of jacobsite and goethite are 317 and 190 Å, respectively.

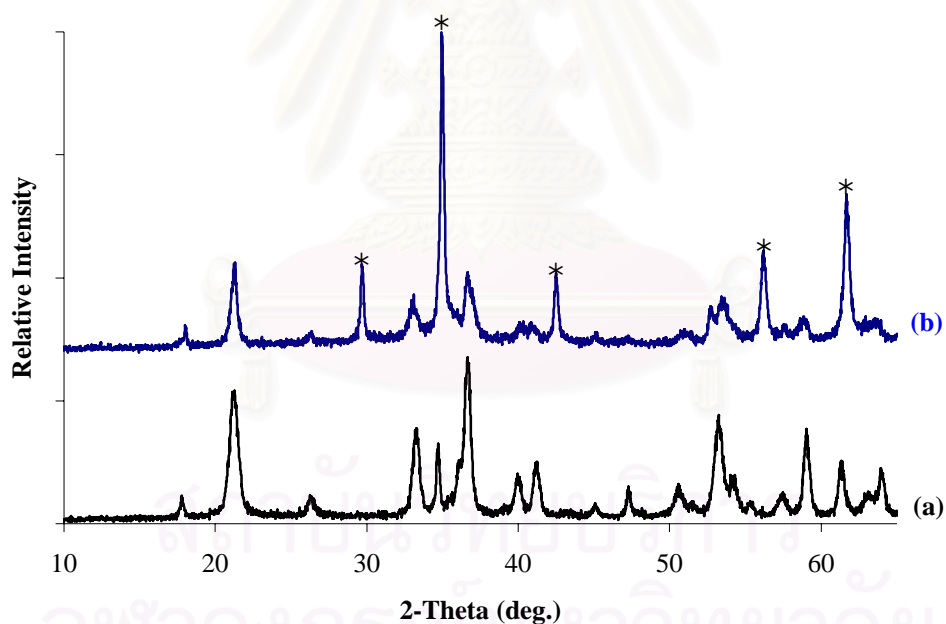


Figure 5.13 XRD patterns of (a) goethite and the product from CP method: (b) CP 70% Fe. * indicates Jacobsite phase.

5.3.4.2 Fourier transform infra-red spectrometer (FT-IR)

Figure 5.14 (b) shows the spectrum of the composite from CP method. As previously mentioned, XRD shows that sample is the mixtures of jacobsite and goethite. The spectra of CP 70% Fe gives the features of mainly α -FeOOH without the presence of other strong bands.

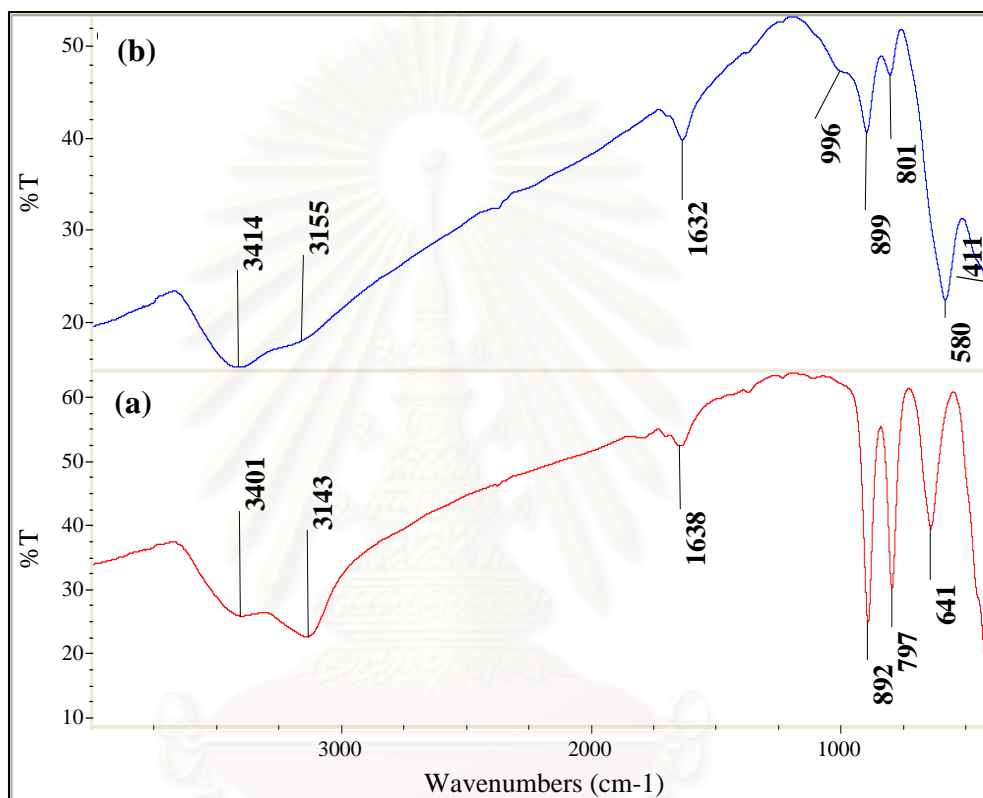


Figure 5.14 Infrared spectra of (a) goethite and the product from CP method: (b) CP 70% Fe.

On the basis IR, the main feature of CP 70 % Fe sample belongs to goethite, while the appearance of MnFe_2O_4 is very small. However, the XRD pattern suggests the presence of crystalline jacobsite. This suggests that it should be noted that the Mn ions may be left in the solution after the synthetic reaction. Most Mn and Fe ions are coprecipitated, resulting to the crystalline jacobsite as a major product, and the remained Fe ions go to precipitate as only goethite phase.

5.3.5 Structural and chemical properties comparison

In this section, the comparison of physical and chemical properties of obtained composites will be presented. The physical structure is characterized by using the fundamental analytical techniques, including XRD, FT-IR, SEM-EDX, and specific surface area. The chemical property is the determination of iron content in samples using permanganate titration.

5.3.5.1 X-ray diffraction (XRD)

The XRD patterns of all composite samples with similar Fe/Mn wt ratio from EP, CP and CT methods are compared in Figure 5.15 along with the patterns of PS 70% Fe. For the composites, prepared from Fe-polycation by using ferric nitrate salt, both patterns are similar to PS method. The XRD analysis also indicates the presence of the goethite crystalline phase with the reflections (110), (111), (130), (111), (021), and (140). The reflection peak broadening comes from the nanometer crystallite sizes of α -FeOOH particles, as listed in Table 5.8.

Table 5.8 The result of phase analysis and crystallite sizes, as determined by the strongest line in XRD pattern, of all Mn-FeO_x composites.

sample	FeOOH phase	Crystallite size (Å)
CIEP	Poorly ordered β -FeOOH	129
CICT	Poorly ordered β -FeOOH	122
NtEP	α -FeOOH	122
NtCT	α -FeOOH	112
CP 70% Fe	α -FeOOH	190
PS 70% Fe	α -FeOOH	169

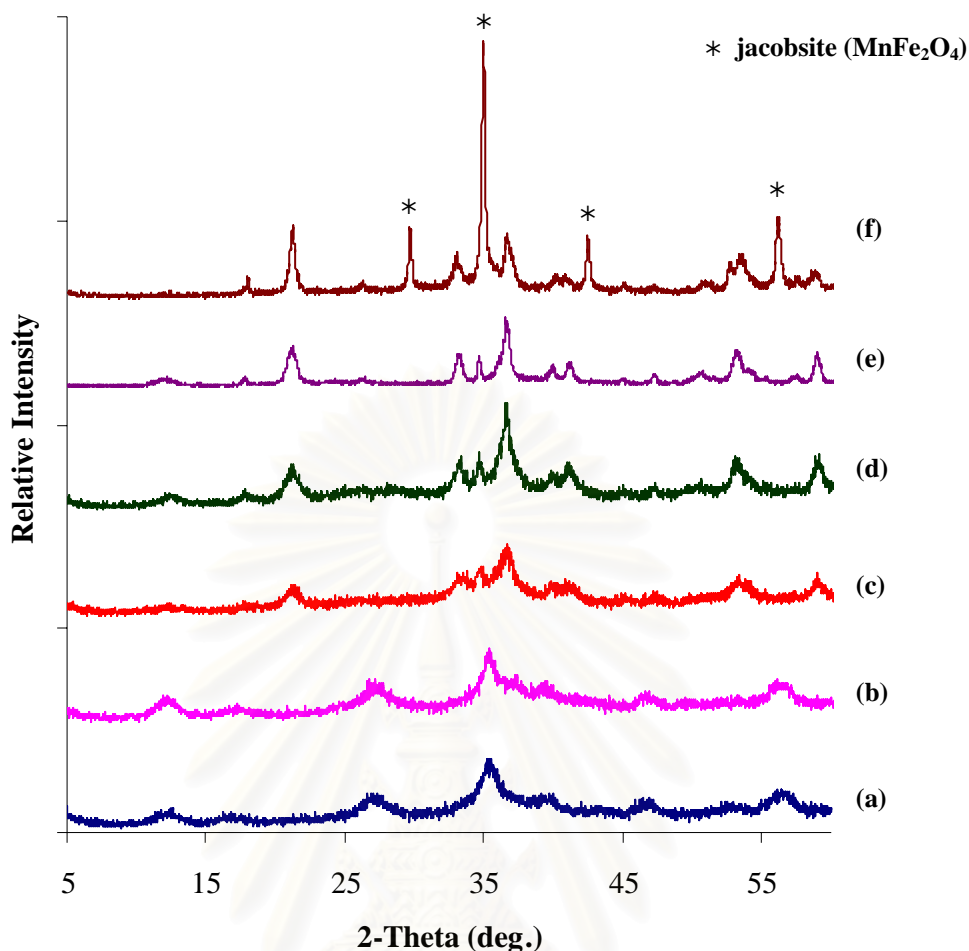


Figure 5.15 XRD patterns of Mn-FeO_x composites from EP method: (a) CIEP and (c) NtEP, CT method: (b) CICT and (d) NtCT, PS method: (e) PS 70% Fe, and CP method: (f) CP 70% Fe.

In both CT and EP samples prepared from ferric chloride salt, the identification of FeOOH phase is difficult because of nearly amorphous structure, and lack of order resulting in the broad and weak peak in the XRD patterns. However, the patterns may regard closely to akaganeite (β -FeOOH). Exceptional CP 70% Fe sample is observed goethite structure, with the presence of manganese-iron oxide compound, jacobsite.

5.3.5.2 Fourier transform infra-red spectrometer (FT-IR)

The FT-IR spectra of composite samples are compared in Figure 5.16. The broad band near 3400 cm^{-1} , together with a relatively strong band at about 1635 cm^{-1} ,

can be assigned to the stretching vibrations and deformation of water, in all spectra. In other word, the hydroxyl group exists in all composite structures, which is also active surface sites for adsorption or ion-exchanged. For the wide band appearing at 400-700 cm^{-1} may be due to the presence of birnessite, which masks some characteristic bands of FeOOH .

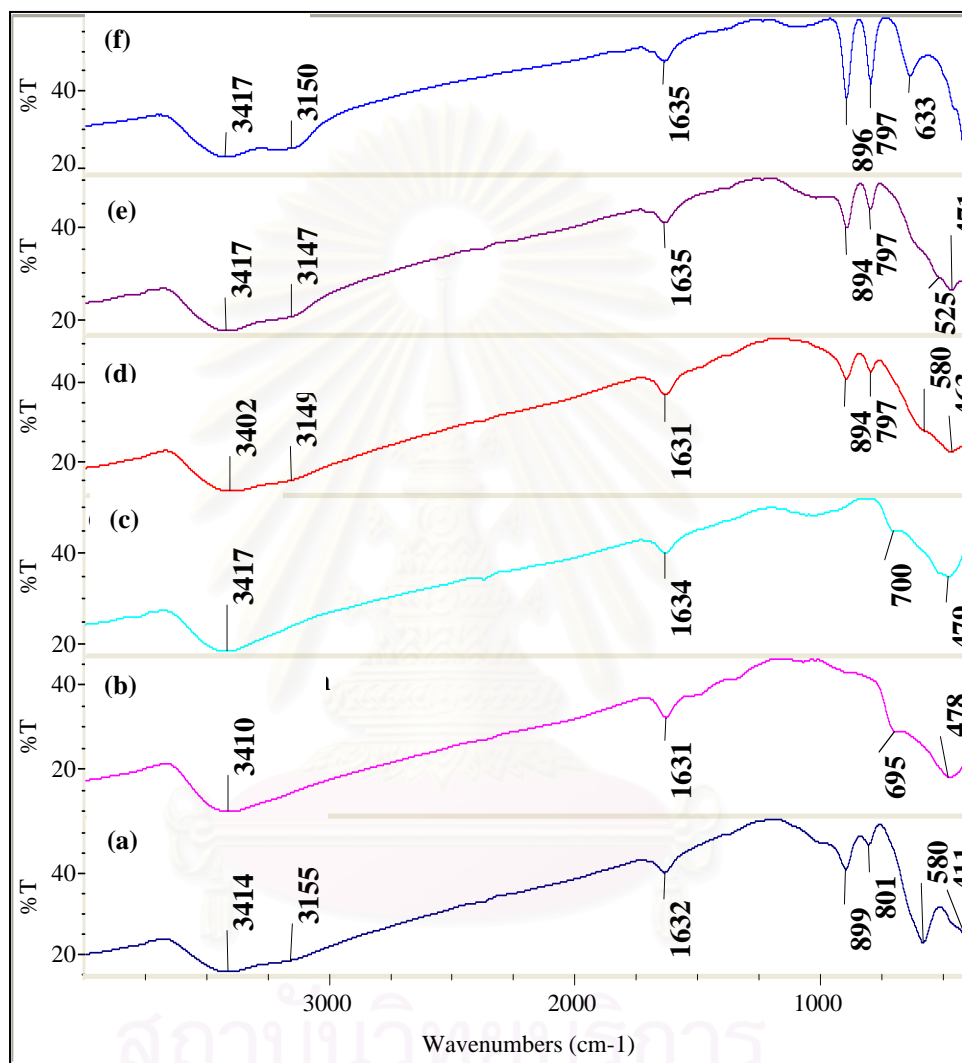


Figure 5.16 Infrared spectra of Mn- FeO_x composite from CP method: (a) CP 70% Fe, EP method: (b) CIEP and (d) NtEP, CT method: (c) CICT and (e) NtCT, and PS method: (f) PS 70% Fe.

IR spectra of the products from nitrate salt are closed to goethite, giving the strongest absorption band at 797 and 894 cm^{-1} characteristics of the Fe-O-H bending in goethite. Whereas the spectrum from chloride salt does not show any absorption band at 800-1100 cm^{-1} , indicating the absence of the α - FeOOH in composite.

In case of CP 70% Fe, the characteristic bands of goethite can be observed and the broad band at 400-700 cm^{-1} appears due to the M-O bonding of jacobsite.

From these results, they confirm that the presence of goethite in Mn-FeO_x composites could be achieved by using ferric nitrate. On the other hand, in the presence of chloride salt, both EP and CT methods do not yield goethite in composites, but poorly crystalline β -FeOOH under the same preparation conditions. Besides, the CP 70% Fe composite is composed of the mixtures of goethite and jacobsite phases. It may be explained that the addition of manganese ion at initial precipitation prefers the coprecipitation of MnFe₂O₄ than the formation of birnessite and goethite.

5.3.5.3 SEM-EDX

To investigate distribution of metal on Mn-FeO_x composites, elemental ion mapping of samples is illustrated in Figure 5.17. Bright points represent the signal of the manganese and iron, respectively from the solid samples. As seen in Figure 5.17(a), elemental mapping from physical mixture sample shows the separated locations of Mn and Fe ions. These results confirm that goethite and birnessite in the PS 70% Fe exhibit discrete oxide particles of each metal. In addition, goethite appears to be more abundant on the sample than the birnessite according to the 70% by weight of Fe. On the other hand, Mn and Fe are spread over all composites synthesized by EP, CT, and CP methods. The relative distributions of Fe and Mn present similar to that amount of iron contents from potassium permanganate titration method. Overall, it can be concluded that separated FeOOH particle does not form in the chemically synthesized composites. Therefore, the synthetic method for the preparation of these composites results in the homogeneous distribution of Fe ion in the composite structures. In other word, a separation of FeOOH phase from birnessite is not form.

We further suggest that the surface morphology, as seen in SEM images, of the CT and CP composites is observed as a rough surface, where as those obtained by EP method present the smooth clean surface. The rough area is due to a non-uniform coating of FeOOH on birnessite substrate surface. On the other hand, the composite

from EP method is built from the dispersed birnessite a encapsulating goethite, showing the smooth sheet structure of birnessite in SEM images.

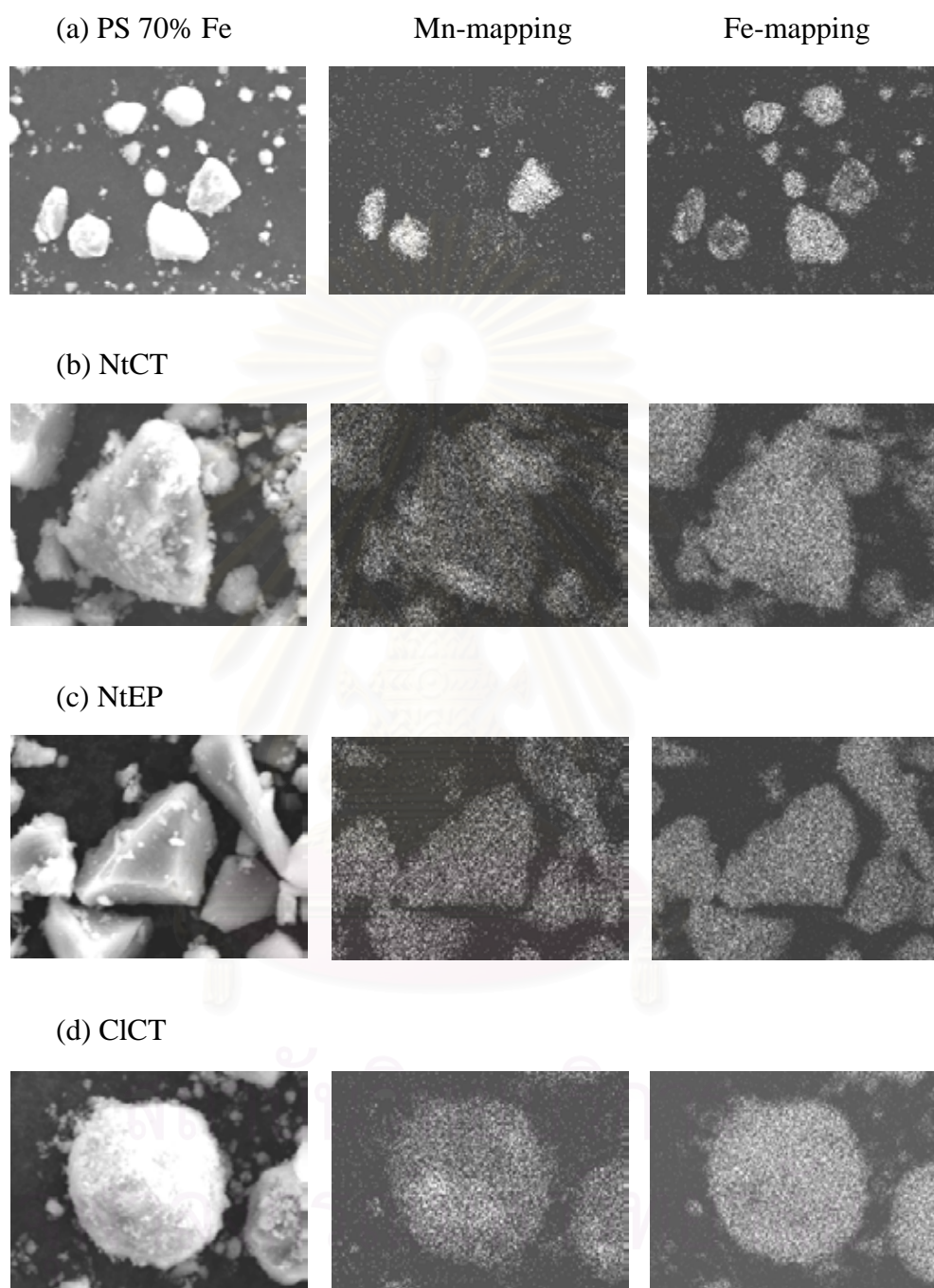


Figure 5.17 EDX mapping of Mn and Fe on Mn-FeO_x composites from PS method: (a) PS 70% Fe, EP method: (c) CIEP and (e) NtEP, CT method: (b) NtCT and (d) CICT, and CP method: (f) CP 70% Fe.

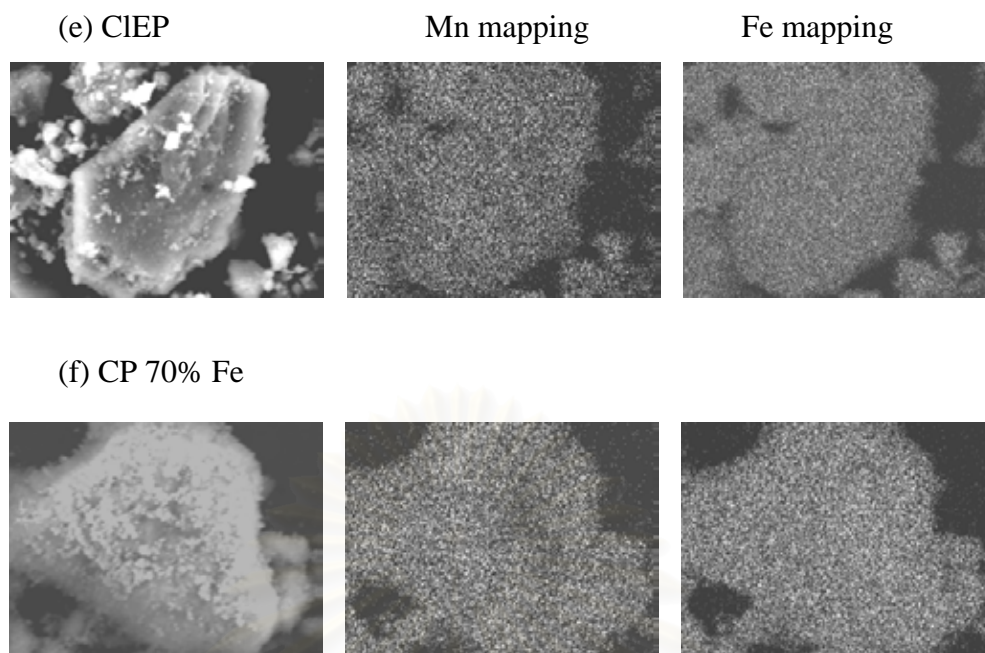


Figure 5.17(cont.) EDX mapping of Mn and Fe on Mn-FeO_x composites from PS method: (a) PS 70% Fe, EP method: (c) CIEP and (e) NtEP, CT method: (b) NtCT and (d) ClCT, and CP method: (f) CP 70% Fe.

5.3.5.4 Determination of iron content in composite

The iron content in composite samples is determined by using redox titration method. Figure 5.18 illustrates the relationship between weight of goethite (mg) and volume of KMnO₄ at the end point. We can calculate the % by weight of Fe from the weight of FeOOH. The results are listed in Table 5.9.

สถาบันวิทยบริการ
จุฬาลงกรณ์มหาวิทยาลัย

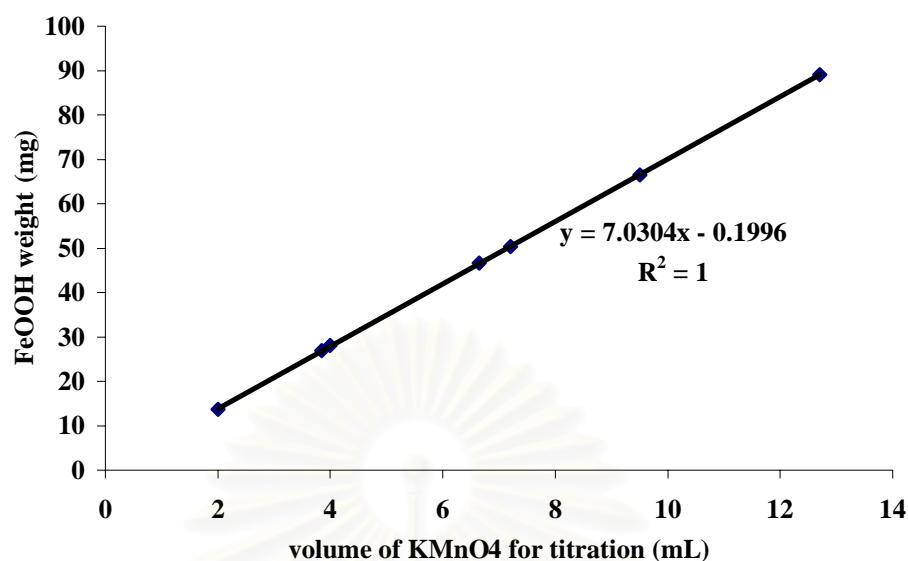


Figure 5.18 Calibration curve for iron content determination by redox titration.

As seen from Table 5.9, the amount of % Fe by weight is nearly similar to the loading amount. The amount of % Fe in all composites, with 70% wt Fe loading, is ranged from 65.74 to 69.01 % wt FeOOH.

Table 5.9 Iron contents in Mn-FeO_x composites.

sample	% wt. Fe in sample					% wt. FeOOH
	first	second	average	SD.	%RSD	
goethite	59.41	59.00	59.21	0.29	0.49	100.00
PS 70% Fe	40.30	40.17	40.24	0.09	0.23	67.96
NtEP	38.94	38.90	38.92	0.03	0.07	65.74
NtCT	40.90	40.82	40.86	0.06	0.14	69.01
ClCT	39.71	39.30	39.51	0.29	0.73	66.73
CIEP	40.00	39.91	39.96	0.06	0.16	67.49
CP 70% Fe	40.61	40.99	40.80	0.27	0.66	68.91

5.3.5.5 N₂ adsorption-desorption isotherms

In order to compare the surface area of all composites, nitrogen adsorption-desorption isotherms are measured at liquid nitrogen temperature. In addition, the surface area and pore size distribution are investigated using BET and BJH analysis, respectively. These results are summarized in Table 5.10. However, the N₂ isotherm of CP 70% Fe sample is not determined because of the unwanted jacobite phase and its lowest adsorption capacity for Cu²⁺ ions.

Upon the chemically synthetic methods for Mn-FeO_x composite, the BET specific surface area largely increases as compared with that of PS 70% Fe. Comparing the type of composite, the surface area decreases in the following order: NtEP ≈ CIEP > NtCT > CICT > PS 70% Fe. In addition, the enhanced surface areas of EP samples are mainly created by disordered structures of birnessite particles that are prepared by exfoliation reaction. Furthermore, both composites prepared by CT method give higher surface area than PS 70% Fe. It may be suggested that some Fe-polycation occupies the interlayer region of birnessite by ion-exchange or/and intercalation process, resulting in the increase of surface area. In case of a higher surface area of composites from NtCT over CICT, it is due to the presence of goethite phase.

Table 5.10 Specific surface area and pore size distribution for birnessite, goethite and various Mn-FeO_x composites.

sample	Pore size (Å)	S _{BET} (m ² /g)
HMnO ₂ ht	37.87	299.55
goethite	280.41	172.45
PS 70% Fe	288.51	211.01
CICT	55.84	274.05
CIEP	48.68	381.54
NtCP	94.09	342.08
NtEP	38.24	372.92

The pore size distribution of all composites has diameter less than 500 Å, indicating the mesopores structure (diameter of 20-500 Å), ranged from 30 to 300 Å. EP and CT composites exhibit dramatically small pore size relative to the parent materials. This is caused by the formation of FeOOH particle under the presence of birnessite condition.

5.4 Adsorption

The batch adsorption studies are conducted under slightly acidic condition of pH 5.5. The main reason is that heavy metals normally start to precipitate under alkaline conditions by forming metal oxides and hydroxides. Copper ion is expected to precipitate as hydroxide species at $\text{pH} \geq 6$. Therefore, a slightly acidic solution ensures that adsorption on specified composites is restricted to Cu divalent ions rather than intervened by copper hydroxide species. Especially, heavy metals are usually found in a cationic form in wastewater.

Therefore, this experiment is carried under the buffer solution of pH 5.5, contact time of 24 h, and copper initial concentration of 100 mg/l.

5.4.1 Birnessite

First of all, birnessite synthesized by solid state and hydrothermal methods are used as adsorbents to measure their copper sorption capacities in order to choose the suitable layered substrate for further development for composite adsorbents. The adsorption capacities of all synthesized birnessites are reported in Table 5.11. The Cu^{2+} ion removal of KMnO_2 ht is higher than that of KMnO_2 ss for 6 times. It can be explained that KMnO_2 ht has a crystallite size smaller than KMnO_2 ss, resulting to large surface area and its sorption affinity. Furthermore, hydrothermal condition creates a higher solvation of water for interlayer K^+ ion than solid state method produces under heat treatment. The K^+ ions in KMnO_2 ht are easily exchanged with the Cu^{2+} ions than KMnO_2 ss.

Table 5.11 The adsorption capacities of Cu^{2+} ions onto birnessite samples.

adsorbent	Adsorption capacity (mg Cu/ g adsorbent)		
	average	SD.	%RSD
KMnO ₂ ht	63.13	2.28	3.61
HMnO ₂ ht	64.50	1.72	2.67
KMnO ₂ ss	10.16	0.23	2.23
HMnO ₂ ss	21.09	0.51	2.44

When the KMnO₂ samples are treated with acid solution, the H⁺ ions are located in the interlayer region instead of K⁺ ions. The sorption of HMnO₂ ht (64.50 mg/g) gives nearly the same value of KMnO₂ ht, whereas HMnO₂ ss (21.09 mg/g) gives 2 folded increase from KMnO₂ ss sample. In the case of hydrothermal method, the amounts of solvated water molecules around K⁺ ions and H⁺ ions are not much different, indicating by closely *d*-values in their XRD patterns. In addition, both KMnO₂ ht and HMnO₂ ht have about the same crystallite sizes. In contrary, after acid-exchange of KMnO₂ ss, H⁺ interlayer appears to be solvated by more water molecules, reaching the same *d*-value as that of HMnO₂ ht, resulting to improve in adsorption capacity. Furthermore, XRD data of KMnO₂ ss and HMnO₂ ss suggests the low sorption is due to the presence of impurity phase of MnO₂ and their large crystallite sizes.

From this result, HMnO₂ ht is chosen as the starting birnessite for synthesis of EP composites.

5.4.2 Composites

The adsorption capacity of Cu^{2+} ion onto various composites is reported in Table 5.12. Removal of Cu^{2+} ion by goethite, synthesized for this project, (8.55 mg/g) is higher than previously reported by Vaughan (2.67 mg/g), Egirani (2.54 mg/g) and, Sherman (7.25 mg/g). This is due to its high surface area, obtained by rapidly hydrolysis of ferric chloride in alkaline solution. The adsorption of goethite is greatly improved by modification with birnessite. Adsorption of Cu^{2+} ions onto Mn-FeO_x composites, prepared by various approaches at 70% wt Fe, decreases in the following

fashion: NtEP (33.29 mg/g) > CIEP (28.89 mg/g) > PS 70% Fe (24.65 mg/g) \approx NtCT (24.13 mg/g) \approx CICT (24.08 mg/g) > CP 70% Fe (15.45 mg/g). Results indicate that the amount of adsorbed copper is higher for EP sample than for the physical mixture. It is due to the great dispersion of birnessite in composite samples, giving high surface areas. CIEP composite presents the higher surface area but the iron oxide phase is not goethite, but resembles to akaganeite instead. This result makes its lower adsorption than NtEP.

Table 5.12 Iron contents, Cu adsorption capacities, and specific surface areas for birnessite, goethite and various Mn-FeO_x composites.

adsorbent	% wt FeOOH from titration	adsorption capacity (mg Cu/g adsorbent)	S _{BET} (m ² /g)
HMnO ₂ ht	0	63.13	299.55
goethite	100	8.55	172.45
PS 70% Fe	68.10	24.65	211.01
CP 70% Fe	68.26	15.45	NA
CICT	66.03	24.08	274.05
CIEP	67.37	28.89	381.54
NtCT	68.82	24.13	342.08
NtEP	66.05	33.29	372.92

The adsorption capacity is greatly improved by EP method, but not CT method. This could be explained that, in the case of EP method, birnessite sheets are separated individually before precipitation by the adsorption of goethite. With this approach, both birnessite and goethite will have high surface area.

In the CP method, its adsorption is the lowest, due to the presence of crystalline phase (MnFe₂O₄) in composite. The large crystallite size is always unappreciable, because it results to low surface area and sorption affinity.

From these results, the NtEP is selected for further Cu²⁺ and Pb²⁺ ions adsorption studies.

5.5 Properties of NtEP composite

Synthesis and characterization of NtEP samples with 5-30 % wt Mn loading are investigated. The characterization is determined by using XRD, and FT-IR and the iron content is identified by titration method. Adsorption capacities towards copper and lead ions are studied, by comparison to the capacities of physical mixtures at similar metal compositions.

5.5.1 X-ray diffraction (XRD)

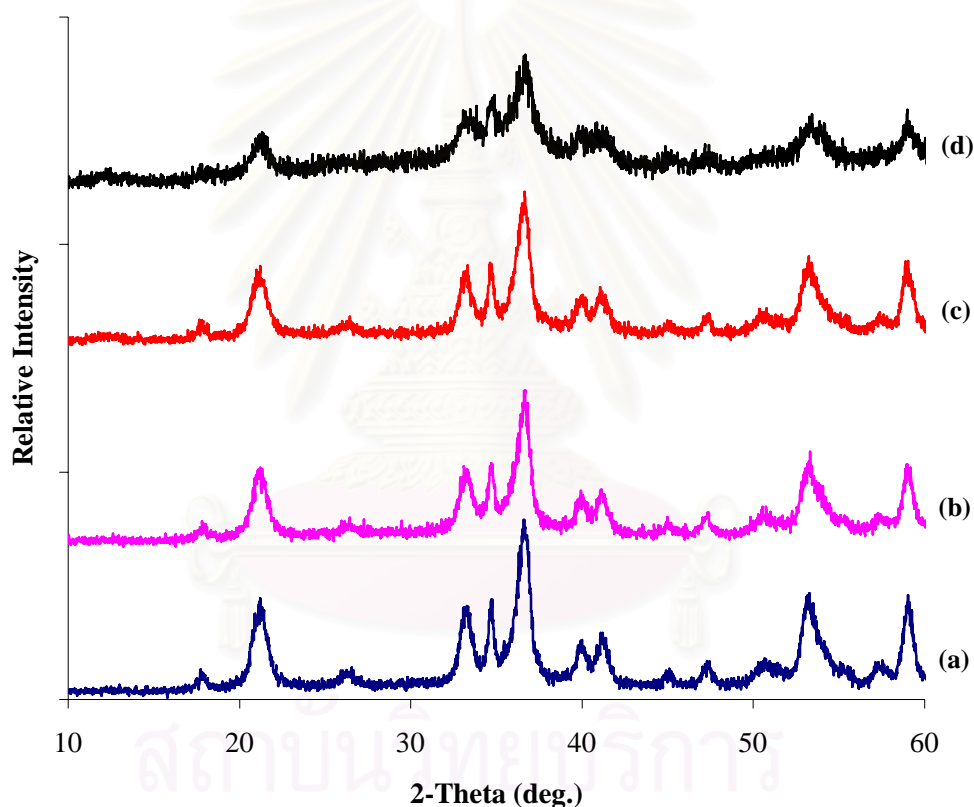


Figure 5.19 XRD patterns of NtEP composites at different % wt Mn loading: (a) 5%, (b) 10%, (c) 20%, and (d) 30%.

Figure 5.19 shows the XRD patterns of the NtEP samples at different % wt Mn loading. When a small amount of birnessite is added (5% wt Mn), the pattern shows only a single phase of goethite. Further addition of Mn slightly changes the pattern to lower relative intensities. Pure birnessite and other iron oxide phases are not found, by increasing Mn proportion. However, as the Mn loading increases to 20% wt

or greater, the patterns are consisted of broad and low intensed peaks of goethite as compares to that of parent. Furthermore, the birnessite is hardly detected in pattern, even for 30% wt Mn loading. It is due to a poorly crystalline or disorder structure of birnessite in the matrix of goethite.

5.5.2 Fourier transform infra-red spectrometer (FT-IR)

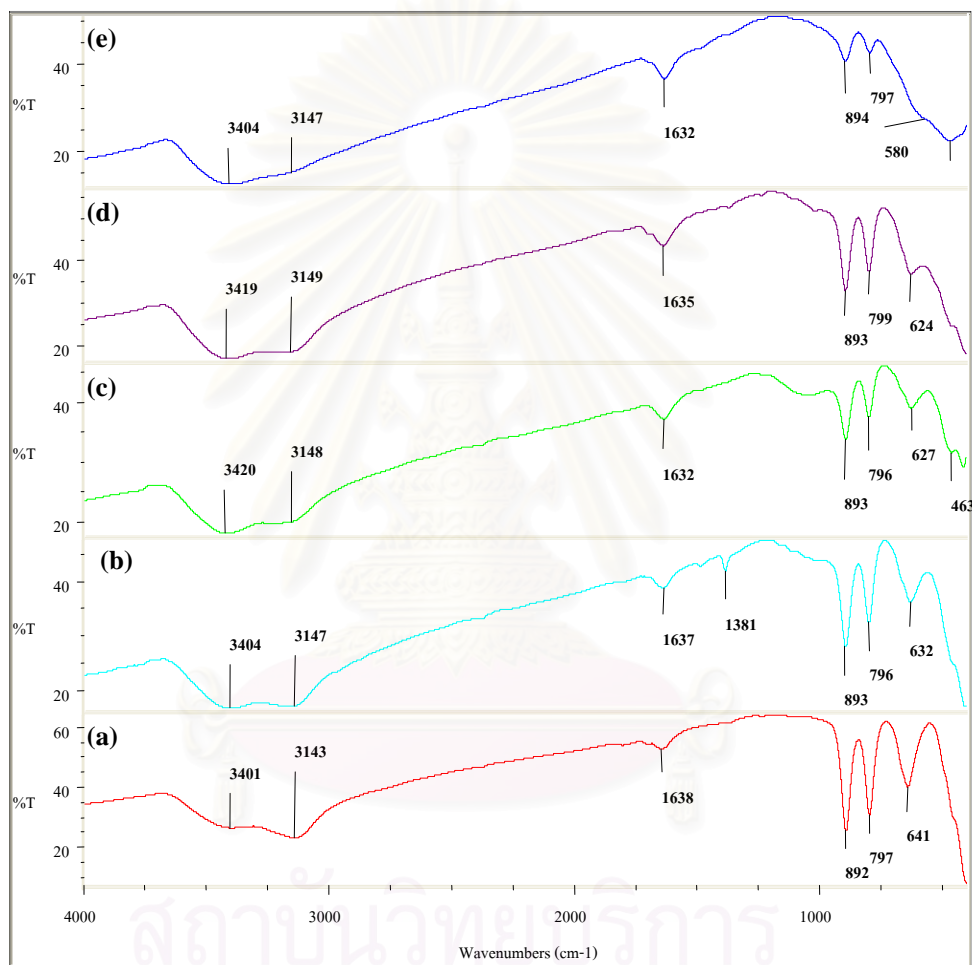


Figure 5.20 Infrared spectra of NtEP composites at different % wt Mn loading: (a) 0%, (b) 5%, (c) 10%, and (d) 20% and (e) 30%.

Figure 5.20 displays the FT-IR spectra of the NtEP samples at different % wt. Mn loading. The Fe pure sample gives absorption bands in good agreement with those previously reported for goethite. When Mn is added, the peak intensity is decreased. It turns into a weak absorption band upon increasing the Mn contents. In the 20% wt Mn

or larger Mn composition, the strong Mn-O stretching vibration bands from birnessite masks the characteristic goethite band (641 and 400 cm^{-1}).

Based on results from XRD and FT-IR, it can be concluded that the addition of birnessite is not largely effect to the phase of iron oxide. The composite is composed of pure goethite with the presence of birnessite within structure.

5.5.3 Iron content in NtEP composite

The iron contents of PS and NtEP samples at varied % Mn loadings are reported in Table 5.13, and 5.14, respectively. The iron content in samples is calculated by using the equation derived form calibration curve of permanganate titration in section 5.3.5.4. The values are converted to % FeOOH by weight in sample in order to easily compare the data for adsorption.

Table 5.13 Iron contents in PS samples using permanganate titration.

sample	% wt. Fe in sample					% wt FeOOH
	first	second	average	SD.	%RSD	
goethite	59.41	59.00	59.21	0.29	0.49	100
Fe 95%	55.06	55.00	55.03	0.04	0.08	92.73
Fe 90%	51.76	51.60	51.68	0.11	0.22	87.05
Fe 80%	45.66	45.80	45.73	0.10	0.22	76.65
Fe 70%	40.30	40.17	40.24	0.09	0.23	68.10
Fe 60%	32.70	32.80	32.75	0.07	0.22	55.74

Table 5.14 Iron contents in NtEP samples using permanganate titration.

Sample % wt Mn loading	% wt Fe in sample					% wt FeOOH
	first	second	average	SD.	%RSD	
Mn 5%	52.10	51.91	52.01	0.13	0.26	87.59
Mn 10%	49.14	49.50	49.32	0.25	0.52	83.07
Mn 20%	46.51	46.63	46.57	0.08	0.18	78.44
Mn 30%	38.94	38.90	38.92	0.03	0.07	65.55

5.5.4 Cu adsorption on NtEP composite

The adsorption capacities of Cu^{2+} ions onto PS and NtEP samples are listed in Table 5.15, and 5.16, respectively.

Table 5.15 Adsorption capacities of Cu^{2+} ions onto PS samples.

sample	% wt FeOOH in sample	Adsorption capacity (mg Cu/ g adsorbent)		
		average	SD.	%RSD
goethite	100 %	8.55	0.27	3.12
Fe 95%	92.73 %	13.66	0.59	4.35
Fe 90%	87.05 %	16.72	0.71	4.27
Fe 80%	76.65 %	19.15	0.91	4.73
Fe 70%	68.10 %	24.65	0.83	3.38
Fe 60%	55.74 %	30.00	1.00	3.32
birnessite	0%	64.50	1.72	2.67

Table 5.16 Adsorption capacities of Cu^{2+} ions onto NtEP samples.

sample	%wt FeOOH in sample	Adsorption capacity (mg Cu/ g adsorbent)		
		average	SD.	%RSD
Mn 5%	Fe 87.59 %	18.77	0.74	3.93
Mn 10%	Fe 83.07 %	19.89	0.23	1.18
Mn 20%	Fe 78.44 %	26.45	0.48	1.83
Mn 30%	Fe 66.55 %	33.29	0.77	2.30

From the table, it is difficult to compare their adsorption capacities of them. This is due to the different in real % FeOOH by weight in sample. Thus, the adsorption data and % wt FeOOH in composite are plotted in Figure 5.21.

Figure 5.21 shows that NtEP composites have a higher adsorption capacities as compared with PS samples at the same % wt FeOOH in sample. The effect of concentration of birnessite on adsorption affinity is investigated. As shown in Figure, dispersion of birnessite in composite improves the performance of goethite for heavy metal removal. Moreover, adsorption on composite is better at higher loading (>21 %

wt Mn) of birnessite. The highest removal is achieved from loaded birnessite with 33.55 % wt Mn.

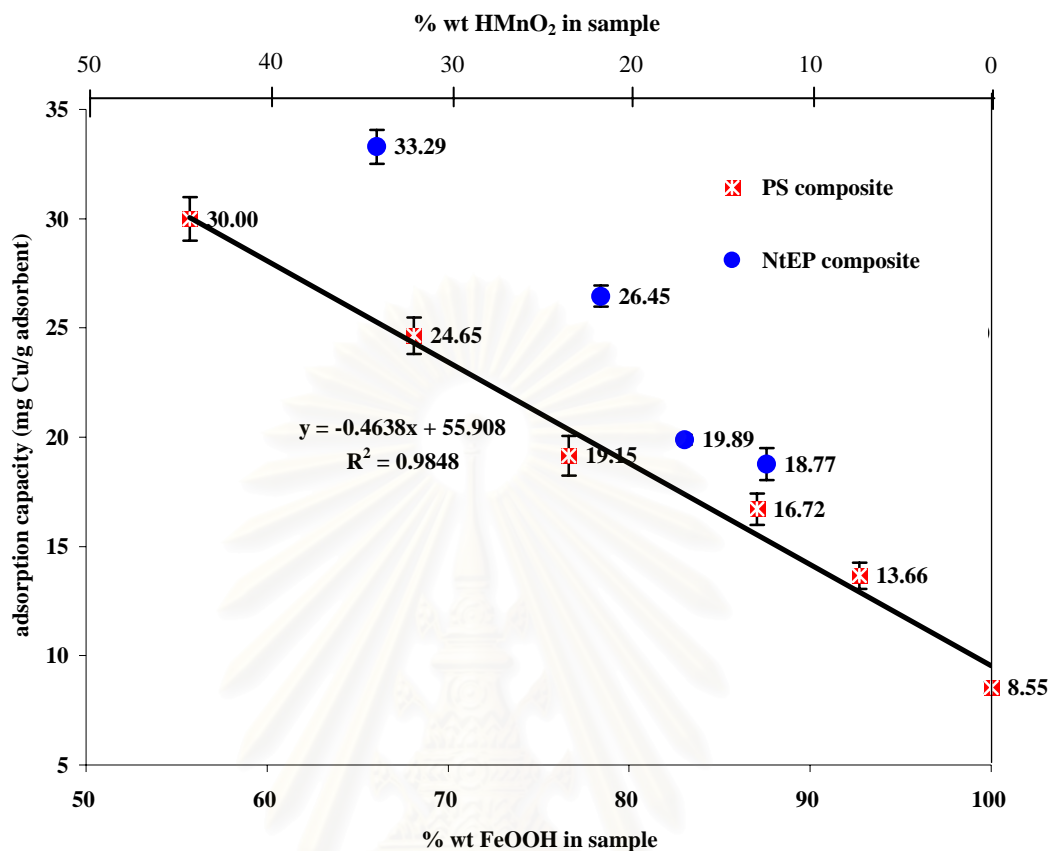


Figure 5.21 Effect of birnessite loading on Cu²⁺ ions adsorption onto NtEP composites.

5.5.5 Pb adsorption on NtEP composite

The Pb²⁺ adsorption studies are conducted under the same conditions (pH 5.5, adsorbent 0.030 g, and equilibrium time 24 h) in copper studies. Pb²⁺ ion adsorption is determined at high initial concentration (300 mg/l) due to the high adsorption capacities of goethite, birnessite and Mn-FeO_x composite for ions. This is due to the fact that metals of higher electronegativity are expected to have higher affinities. Thus, Pb²⁺ ion has a higher capacity than Cu²⁺ ion for those samples.

The effect of birnessite loading in composite on Pb²⁺ removal is shown in Figure 5.22. The modification of goethite results in increasing of adsorption with higher % wt Mn. With lower loading, a large modified surface area gives a large

higher capacity than physical mixture for Pb^{2+} ions. At higher loading, composite efficiency levels off. This can be attributed to distribution of birnessite on all areas of the goethite. However, higher quantities of birnessite may lead to saturation of dispersed surface. It means that some birnessite is separated as discreted oxide, resulting low adsorbed value than expected.

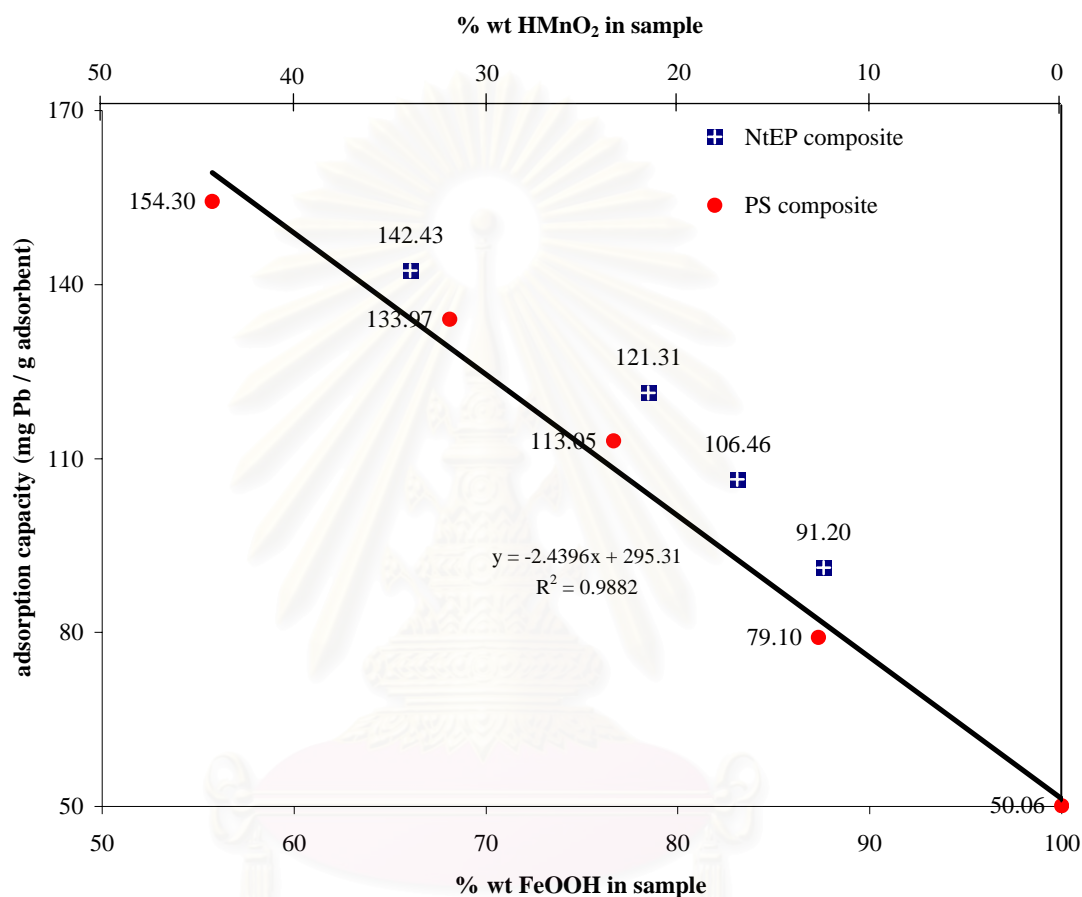
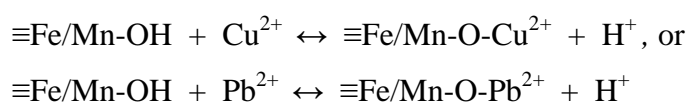


Figure 5.22 Effect of birnessite loading on Pb^{2+} ions adsorption onto NtEP composites.

In addition, the adsorption mechanism involves an exchange reaction of metal ion with H^+ on the composite surfaces. Based on the principle of ion exchanged, the more metal ions that are adsorbed onto composite, the more hydrogen ions are released. The complex reactions of $\text{Cu}^{2+}/\text{Pb}^{2+}$ ions with hydroxyl groups on Mn-FeO_x surface may be written as follows:



5.5.6 Filtration qualities

Filtration quality is an important property of adsorbents used in water treatment. The separation ability of adsorbents (goethite, birnessite, and NtEP at 75-95 % wt Fe) from adsorbate solution is evaluated. The centrifugation (3000 rpm) is used to categorize the adsorbents at 10, 20, and 30 min, respectively. After 10 min of centrifugation, 80% wt Fe sample separates from adsorbate solution, resulting to the clear solution. After 20 min, the separation of other adsorbent is not observed. In the case of birnessite and other composites, transparent colloidal solutions are obtained with most precipitates. Further centrifugation gives the results unchanged. However, in the case of goethite as adsorbent, the solution is still yellow turbid solution, even after 30 min of centrifugation. The increase in separation of composite is mainly due to the surface aggregation of goethite and birnessite. It would appear that dispersed birnessite changes the colloidal properties of goethite and increases aggregation of the particles, which results in the improved separation.

CHAPTER VI

CONCLUSIONS AND SUGGESTIONS

6.1 Conclusions

Manganese oxide-iron oxide composites are synthesized using four approaches: physical mixture (PS), exfoliation-precipitation (EP), coating (CT), and co-precipitation (CP). The hydrothermal method is chosen to prepare the starting birnessite for some approaches, because its completion for ion-exchange, ease of intercalation processes, and high surface area. Goethite is the chosen phase for absorption study because of its high adsorption capacity among other iron oxides.

The physical mixtures of goethite and birnessite, 70 - 95 % Fe to total metal, give no change in the chemical and structural properties, compared to their individual counterparts, pure goethite and proton birnessite. Their XRD patterns, IR spectra, specific surface areas, and heavy metal adsorption capacities provide features of each component. The dispersion of Fe and Mn over samples is poorly distributed.

EP and CT methods result higher dispersion of Fe and Mn over the composite samples. The anionic counter ion of ferric salts plays the important role to control the iron oxide phase. Although both ferric nitrate (Nt) and ferric chloride (Cl) give the FeOOH phase, the nitrate anion yields α -FeOOH (goethite), whereas the chloride anion leads to poorly crystalline β -FeOOH (akaganeite). For all cases, the manganese oxide phase is still birnessite, indicating both methods do not destroy the structure of starting preformed manganese oxide. The EP method, which the birnessite structure is dispersed prior to form composites with Fe-polycation, results to the Mn-FeO_x composites with higher BET surface area and higher adsorption capacities, comparing to the simple CT method. In

addition, goethite phase shows the higher surface area and higher adsorption capacities than akaganeite phase, for the same synthetic approach.

The CP approach leads to the composites of goethite and unwanted jacobite, MnFe_2O_4 . Jacobite has high crystallinity and low surface area, leading to lower adsorption capacity, even comparing to the PS of goethite and birnessite.

The adsorption capacities of composites, with 66 wt. % Fe to total metal, are tested with copper ion. The composite prepared by nitrate ion and EP method shows higher adsorption capacities for approximately 32 %, comparing to the PS of goethite and birnessite. The adsorption capacities could be arranged as the following trends: $\text{NtEP} > \text{CIEP} > \text{NtCT} \approx \text{CICT} \approx \text{PS} > \text{CP}$.

At pH 5.5, the composites, NtEP, have the adsorption capacities towards copper ion and lead ion higher than the PS of goethite and birnessite at all similar weight percent of Fe to total metal.

The filtration quality of the composites is dramatically improved, as compared to the PS. However, the clear solution is only obtained by using the composites with 80 wt % Fe to total metal as an adsorbent.

6.2 Suggestion for further work

From the obtained results, further work shall be focused on the following:

1. To observe the adsorption capacity for other heavy metal ions such as nickel, zinc, and cadmium onto obtained composites.
2. To determine the adsorption isotherm of copper and lead ions onto NtEP composites.

REFERENCES

1. Alexandrova, L.; Grigorov, L. Precipitate and adsorbing colloid flotation of dissolved copper, lead and zinc ions. *International Journal of Mineral Processing*, **1996**, *48*, 111-125.
2. Blöcher, C.; Dorda, J.; Mavrov, V.; Chimel, H.; Lazaridis, N. K.; Matis, K. A. Hybrid flotation-membrane filtration process for the removal of heavy metal ions from wastewater. *Water Research*, **2003**, *37*, 4018-4026.
3. Dabrowski, A.; Hubicki, Z.; Podkoscielny, P.; Robens, E. Selective removal of the heavy metal ions from waters and industrial wastewaters by ion-exchange method. *Chemosphere*, **2004**, *56*, 91-106.
4. Bailey, S. E.; Olin, T. S.; Bricka, R. M.; Adrain, D. D. A review of potentially low-cost sorbents for heavy metals. *Water Research*, **1998**, *33*, 2469-2479.
5. Gabaldon, C.; Marzal, P.; Ferrer, J.; Seco, A. Single and competitive adsorption of Cd and Zn onto a granular activated carbon. *Water Research*, **1996**, *12*, 3050-3060.
6. Gupta, V. K.; Srivastava, S. K.; Mohan, D.; Sharma, S. Design parameters for fixed bed reactors of activated carbon developed from fertilizer waste for the removal of some heavy metal ions. *Waste Management*, **1997**, *17*, 517-522.
7. Kadirvelu, K.; Thamaraiselvi, K.; Namasivayam, C. Removal of heavy metals from industrial wastewaters by adsorption onto activated carbon prepared from an agricultural solid waste. *Bioresource Technology*, **2001**, *76*, 63-65.
8. Babel, S.; Kurniawan, T. A. Low-cost adsorbents for heavy metals uptake from contraminated water: a review. *Journal of Hazardous Materials*, **2003**, *B97*, 219-243.
9. Rajeshwarisivaraj; Sivakumar, S.; Senthilkumar, P.; Subburam, V. Carbon fom Cassava pell, an agricultural waste, as an adsorbent in the removal of dyes and metal ions from aqueous solution. *Bioresource Technology*, **2001**, *80*, 233-235.

10. Sheta, A. S.; Falatah, A. M.; Al-Sewailem, M. S.; Khaled, E. M.; Sallam A. S. Sorption characteristics of zinc and iron by natural zeolite and bentonite. *Microporous and Mesoporous Materials*, **2003**, *61*, 127-136.
11. Sen, T. K.; Mahajan, S. P.; Khailar, K. C. Adsorption of Cu^{2+} and Ni^{2+} on iron oxide and its importance on Ni^{2+} transport in porous media. *Colloids and Surfaces A: Physicochemical Engineering Aspects*, **2002**, *211*, 91-102.
12. Kanungo, S. B.; Tripathy, S. S.; Mishra, S. K.; Sahoo, B.; Rajeev. Adsorption of Co^{2+} , Ni^{2+} , Cu^{2+} , and Zn^{2+} onto amorphous hydrous manganese dioxide from simple (1-1) electrolyte solutions. *Journal of Colloid and Interface Science*, **2004**, *269*, 11-21.
13. Juang, R. S.; Wu, W. L. Adsorption of sulfate and Copper(II) on goethite in relation to the changes of zeta potentials. *Journal of Colloid and Interface Science*, **2002**, *249*, 22-29.
14. Rietra, R. P. J. J.; Hiemstra, T.; van Riemsdijk, W. H. Sulfate adsorption on goethite. *Journal of Colloid and Interface Science*, **1999**, *218*, 511-521.
15. Manceau, A. The mechanism of anion adsorption on iron oxides: evidence for the bonding of arsenate tetrahedra on free $\text{Fe}(\text{O},\text{OH})_6$ edges. *Geochimica et Cosmochimica Acta*, **1995**, *59*, 3647-3653.
16. Parkman, R. H.; Charnock, J. M.; Bryan, N. D.; Livens, F. R.; Vaughan, D. J. Reactions of copper and cadmium ions in aqueous solution with goethite, lepidocrocite, mackinawite, and pyrite. *American Mineralogist*, **1999**, *84*, 407-419.
17. Beukes, J. P.; Giesekke, E. W.; Elliott, W. Nickel retention by goethite and hematite. *Minerals Engineering*, **2000**, *13*, 1573-1579.
18. Pivovarov, S. Adsorption of cadmium onto hematite: Temperature dependence. *Journal of Colloid and Interface Science*, **2001**, *234*, 1-8.
19. Vaclavikova, M.; Jakabsky, S.; Hredzak, S. Magnetic nanoscale particles as sorbents for removal of heavy metal ions. 497-484.
20. Gadde, R. R.; Laitinen, H. A. Studies of heavy metal adsorption by hydrous iron and manganese oxides. *Analytical Chemistry*, **1974**, *46*, 2022-2026.

21. Chorover, J.; Amistadi, M. K. Reaction of forest floor organic matter at goethite, birnessite and smectite surface. *Geochimica et Cosmochimica Acta*, **2001**, *65*, 95-109.
22. Dong, D.; Nelson, Y. M.; Lion, L. W.; Shuler, M. L.; Ghiorse, W. C. Adsorption of Pb and Cd onto metal oxides and organic material in natural surface coatings as determined by selective extractions: new evidence for the importance of Mn and Fe oxides. *Water Research*, **1999**, *34*, 427-436.
23. Lo, S. L.; Jeng, H. J.; Lai, C. H. Characteristics and adsorption properties of iron-coated sand. *Water Science and Technology*, **1997**, *35*, 63-70.
24. Khaodhair, S.; Azizian, M. F.; Osathaphan, P. O. Copper, chromium, and arsenic adsorption and equilibrium modeling in an iron-oxide-coated sand, background electrolyte system. *Water air and Soil Pollution*, **2000**, *119*, 105-120.
25. Lai, C. H.; Lo, S. L.; Lin, C. F. Evaluating an iron-coated sand for removing copper from water. *Water Science and Technology*, **1994**, *30*, 175-182.
26. Lai, C. H.; Chen, C. Y.; Shin, P. H.; Hsia, T. H. Competitive adsorption of copper and lead ions on an iron-coated sand from water. *Water Science and Technology*, **2000**, *42*, 149-154.
27. Vaishaya, R. C.; Gupta, S. K. Coated sand filtration: an emerging technology for water treatment. *Journal of Water Supply Research and Technology-aqua*, **2003**, *52*, 299-306.
28. Xu, Y.; Axe, L. Synthesis and characterization of iron oxide-coated silica and its effect on metal adsorption. *Journal of Colloid and Interface Science*, available online at www.sciencedirect.com
29. Lee, C. I.; Yang, W. F.; Hsieh, C. I. Removal of copper (II) by manganese-coated sand in a liquid fluidized-bed reactor. *Journal of Hazardous Materials*, **2004**, *B114*, 45-51.
30. Hu, P. Y.; Hsieh, Y. H.; Chen, J. C.; Chang, C. Y. Characteristics of manganese-coated sand using SEM and EDAX analysis. *Journal of Colloid and Interface Science*, **2004**, *272*, 308-313.

31. Khraisheh, M. A. M.; Al-degs, Y. S.; Mcminn, W. A. M. Remediation of wastewater containing heavy metals using raw and modified diatomite. *Chemical Engineering Journal*, **2004**, *99*, 177-184.
32. Liu, D.; Teng, Z.; Sansalone, J. J. Cartledge, F. K. Surface characteristics of sorptive-filtration storm water media. II: higher specific gravity ($\rho_s > 1.0$) oxide-coated fixed media. *Journal of Environmental Engineering*, **2001**, *127*, 879-888.
33. Villalobos, M.; Bargar, J.; Sposito, G. Mechanisms of Pb(II) sorption on a biogenic manganese oxide. *Environmental Science & Technology*, **2005**, *39*, 569-576.
34. Tamura, H.; Furuichi, R. Adsorption affinity of divalent heavy metal ions for metal oxides evaluated by modeling with the Frumkin isotherm. *Journal of Colloid and Interface Science*, **1997**, *195*, 241-249.
35. Choy, J. H.; Lee, H. C.; Jung, H.; Kim, H.; Boo, H. Exfoliation and restacking route to anatase-layered titanate nanohybrid with enhanced photocatalytic activity. *Chemistry of Materials*, **2002**, *14*, 2486-2491.
36. Kooli, F.; Sasaki, T.; Watanabe, M. Microporosity and acidity properties of alumina pillared titanates. *Langmuir*, **1999**, *15*, 1090-1095.
37. Liu, Z. H.; Yang, X.; Makita, Y.; Ooi, K. Preparation of a polycation-intercalated layered manganese oxide nanocomposite by a delamination/reassembling process. *Chemistry of Materials*, **2002**, *14*, 4800-4806.
38. Wang, L.; Sasaki, N.; Ebina, Y.; Takada, K.; Sasaki, T. Inorganic multilayer films of manganese oxide nanosheets and aluminum polyoxocations: fabrication, structure, and electrochemical behavior. *Chemistry of Materials*, **2005**, *17*, 1352-1357.
39. Egirani, D. E.; Baker, A. R. ; Andrews, J. E. Copper and zinc removal from aqueous solution by mixed mineral systems I. reactivity and removal kinetics. *Journal of Colloid and Interface Science*, available online at www.sciencedirect.com.
40. Podda, D. P.; Johnson, B. B.; Wells, J. D. Modeling the effect of temperature on adsorption of Lead(II) and zinc(II) onto goethite at constant pH. *Journal of Colloid and Interface Science*, **1996**, *184*, 365-377.

41. Peacock, C. L.; Sherman, D. M. Copper(II) sorption onto goethite, hematite and lepidocrocite: a surface complexation model based on ab initio molecular geometries and EXAFS spectroscopy. *Geochimica et Cosmochimica Acta*, **2004**, *68*, 2623–2637.
42. Trivedi, P.; Axe, L.; Dyer, J. Adsorption of metal ions onto goethite: single-adsorbate and competitive systems. *Journal of Colloid and Interface Science*, **2001**, *191*, 107-121.
43. Kanungo, S. B.; Tripathy, S. S.; Rajeev Adsorption of Co, Ni, Cu, and Zn on hydrous manganese dioxide from complex electrolyte solutions resembling sea water in major ion content. *Journal of Colloid and Interface Science*, **2004**, *269*, 1-10.
44. Thipathy, S. S.; Kanungo, S. B. Adsorption of Co^{2+} , Ni^{2+} , Cu^{2+} and Zn^{2+} from 0.5 M NaCl and major ion sea water on a mixture of $\delta\text{-MnO}_2$ and amorphous FeOOH. *Journal of Colloid and Interface Science*, available online at www.sciencedirect.com.
45. Li, X.; Pan, G.; Qin, Y.; Hu, T.; Wu, Z.; Xie, Y. EXAFS studies on adsorption–desorption reversibility at manganese oxide–water interfaces II. reversible adsorption of zinc on $\delta\text{-MnO}_2$. *Journal of Colloid and Interface Science*, **2004**, *271*, 35-40.
46. Lai, C. H.; Lo, S. L.; Chiang, H. L. Adsorption/desorption properties of copper ions on the surface of iron-coated sand using BET and EDAX analyses. *Chemosphere*, **2000**, *41*, 1249-1255.
47. Green-Pedersen, H.; Pind, N. Preparation, characterization, and sorption properties for Ni(II) of iron oxyhydroxide–montmorillonite. *Colloids and Surfaces A: Physicochemical and Engineering Aspects*, **2000**, *168*, 133–145.
48. Boonfueng, T.; Axe, L.; Xu, Y. Properties and structure of manganese oxide-coated clay. *Journal of Colloid and Interface Science*, **2005**, *281*, 80-92.
49. Benjamin, M. M.; Sletten, R. S.; Bailay, R. P.; Bennett, T. Sorption and filtration of metals using iron-oxide-coated-sand. *Water Research*, **1996**, *30*, 2609-2620.
50. Al-Sewailem M. S.; Khaled, E. M.; Mashhady, A. S. Retention of copper by desert sands coated with ferric hydroxides. *Geoderma*, **1999**, *89*, 249-258.

51. Ebina, Y.; Sasaki, T.; Harada, M.; Watanabe, M. Restacked perovskite nanosheets and their Pt-loaded materials as photocatalysts. *Chemistry of Materials*, **2002**, *14*, 4390-4395.
52. Belver, C.; Vicente, M. A.; Martinez, A. A.; Fernandez, G. M. Fe-saponite pillared and impregnated catalysts II. nature of the iron species active for the reduction of NO_x with propene. *Applied Catalysis B: Environmental*, **2004**, *50*, 227-234.
53. Kooli, F.; Sasaki, T.; Rives, V.; Watanabe, M. Synthesis and characterization of a new mesoporous alumina-pillared titanate with a double-layer arrangement structure. *Journal of Materials Chemistry*, **1999**, *10*, 497-501.
54. Wang, L.; Takada, K.; Kajiyama, A.; Onoda, M.; Michiue, Y.; Zang, L.; Watanabe, M.; Sasaki, T. Synthesis of a Li-Mn-oxide with disordered layer stacking through flocculation of exfoliated MnO₂ nanosheets, and its electrochemical properties. *Chemistry of Materials*, **2003**, *15*, 4508-4514.
55. Xu, Y.; Feng, Q.; Kajiyoshi, K.; Yanagisawa, K.; Yang, X.; Makita, Y.; Kasaishi, S.; Ooi, K. Hydrothermal syntheses of layered lithium nickel manganese oxides from mixed layered Ni(OH)₂-manganese oxides. *Chemistry of Materials*, **2002**, *14*, 3844-3851.
56. Gumton, C. Adsorption: should we care. *Regolith*, **2004**, 112-116.
57. Drever, J. I. The geochemistry of natural water, Eaglewood Criffs, USA, Prentice-Hall, **1982**.
58. Oxide and hydroxide minerals. Available from: <http://mineral.gly.bris.ac.uk/mineralogy/17.oxides>.
59. Oxides and hydroxides. Available from: www.soils.edu/courses/SS325/oxides.
60. Post, J. E. Manganese oxide minerals: crystal structures and economic and environmental significance. *Proceedings of the National Academy of Sciences of the United States of America*, **1999**, *96*, 3447-3454.
61. Ching, S.; Petrovay, D. J.; Jorgensen, M. L. Sol-gel synthesis of layered birnessite-type manganese oxides. *Inorganic Chemistry*, **1997**, *36*, 883-890.
62. Robert, A. S.; Tom, P.; Gerhard, L.; Nick, G. Pillared clays and pillared layered solids (technical report). *Pure Apply Chemistry*, **1999**, *71*, 2367-2371.

63. Moore, D. M.; Reynolds, Jr. R. C. X-ray diffraction and the identification and analysis of clay minerals, New York, USA, Oxford University Press, **1989**.
64. Basic operating principles of the sorptomatic 1990. Available from: <http://saf.chem.ox.ac.uk/Instruments/BET/sorpoptprin>.
65. Gilbert, H. A. Quantitative chemical analysis, New York, USA, Harper & Row, **1968**.
66. Kosmulshi, M.; Maczka, E.; Jartych, E.; Rosenholm, J. B. Synthesis and characterization of goethite and goethite-hematite composite: experimental study and literature survey. *Advances in Colloid and Interface Science*, **2003**, *103*, 57-76.
67. Lui, Z. H.; Ooi, K.; Kanoh, H.; Tang, W. P.; Tomida, T. Swelling and delamination behaviors of birnessite-type manganese oxide by intercalation tetraalkyl-ammonium ions. *Langmuir*, **2000**, *16*, 4154-4164.
68. Wang, L.; Takada, K.; Kajiyama, A.; Onoda, M.; Michiu, Y.; Zhang, L.; Watanabe, M.; Sasaki, T. Preparation of nanometer-sized manganese oxide by intercalation of organic ammonium ions in synthetic birsite OL-1. *Chemistry of Materials*, **2003**, *15*, 4508-4514.
69. Govea, L. V.; Steinfink, H. Thermal stability and magnetic properties of Fe-polyoxocation intercalated montmorillonite. *Chemistry of Materials*, **1997**, *9*, 894-856.
70. Krehula, S.; Popović, S.; Musić, S. Synthesis of acicular α -FeOOH particles at a very high pH. *Materials Letters*, **2002**, *54*, 108-113.
71. Yang, X.; Makita, Y.; Liu, Z. H.; Sakane, K.; Ooi, K. Structural characterization of a self-assembled MnO₂ nanosheets from birnessite manganese oxide single crystals. *Chemistry of Materials*, **2004**, *16*, 2002-2010.
72. Brock, S. L.; Sanabria, M.; Suib, S. L. Particle size control and self-assembly processes in novel colloids of nanocrystalline manganese oxide. *The Journal of Physical Chemistry B*, **1999**, *103*, 7416-7428.
73. Heylen, I.; Vansant, E. F. The difference in adsorption capacity between Fe-PILCs and modified Fe-BuA- and Fe-Zr-PILCs. *Microporous Materials*, **1997**, *10*, 41-50.

74. Cai, J.; Liu, J.; Gao, Z.; Navrotsky, A.; Suib S. L. Synthesis and anion exchange of tunnel structure akaganeite. *Chemistry of Materials*, **2001**, *13*, 4595-4602.
75. Deliyanni, E. A.; Bakoyannakis, D. N.; Zouboulis A. I.; Matis, K. A.; Nalbandian, L. Akaganeite-type β -FeO(OH) nanocrystals: preparation and characterization. *Microporous and Mesoporous Materials*, **2001**, *42*, 49-57.



สถาบันวิทยบริการ
จุฬาลงกรณ์มหาวิทยาลัย



Appendices

สถาบันวิทยบริการ
จุฬาลงกรณ์มหาวิทยาลัย

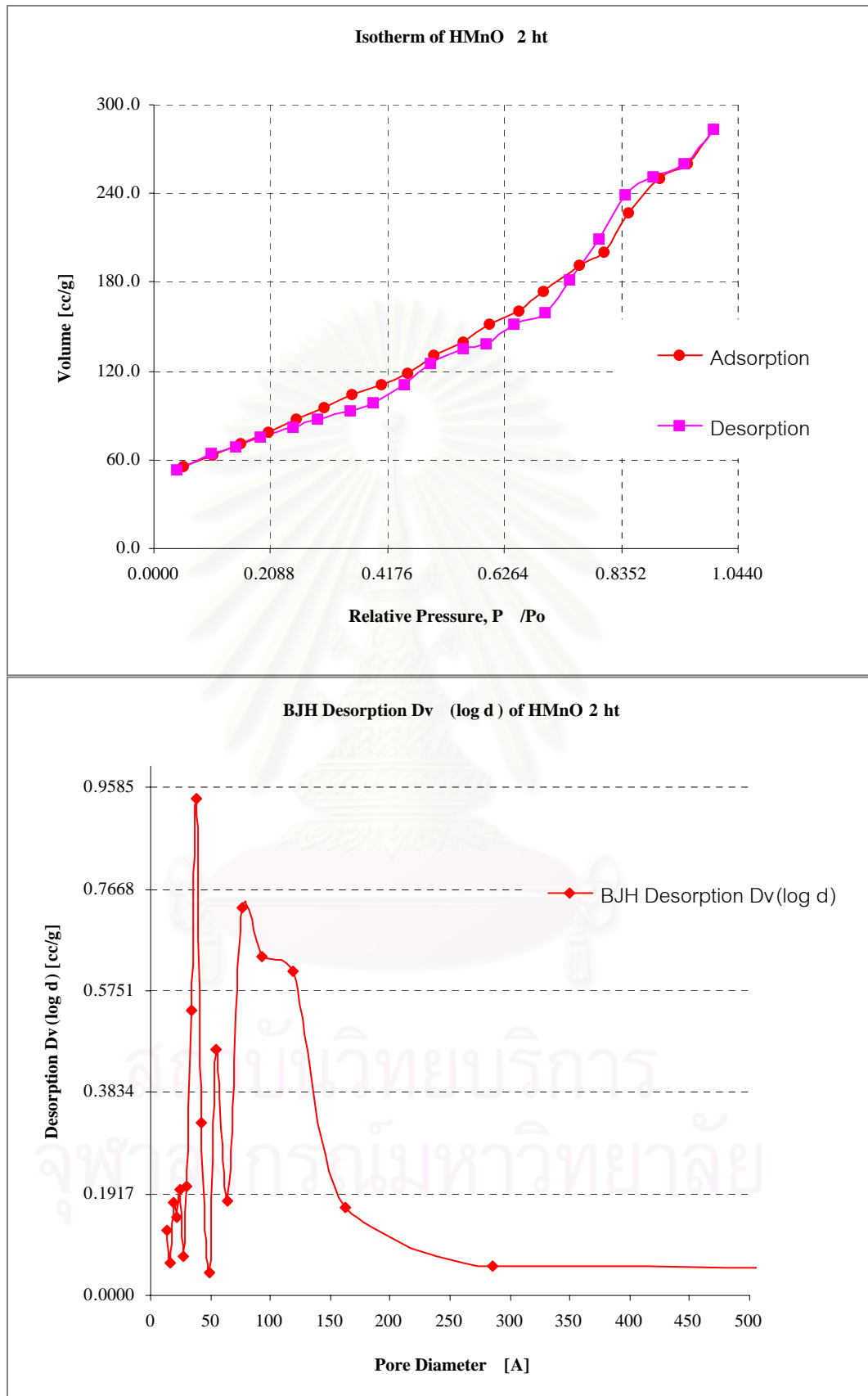


Figure A-1 N₂ adsorption-desorption isotherm and pore sizes distribution of HMnO₂ ht.

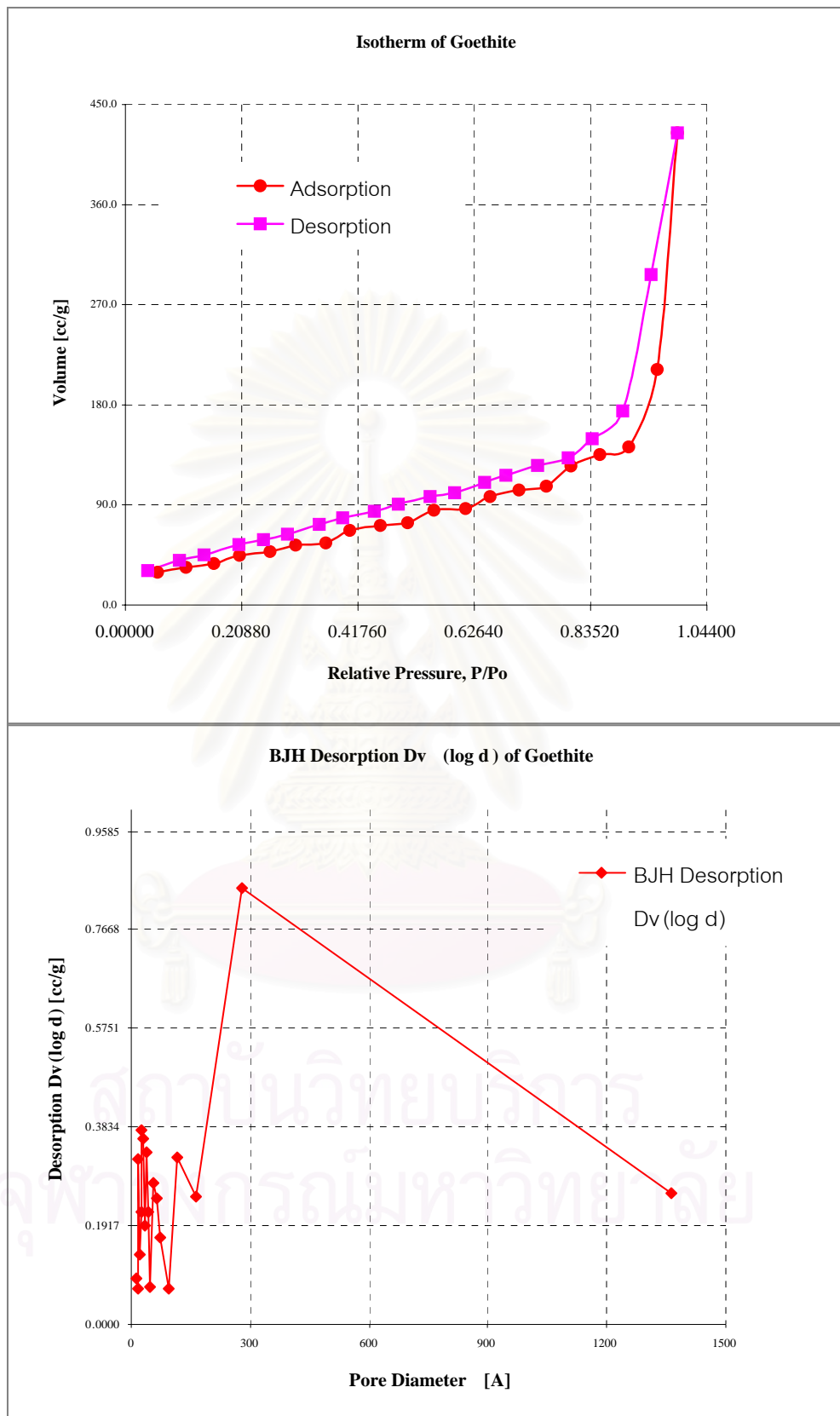


Figure A-2 N_2 adsorption-desorption isotherm and pore sizes distribution of Goethite.

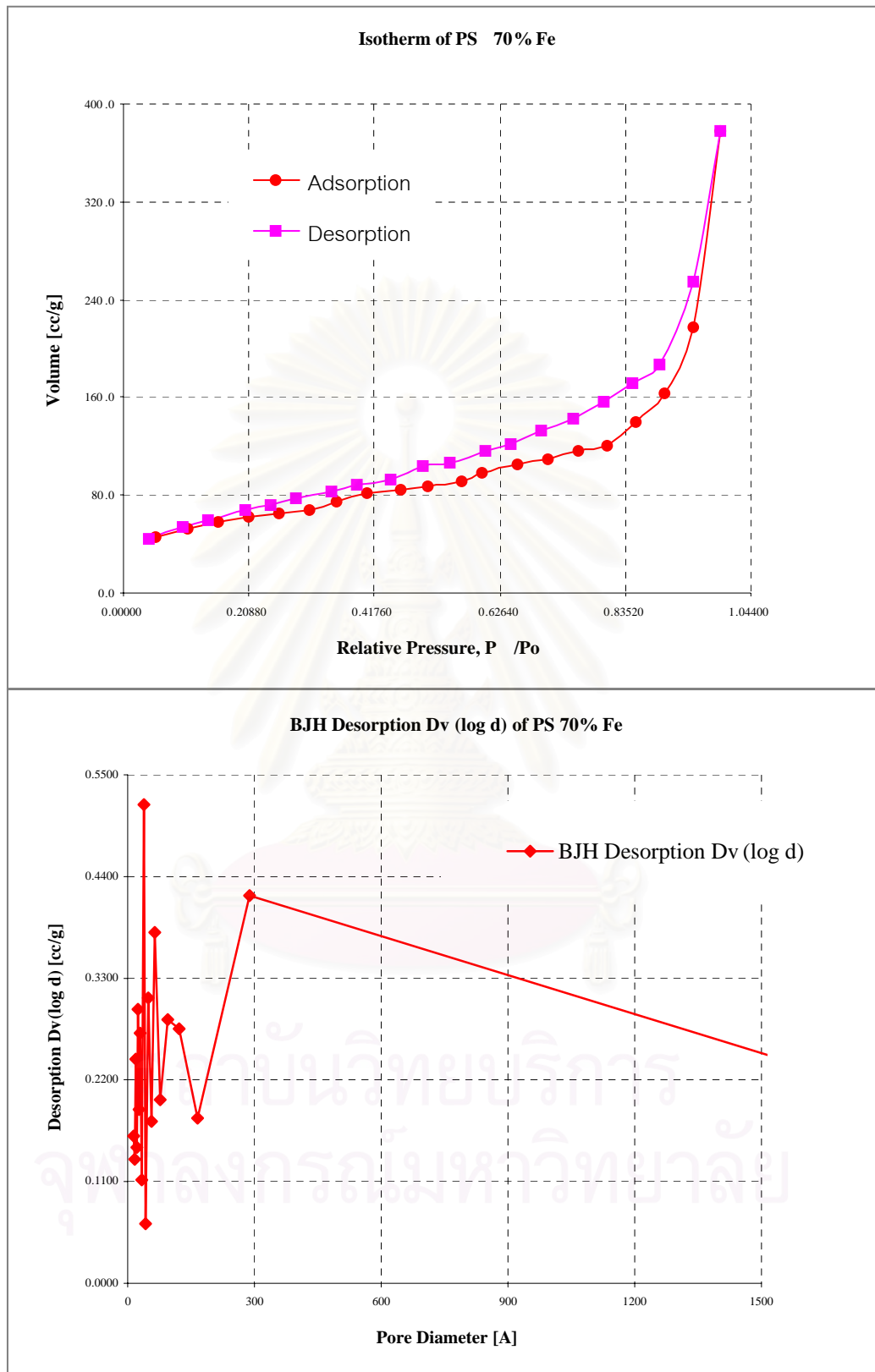


Figure A-3 N_2 adsorption-desorption isotherm and pore sizes distribution of PS 70% Fe.

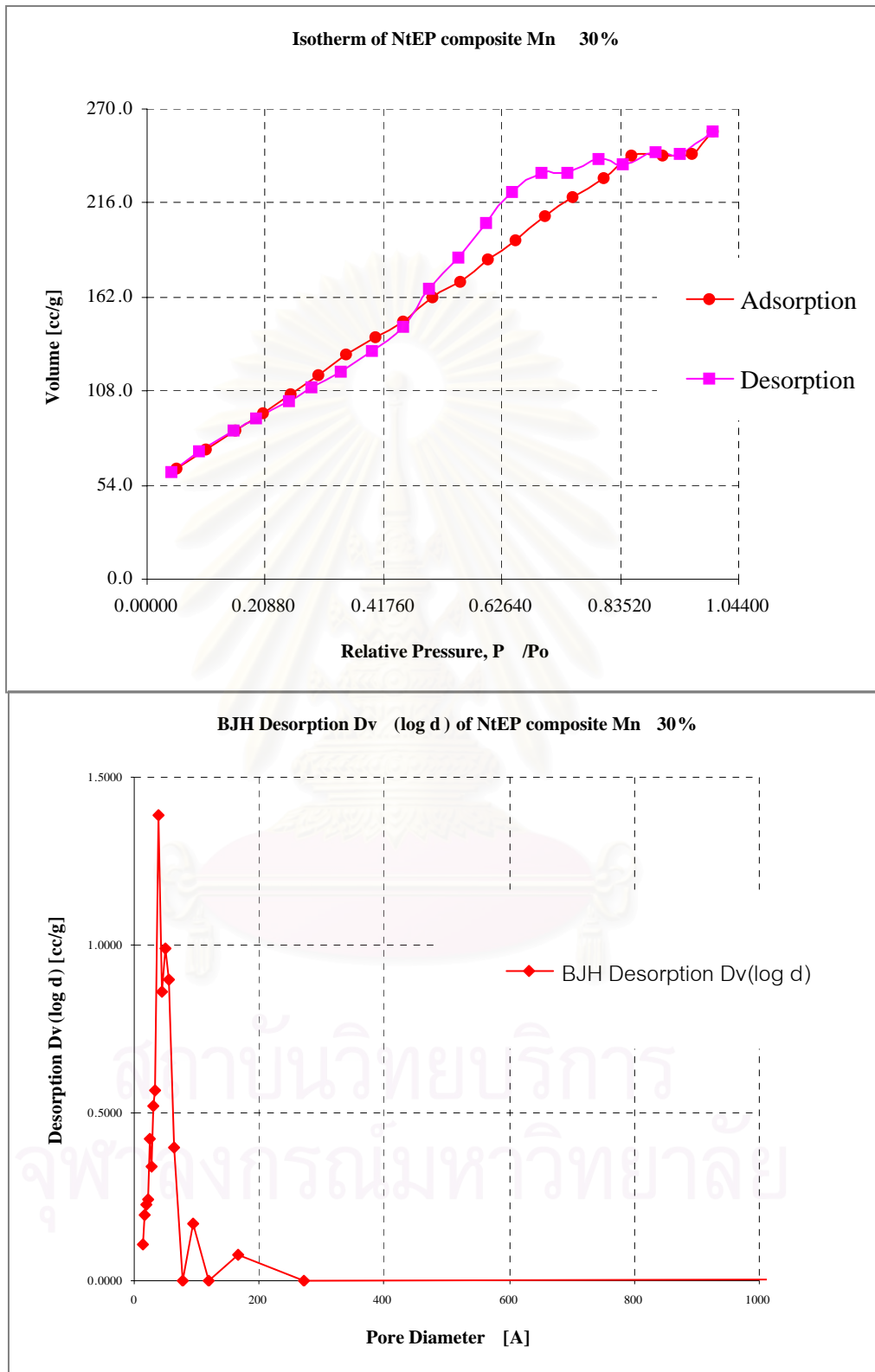


Figure A-4 N_2 adsorption-desorption isotherm and pore sizes distribution of NtEP composite.

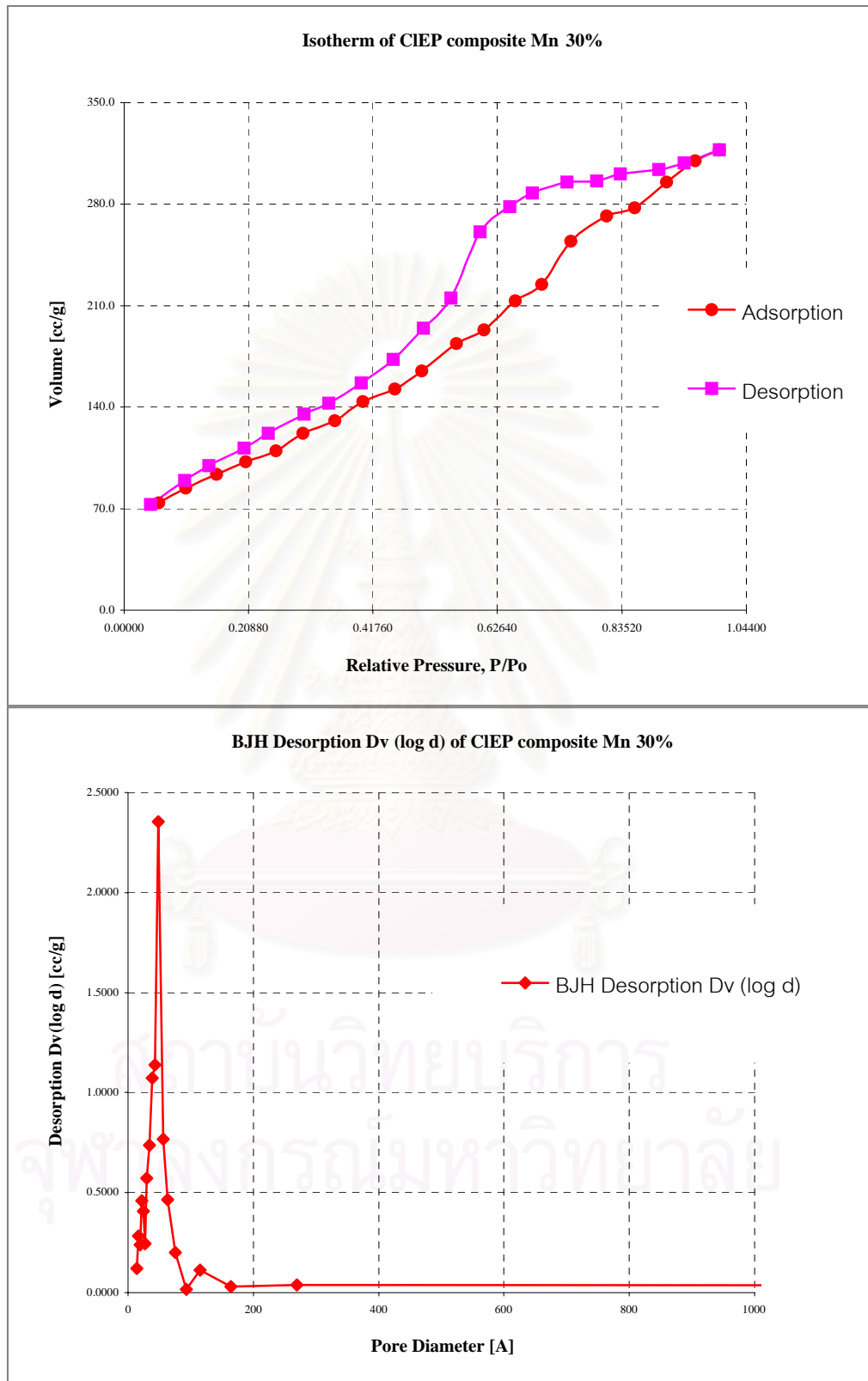


Figure A-5 N_2 adsorption-desorption isotherm and pore sizes distribution of CIEP composite.

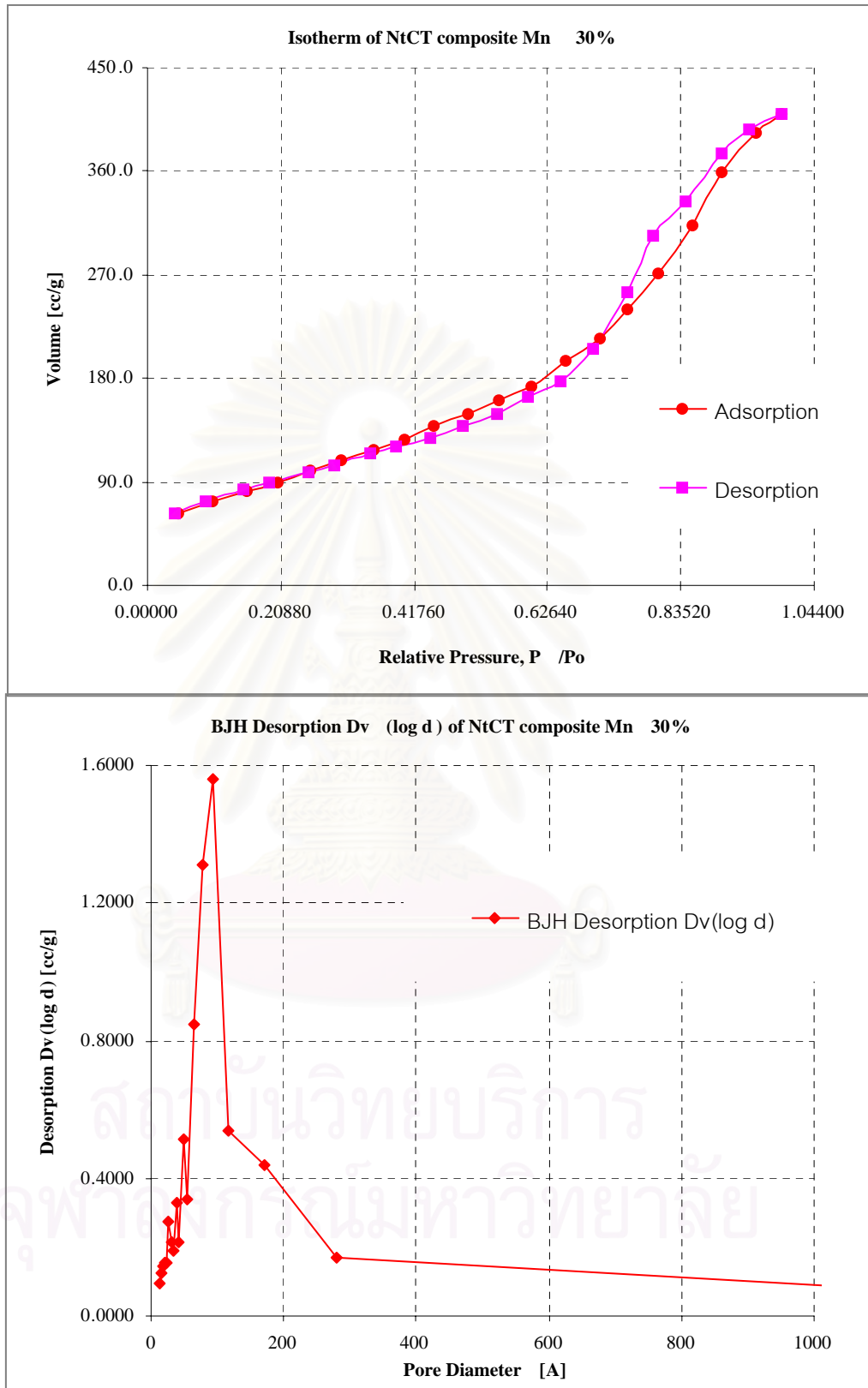


Figure A-6 N_2 adsorption-desorption isotherm and pore sizes distribution of NtCT composite.

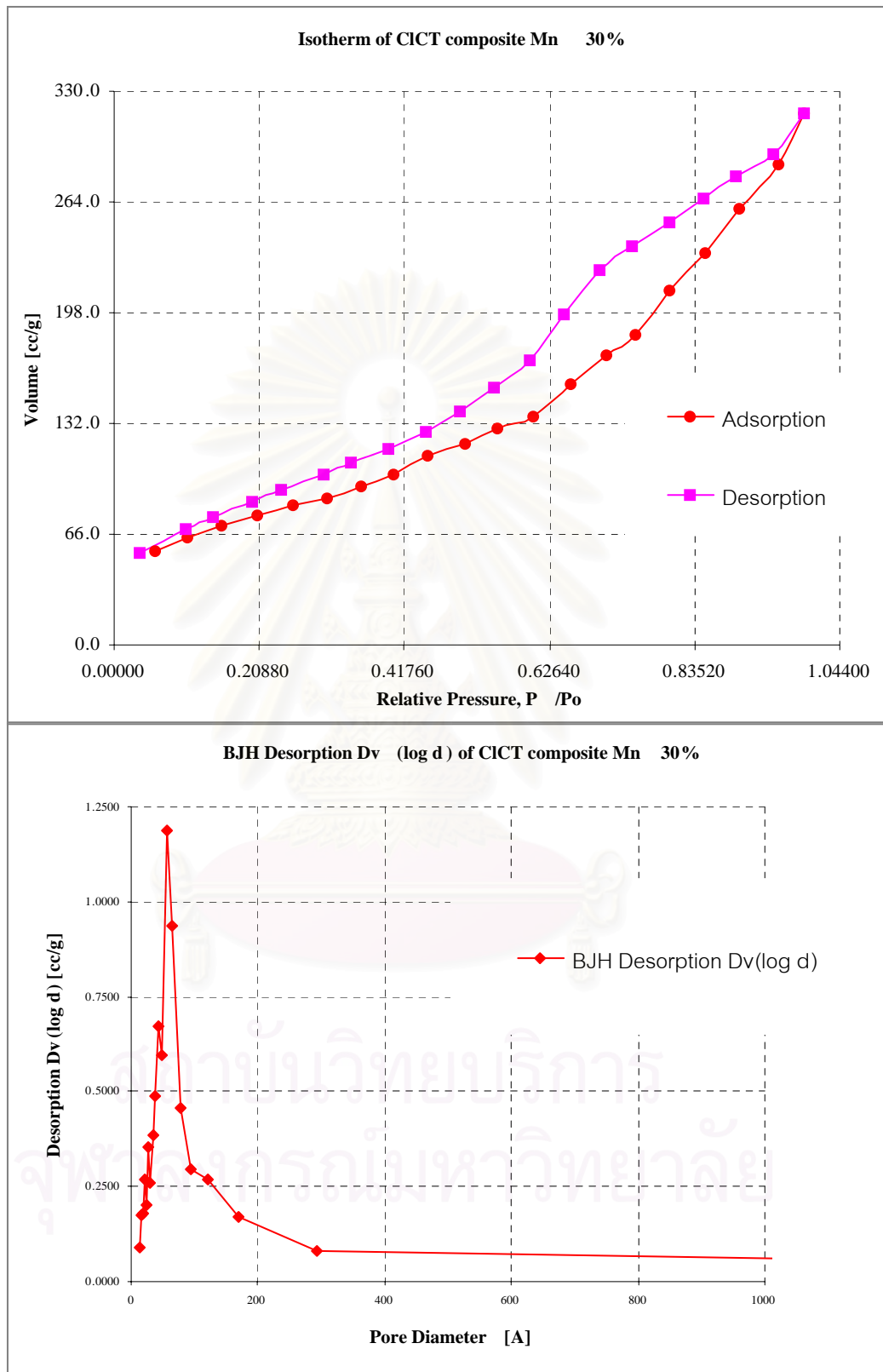


Figure A-7 N₂ adsorption-desorption isotherm and pore sizes distribution of CICT composite.

VITAE

Miss Khwannapa Kongsanoa was born on September, 1980 in Rayong, Thailand. She received a Bachelor Degree of Science in Chemistry from Chulalongkorn University in 2003. Since then, she has been a graduate student in major of Inorganic Chemistry, Faculty of Science, Chulalongkorn University. During her graduate studies towards the Master's Degree, she also receives a teaching assistant from Department of Chemistry, Faculty of Science in 2003, and a research granted from the Graduate School, Chulalongkorn University.

Her present address is 79/3 Moo 10, Kached, Muang, Rayong, 21100. Tel 0-1868-0899.



สถาบันวิทยบริการ
จุฬาลงกรณ์มหาวิทยาลัย